Università degli Studi di Ferrara

DOTTORATO DI RICERCA IN
"Farmacologia e oncologia molecolare"

CICLO XXII

COORDINATORE Prof. Pier Andrea Borea

The Ca^{2+} signal as common target of three different proteins involved in the apoptotic process

Settore Scientifico Disciplinare **MED/04**

Dottorando
Dott. Marchi Saverio

Tutore
Prof. Rimessi Alessandro

Anni 2007/2009

Index

Abstract

Ca^{2+} signal plays a fundamental role in modulating diverse cellular responses as muscle contraction, exocytosis, motility, fertilization, proliferation and apoptosis. Therefore, several proteins involved in this wide range of biological processes “manipulate” intracellular Ca^{2+} to (dis)regulate these events. To analyse Ca^{2+} homeostasis at the subcellular level, we employed the Ca^{2+}-sensitive photoprotein aequorin, targeted to defined intracellular locations (organelles, such as mitochondria, endoplasmic reticulum, and cytoplasmic regions).

Using this experimental approach, we investigated multiple effects on Ca^{2+} dynamics of three different proteins: i) the 66 KDa isoform of Shc protein (p66Shc) and its role on the alterations of mitochondrial Ca^{2+} homeostasis during oxidative stress. ii) The tumor suppressor protein Fhit and its role as sensitizer of the low-affinity Ca^{2+} transporters of mitochondria, and in turn potentiating the effect of apoptotic agents. iii) The proto-oncogene Akt, a potent inhibitor of apoptosis, through the reduction of Ca^{2+} release from the ER during apoptotic stimulation.

Taken together, these data remark the practical useful of Ca^{2+}-dynamics investigation as a “reporter system” to understand different molecular mechanisms of different proteins and may provide ways to act on apoptotic cell death and its derangement in cancer.

Riassunto

Il segnale Ca^{2+} gioca un ruolo fondamentale nel modulare diverse risposte cellulari come contrazione muscolare, esocitosi, mobilità cellulare, fertilità, proliferazione ed apoptosi. Perciò, diverse proteine implicate in questa ampia gamma di processi biologici "manipolano" la concentrazione di Ca^{2+} intracellulare per (dis)regolare questi processi.

Per analizzare l'omeostasi del Ca^{2+} a livello sub-cellulare, il nostro laboratorio si avvale della tecnica dell'equorina, una foto-proteina sensibile al Ca^{2+} che può essere direzionata ai vari sub-compartimenti cellulari (organelli come mitocondri, reticolo endoplasmico e citoplasma).

Usando questo approccio sperimentale, abbiamo studiato i diversi effetti riguardanti le dinamiche del Ca^{2+} di 3 proteine: i) la proteina p66Shc e il suo ruolo nell'alterazione dell'omeostasi del Ca^{2+} in condizioni di stress ossidativo. ii) l'oncosoppressore Fhit e la sua capacità nel sensibilizzare i trasportatori del Ca^{2+}a bassa affinità e nel potenziare gli effetti di agenti apoptotici. iii) il proto-oncogene Akt, un potente inibitore del processo apoptotico, capace di inibire il rilascio di Ca^{2+} dal reticolo endoplasmico dopo stimolo apoptotico.

Nel complesso questi dati sottolineano l'importanza dello studiare le dinamiche del segnale Ca^{2+}, essendo questo un formidabile "sistema reporter" per meglio comprendere i meccanismi molecolari di proteine diverse. Inoltre, nello specifico, esso puo essere considerato un processo su cui poter agire per modificare il processo apoptotico e la sua disregolazione nel tumore.

1. Introduction

1.1 The concept of Ca^{2+} as a cellular signal

In the past two decades, our understanding of how extracellular signals are conveyed to eukaryotic cells via an increase in intracellular Ca^{2+} concentration has widely expanded. It is today common knowledge that a variety of extracellular stimuli (ranging from the binding of hormones, neurotransmitters, growth factors to phenomena such as cell-cell interactions), through diverse mechanisms (e.g. receptors that are themselves ion channels, or have an intrinsic enzymatic activity or are coupled to enzymatic effectors via G proteins) induce a rise in cytoplasmic Ca^{2+} concentration ($[Ca^{2+}]_{cyt}$) with defined amplitude and kinetics [1, 2].

In most eukaryotic cells, a large electrochemical gradient for Ca^{2+} exists across the plasma membrane. The transmembrane potential across the membrane is 70 to 90 mV. The interior of the cell is the more negative, yet the cytoplasmic concentration of Ca^{2+} ($[Ca^{2+}]_{cyt}$) is less than one-ten thousandth of that in the extracellular milieu. There are also intracellular organelles, such as the endoplasmic reticulum (ER) and secretory granules, which contain one- to ten thousand fold greater concentrations of Ca^{2+} than the cytoplasm.

Moreover, the technological advancements in probe design and imaging systems, by allowing the accurate measurement $[Ca^{2+}]$ at the single cell level, has revealed a marked asynchronicity in cell response and a high spatio-temporal complexity of the intracellular Ca^{2+} signal. We now know that the Ca^{2+} signal can be conveyed as repetitive $[Ca^{2+}]_{cyt}$ spikes (commonly referred to as Ca^{2+} oscillations) [3], as well as localised $[Ca^{2+}]_{cyt}$ increases that may either be confined or gradually propagate to the rest of the cell ("Ca^{2+} waves") [4, 5].

An extensive Ca^{2+}-signalling toolkit is used to assemble signalling systems with very different spatial and temporal dynamics. Rapid highly localized Ca^{2+} spikes regulate fast responses, whereas slower responses are controlled by repetitive global Ca^{2+} transients or intracellular Ca^{2+} waves. The Ca^{2+} has a direct role in controlling the expression patterns of its signalling systems that are constantly being remodelled in both health and disease. During the *on reaction*, stimuli induce both the entry of external Ca^{2+} and the formation of second messengers that release internal Ca^{2+} that is stored within the endoplasmic reticulum or Golgi apparatus. Most of this calcium is bound to buffers, whereas a small proportion binds to the effectors that activate various cellular processes. During the *off reactions*, Ca^{2+} leaves the effectors and buffers and is removed from the cell by various

exchangers and pumps. The Na^+/Ca^{2+} exchanger (NCX) and the plasma membrane Ca^{2+}-ATPase (PMCA) extrude Ca^{2+} to the outside, whereas the sarco/endoplasmic reticulum Ca^{2+}-ATPase (SERCA) pumps Ca^{2+} back into the ER.

Mitochondria also have an active function during the recovery process in that they sequester Ca^{2+} rapidly trough a uniporter, and release more slowly back into the cytosol to be dealt with by the SERCA and the PMCA. Cell survival is dependent on Ca^{2+} homeostasis, whereby the Ca^{2+} fluxes during the off reactions exactly match those during the on reaction.

1.2 Generation (on reaction) and extinction (off reaction) of Ca^{2+} signalling

Cells maintain a rigid control over the intracellular level of Ca^{2+}, thus ensuring that the level is kept low during periods of inactivity. In order to use Ca^{2+} as a messenger, cells overcome this tight homeostatic control by using sophisticated mechanisms. An increase in the intracellular level of Ca^{2+} depends upon entry channels in the plasma membrane and release channels in the membranes of the internal stores, the endoplasmic reticulum (ER) or the Golgi apparatus. In first case, there are many different plasma membrane channels that control Ca^{2+} entry from the external medium in response to stimuli that include membrane depolarization, stretch, noxious stimuli, extracellular agonists.

Entry of Ca^{2+} is driven by the presence of a large electrochemical gradient across the plasma membrane. The cells use this external source of signal Ca^{2+} by activating various entry channels with widely different properties. We know the most about the voltage-operated channels (VOCs), which are found in excitable cells and generate the rapid Ca^{2+} fluxes that control fast cellular process such as muscle contraction or exocytosis at synaptic endings.

There are many other Ca^{2+}-entry channels that open in response to different external signals, such as the *receptor-operated channels* (ROCs), for example the NMDA receptor that respond to glutamate. There also are *second-messenger-opereted channels* (SMOCs) that are controlled by internal messengers, such us the cyclic-nucleotide-gated channels that are found in sensory systems and the arachidonic-acid-sensitive channel. In addition to these more clearly defined channel-opening mechanisms, there are many other channel types that are sensitive to a diverse array of stimuli, such as the *store-operated channels* (SOCs) or *G protein-operated-calcium channels* (GOCCs).

The G protein-coupled receptors contains upwards of 1000 distinct members that mediate the vast majority of all responses to hormones, neurotransmitters, autocrine and paracrine factors. These integral membrane proteins have a conserved primary structure that contains seven stretches of 20-25 hydrophobic amino acid residues that span the plasma membrane. Hence, these important convertors of extracellular signals into intracellular signals are called seven transmembrane spanning domain receptors. Upon binding of agonist, GOCCs undergo a conformational change which then allows for productive coupling to heterotrimeric guanine regulatory proteins (G proteins). The active conformation of the agonist-occupied G protein-coupled receptor acts as a guanine nucleotide exchange factor for the heterotrimeric G protein and activates the G protein by promoting the dissociation of GDP and loading of GTP onto the G protein α subunit. In order to limit the magnitude and duration of the extracellular stimulus, the signalling cascade has to be dynamically regulated. In fact, most stimuli are short lived (milliseconds to minutes) as their response wanes over time even in the presence of saturating concentrations of agonist. This phenomenon is termed desensitization. Several different processes with varying time frames are responsible for desensitization.

The release of Ca^{2+} from internal store is controlled by Ca^{2+} itself, or by an expanding group of messengers, such as inositol–1,4,5–triphosphate (IP_3), cyclic ADP ribose (cADPr), nicotinic acid adenine dinucleotide phosphate (NAADP) and sphingosine-1-phosphate, that either stimulate or modulate the release channels on the internal stores. The most ubiquitous of the intracellular Ca^{2+} release mechanisms involves the phosphoinositide specific phospholipase C-derived second messenger (IP_3), which acts by binding to a specific receptor (IP_3R) on the endoplasmic reticulum. Distinct subtypes of the receptor exist, representing products of at least three distinct genes, and additional forms arise as a result of alternative splicing of mRNA. The interaction of IP_3 with its receptor involves complex and poorly understood regulatory interactions among the receptor, IP_3 and Ca^{2+}, the latter exerting influence from both the cytoplasmic and luminal aspects of the receptor. Ca^{2+} in the lumen of the ER appears to sensitize the receptor to IP_3. On the cytoplasmic surface, low concentrations of Ca^{2+} sensitize the receptor, while higher concentrations are inhibitory. These actions may contribute to the "all-or-none" oscillatory behaviour of $[Ca^{2+}]_{cyt}$ signals observed in some cell types.

The other major type of intracellular Ca^{2+}-mobilizing receptor is the ryanodine receptor (RYR). The ryanodine receptor family comprising three members: RYR1 found in skeletal muscle and certain neurones (e.g. Purkinje cells), RYR2 found in cardiac muscle,

brain and some other cells, and RYR3 found in smooth muscle, brain and other cells [6], [7]. In its most specialized setting, in skeletal muscle, the RYR is gated by a direct conformational interaction with a dihydropyridine receptor in the *t*-tubule membrane. This coupling allows for rapid release of stored Ca^{2+} when an action potential invades the *t*-tubule system. However, the physiological ligand for the RYR is usually Ca^{2+} itself; because of this, it is considered to be a *Calcium-Induced Calcium Release* receptor-Ca^{2+} channel. Because Ca^{2+} can sensitize the IP_3 receptor to IP_3, the IP_3 receptor also can exhibit a *Calcium-Induced Calcium Release* behaviour. However, some IP_3 is always required for its action, while the ryanodine receptor can function as a "pure" *Calcium-Induced Calcium Release* receptor. Although the RYR is thought to be regulated primarily by *Calcium-Induced Calcium Release*, there is also a small water-soluble molecule that can function as a regulatory ligand for at least some forms of the ryanodine receptor. Cyclic adenosine diphosphate ribose (cADPr) functions in a manner somewhat similar to IP_3: it increases the probability of the ryanodine receptor channel opening by increasing its sensitivity to Ca^{2+}.

During the course of a typical Ca^{2+} transient, the generation of Ca^{2+} signalling is counteracted by the systems of switching off of Ca^{2+} signalling, during which time various pumps and exchangers remove Ca^{2+} from the cytoplasm.

The pumping mechanisms have important homeostatic functions in that they maintain the resting level of Ca^{2+} and ensure that the internal stores are kept loaded. Four different pumping mechanisms are responsible for the off reaction: the plasma-membrane Ca^{2+}-ATPase (PMCA), the Na^{+}/Ca^{2+} exchanger (NCX), SERCA (sarco/endoplasmic reticulum Ca^{2+}-ATPase) and the mitochondrial calcium uniporter (MCU). PMCA and SERCA pumps have lower transport rates but high affinities, therefore they can respond to modest elevations in Ca^{2+} levels and set basal Ca^{2+} levels. The NCX and mitochondrial uniporter have much greater transport rates, and can limit Ca^{2+} transient over a wider dynamic range.

Ca^{2+}-ATPases constitute a large family of proteins that fall into two distinct groups, the sarco(endo)plasmic reticulum Ca^{2+}-ATPase (SERCA), and the plasma membrane Ca^{2+}-ATPase (PMCA). Most eukaryotic cells co-express, in a tissue-specific and differentiation stage-specific manner, one or more types of SERCA and PMCA pumps.

The PMCA are calcium pumps of the plasma membrane, largely responsible for the regulated transport of Ca^{2+} between the intracellular and the extracellular milieu. Mammals have four genes encoding the proteins PMCA1 through PMCA4. Each gene transcript is

alternatively spliced to generate several variants. Their distribution is tissue- and cell-specific and undergoes regulation during cell development and differentiation. Traditionally, these pumps have been considered to play a housekeeping role in controlling basal Ca^{2+} levels, but more recently, it became clear that the presence (and the co-expression) of different isoforms must be related to a more specialized function [8].

The only known mechanism for accumulation of Ca^{2+} by the endoplasmic reticulum is through the actions of SERCA pumps. SERCA are calcium pumps involved in the transport of calcium from the cytosol to various intracellular stores such as the sarcoplasmic reticulum (SR), the endoplasmic reticulum (ER) and calciosomes. It catalyses Ca^{2+} transport to the lumen of the SR or ER by an active process that requires adenosine triphosphate (ATP). Enzyme phosphorylation and ATP hydrolysis result in translocation of the two Ca^{2+} ions bound to the enzyme from a high affinity site to a low affinity site. The two calcium ions are then released into the lumen of the intracellular stores [9].

Three separate genes encode the SERCA family. The SERCA 1 gene is exclusively expressed in fast twitch skeletal muscle. Developmentally regulated alternative splicing of SERCA 1 results in an adult isoform (SERCA 1a) and a neonatal isoform (SERCA 1b) [10-12]. The SERCA 2 gene is expressed in slow-twitch skeletal muscle, cardiac muscle, smooth muscle and non-muscle tissues. Tissue-dependant processing of the SERCA 2 gene transcript yields four SERCA 2 messenger ribonucleic acids (mRNAs) (classes 1–4). Class 1 mRNA encodes the SERCA 2a isoform, found in cardiac, smooth and slow twitch skeletal muscles. Class 2, 3 and 4 mRNAs encode the SERCA 2b isoform, ubiquitously expressed at low levels in all cell types [13, 14]. A third isoform, SERCA 3, is less well documented, but like the SERCA 2 gene, shows widespread tissue distribution [15]. Phospholamban (cardiac muscle) and sarcolipin (skeletal muscle) regulate SERCA activity, current models of Ca^{2+}-ATPase regulation by phospholamban depict unphosphorylated phospholamban as an inhibitor of the Ca^{2+}-ATPase, the inhibition is exerted by association of the two proteins [16, 17].

Na^{+}/Ca^{2+} exchangers cooperate with the PMCA pumps to export Ca^{2+} from the cytosol using the energy of the Na^{+} (K^{+}) gradient across the plasma membrane [18, 19]. Two basic types of Na^{+}/Ca^{2+} exchangers have been characterized. They differ in the nature and stoichiometry of the transported ions: the protein found in the plasma membranes of cardiac and a number of other cells (the prototype of the Na^{+}/Ca^{2+} exchangers denominated NCX) exchanges three Na^{+} for one Ca^{2+} [20], whereas the protein originally found in the outer segment of retinal rods and cones and latter in other

cells as well (denominated NCKX) imports four Na^+ ions in the cytosol in exchange for one Ca^{2+} and one K^+ [21]. Thus, the exchanger functions electrogenically, using the energy potential stored in the transmembrane Na^+ gradient to extrude the Ca^{2+} against its concentration gradient. The exchangers are expressed at high level in brain and a few other tissues, in particular skeletal muscles, where the presence of multiple isoforms underlines the critical role of the exchanger in the control of cytosolic Ca^{2+} concentration in neurons. A particular case is that of synaptic transmission, a process that demands that the cytosolic Ca^{2+} concentration is constantly re-adjusted and where the exchanger has a key role.

Mitochondrial Ca^{2+} uptake plays a key role in the regulation of many cell functions, ranging from ATP production to cell death. However, the molecular mechanism underlying this phenomenon has not yet been completely explained, indeed, while the contribution of OMM Ca^{2+} channels (VDAC) has been well characterized, little is known about the so-called mitochondrial Ca^{2+} uniporter (MCU). MCU is a highly selective ion channel located in the mitochondrial inner membrane, with a dissociation constant ≤ 2 nM over monovalent cations, reaching saturation only at supraphysiological $[Ca^{2+}]_{cyt}$. Ca^{2+} crosses the inner mitochondrial membrane through the MCU thanks to the considerable driving force represented by the negative transmembrane potential [22]. Studies performed on isolated mitochondria allowed the identification of some regulatory molecules acting on MCU, in particular the most effective inhibitors are the hexavalent cation Rutenium Red (RuR) and its related compound RuR360 [23], clonazepam and CGP37157 [24]. Another important regulator of MCU is Ca^{2+} itself. As demonstrated by Moreau and its group [25], in fact, MCU has a biphasic dependence on cytosolic Ca^{2+} concentration: $[Ca^{2+}]_{cyt}$ increase can both activate or inactivate mitochondrial Ca^{2+} uptake.

1.3 Mitochondrial Ca^{2+} signalling: a turning point controlling cell fate

In the past years, mitochondria have been shown to be a critical checkpoint, capable of releasing structural components into the cytoplasm of cells doomed to die via apoptosis [26]. These proteins normally retained in the organelle (that include an important component of the respiratory chain, cytochrome *c*, as well as newly discovered proteins, such as AIF and Smac/Diablo) are released into the cytoplasm, where they activate effector caspases and drive cells to apoptotic cell death [27]. Interestingly, Ca^{2+} has been shown to play an important function in this process, thus representing a complex signal

within the organelle, which can be decoded into radically different biological consequences [28-31].

Indeed, work from various labs has revealed that the alteration of the Ca^{2+} signal reaching the mitochondria and/or the combined action of apoptotic agents or pathophysiological conditions (e.g., oxidative stress, Cadmium injury) can induce a profound alteration of organelle structure and function [32, 33]. Different effects have been described. Szalai et al. showed in hepatocytes that, upon treatment with sub-optimal doses of the lipid mediator of apoptosis ceramide, the repetitive spiking of cytosolic Ca^{2+} concentration ($[Ca^{2+}]_{cyt}$) rather than triggering the activation of matrix dehydrogenases (and thus the stimulation of aerobic metabolism), causes opening of mitochondrial permeability transition pore (MPTP, the channel that allows the release in the cytosol of intermembrane-residing apoptotic factors) mitochondrial swelling and the release of cytochrome *c* [34]. Thus, a mechanism of coincidence detection of physiological agonists and apoptotic stimuli allows the specific induction of the apoptotic program (with mitochondria acting as the site where this differential decoding is operated). Subsequently, we have shown that in HeLa cells, ceramide directly causes the release of Ca^{2+} from the ER, and Ca^{2+} loading in mitochondria possibly in combination with a direct activity of the lipid mediator causes the morphological alteration of the organelle (fragmentation, swelling) and the ensuing release of cytochrome *c* and other caspase cofactors [33].

In all cases, the amount of Ca^{2+} released from the ER and the ability of mitochondria to accumulate it appear to play a critical role. In fact, a decrease of ER Ca^{2+} content protects cells from apoptotic cell death [35]; conversely, amplification of Ca^{2+} signals has a proapoptotic effect. In this respect, both in neurons and in hepatic cells it was observed that apoptotic signals (staurosporin in the former case, the proapoptotic X protein of Hepatitis B virus in the latter) cause the activation of caspase 3, with ensuing cleavage of the plasma membrane Ca^{2+} ATPase (that contain a consensus for caspase cleavage in its sequence) [36, 37]. Thus, the mechanism that allows the termination of the agonist induced Ca^{2+} signals is impaired, and $[Ca^{2+}]_{cyt}$ rises are enhanced and prolonged. This causes mitochondrial Ca^{2+} overload and the apoptotic morphological and functional alterations of the organelles [31].

Therefore, is a general agreement in the literature that the increased energy demand required for carrying out different processes, such as muscle contraction, exocytosis, motility, fertilization, proliferation and gene expression, is met, in part, from the accumulation of some of the released Ca^{2+} by the mitochondria with the resulting Ca^{2+}-

dependent activation of key intramitochondrial enzymes linked to ATP production [38, 39]. The efficiency of this process is greatly enhanced by placement of ER and mitochondrial membranes in close proximity [40]. Thus the physiological release of Ca^{2+} through IP_3Rs serves important signaling and “housekeeping” roles in maintaining normal function during agonist-mediated cell activation. However, in the presence of an apoptotic stimulus, the IP_3R-mediated Ca^{2+} release can activate apoptotic pathways by inducing the release from mitochondria of a number of pro-apoptotic factors including cytochrome *c*.

The present thesis is focused on studying the signal transduction pathways in living cells with particular emphasis on calcium signalling. In these studies I used a well established technique for measuring Ca^{2+} in subcellular compartments, that is based on the recombinant expression of the Ca^{2+}-sensitive photoprotein aequorin, modified in order to include specific targeting sequences. This approach provides a formidable “read-out system” to understand how different proteins “manipulate” intracellular Ca^{2+} homeostasis in order to exert their biological functions.

2. Tools

The wide expansion of molecular biology techniques, with the possibility of modifying and expressing exogenous cDNAs in virtually all cell types, has been responsible for the growing success in the use of protein probes in cell biology. Two groups of reporter proteins are currently employed, derived from the wide variety of bioluminescent organisms: the chemiluminescent proteins (e.g. the different types of aequorin), and the fluorescent proteins (e.g. the green fluorescent protein, GFP).

The Ca^{2+}-sensitive photoprotein aequorin was targeted to defined intracellular locations (organelles, such as mitochondria, endo- and sarcoplasmic reticulum, Golgi apparatus and nucleus, and cytoplasmic regions, such as the bulk cytosol and the subplasmalemmal rim) and used to analyse Ca^{2+} homeostasis at the subcellular level.

2.1 Aequorin

Aequorin is a Ca^{2+} sensitive photoprotein of a coelenterate, isolated from the jellyfish *Aequorea Victoria.* The protein is composed of a 21 kDa apoprotein and a hydrophobic prosthetic group, coelenterazine (MW~400 Da). The 2 components must be associated for the Ca^{2+}-triggered light emission to occur. The holoprotein possesses 3 high affinity Ca^{2+} binding sites (homologous to the sites present in other Ca^{2+} binding proteins, such as calmodulin). Upon binding of Ca^{2+} ions, the coelenterazine is oxidized to coelenteramide, with a concomitant release of carbon dioxide and emission of light; this is an irreversible reaction where one photon is emitted.

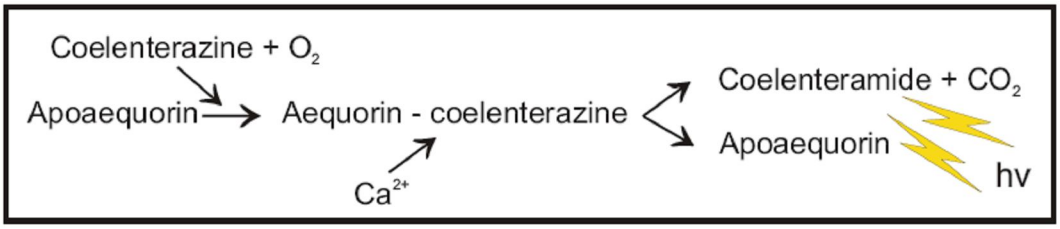

Fig. 1: The aequorin reaction: Aequorin is composed of an apoprotein and a prosthetic group, coelenterazine, and its polypeptide sequence includes three high affinity Ca^{2+}-binding sites. Ca^{2+} binding causes the rupture of the covalent link between the apoprotein and the prosthetic group, a reaction associated with the emission of one photon.

Although this reaction is irreversible, in vitro an active aequorin can be obtained by incubating the apoprotein with coelenterazine in the presence of oxygen and 2-mercaptoethanol. Reconstitution of an active aequorin (expressed recombinantly) can be obtained also in living cells by simple addition of coelenterazine to the medium. Coelenterazine is highly hydrophobic and has been shown to permeate cell membranes of various cell types, ranging from the slime mold *Dictyostelium discoideum* to mammalian cells and plants [41].

The possibility of using aequorin as a calcium indicator is based on the existence of a well-characterized relationship between the rate of photon emission and the free Ca^{2+} concentration. The rate of this reaction depends on the Ca^{2+} concentration ($[Ca^{2+}]$) to which the photoprotein is exposed. In particular, at $[Ca^{2+}]$ between 10^{-7} and 10^{-5} M (the concentration normally occurring in the cytoplasm of living cells), there is a direct relationship between $[Ca^{2+}]$ and the fractional rate of consumption of the photoprotein.

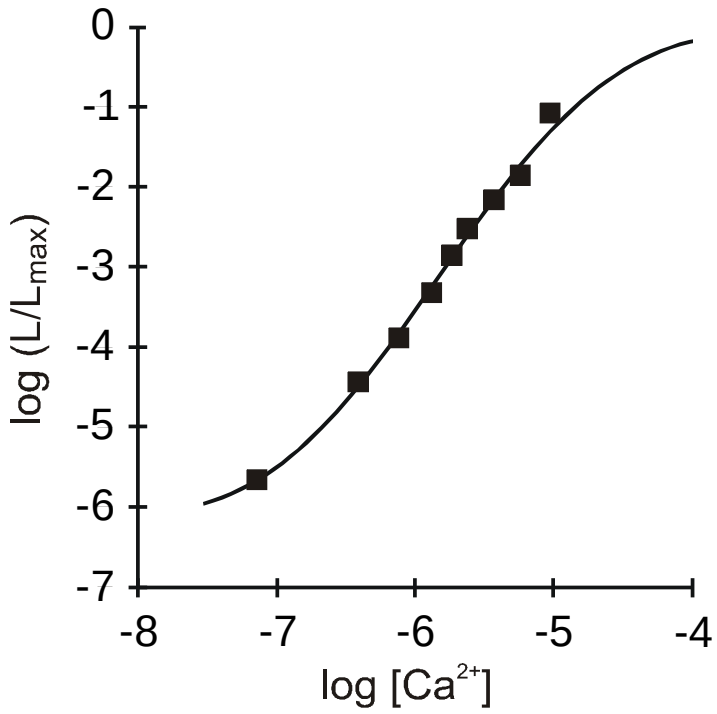

Fig. 2: Relationship between the free Ca^{2+} concentration and the rate of aequorin photon emission.
The fractional rate of aequorin consumption is expressed as the ratio between the emission of light at defined $[Ca^{2+}]$ (L) and the maximal rate of the light emission at saturating $[Ca^{2+}]$ (L max).

Figure 2 shows the Ca^{2+} response curve of aequorin, at physiological conditions of pH, temperature, and ionic strength. It is apparent that the fractional rate of aequorin consumption expressed as the ratio between the emission of light at a defined Ca^{2+}

concentration (L) and the maximal rate of the light emission at saturating [Ca^{2+}] (Lmax) is proportional to the 2nd-3rd power of [Ca^{2+}]. Indeed, if all the light emitted by the photoprotein throughout an experiment, as well as that discharged at the end are collected it is possible to estimate Lmax and then calculate back the [Ca^{2+}] to which the photoprotein is exposed in every moment.

Although aequorin luminescence is not influenced either by K^+ or Mg^{2+} (which are the most abundant cations in the intracellular environment and thus the most likely source of interference in physiological experiments) both ions are competitive inhibitors of Ca^{2+} activated luminescence. Aequorin photon emission can be also triggered by Sr^{2+} but its affinity is about 100 fold lower than that of Ca^{2+}, while lanthanides have high affinity for the photoprotein (e.g. are a potential source of artifacts in experiments where they are used to block Ca^{2+} channels). pH was also shown to affect aequorin luminescence but at values below 7.

In fact all experiments of this thesis with aequorin need to be done in well-controlled conditions of pH and ionic concentrations, notably of Mg^{2+}.

2.1.1 Recombinant Aequorin

In the past, was widely employed to measure Ca^{2+} concentration in living cells, in fact the purified protein was widely used to monitor cytoplasmic [Ca^{2+}] changes in invertebrate muscle cells after microinjection. However, due to the time-consuming and traumatic procedure of microinjection, the role of aequorin in the study of Ca^{2+} homeostasis remained confined to a limited number of cells (giant cells) susceptible to microinjection.

The cloning of aequorin cDNA [42] and the explosive development of molecular biology offered new possibilities in the use of aequorin, as microinjection has been replaced by the simpler technique of cDNA transfection, opening the way to recombinant expression and thus has largely expanded the applications of this tool for investigating Ca^{2+} handling in living cells. As a polypeptide, aequorin allows the endogenous production of the photoprotein in cell systems as diverse as bacteria, yeast, plants and mammalian cells.

In particular, recombinant aequorin can be expressed not only in the cytoplasm, but also in specific cellular locations by including specific targeting sequencing in the engineered cDNAs.

Extensive manipulations of the N-terminal of aequorin have been shown not to alter the chemiluminescence properties of the photoprotein and its Ca^{2+} affinity. On the other hand, even marginal alterations of the C-terminal either abolish luminescence altogether or drastically increase Ca^{2+} independent photon emission [43]. As demonstrated by Watkins and Campbell [44], the C-terminal proline residue of aequorin is essential for the long-term stability of the bound coelenterazine. For these reasons, all targeted aequorins synthesized in our laboratory include modifications of the photoprotein N-terminal. Three targeting strategies have been adopted:

1. Inclusion of a minimal targeting signal sequence to the photoprotein cDNA.
2. Fusion of the cDNA encoding aequorin to that of a resident protein of the compartments of interest.
3. Addition to the aequorin cDNA of sequences that code for polypeptides that bind to endogenous proteins.

2.1.2 Chimeric Aequorin cDNAs (Fig. 3)

Below I briefly describe the constructs that were present in our laboratory and that I used for the thesis.

- *Aequorin targeted to cytoplasm (cytAEQ)*

An unmodified aequorin cDNA encodes a protein that, in mammalian cells is located in the cytoplasm and, given its small size, also diffuses into the nucleus. An alternative construct was also available that is located on the outer surface of the ER and of the Golgi apparatus. This construct was intended to drive the localization of aequorin to the inner surface of the plasma membrane given that it derives from the fusion of the aequorin cDNA with that encoding a truncated metabotropic glutamate receptor (mgluR1). The encoded chimeric protein, however, remains trapped on the surface of the ER and Golgi apparatus, with the aequorin polypeptide facing the cytoplasmic surface of these organelles. The cytoplasmic signal revealed by this chimeric aequorin is indistinguishable from that of a cytoplasmic aequorin, but it has the advantage of being membrane bound and excluded from the nucleus.

- *Aequorin targeted to mitochondria (mtAEQ)*

The mtAEQ probe has been successfully employed to measure the $[Ca^{2+}]$ of the mitochondrial matrix of various cell types. This construct includes the targeting presequence of subunit VIII of human cytochrome c oxidase fused to the aequorin cDNA [45].

- *Aequorin targeted to Endoplasmic reticulum (erAEQ)*

The erAEQ includes the leader (L), the VDJ and Ch1 domains of an Ig2b heavy chain fused at the N-terminus of aequorin. Retention in the ER depends on the presence of the Ch1 domain that is known to interact with high affinity with the luminal ER protein BiP [46].

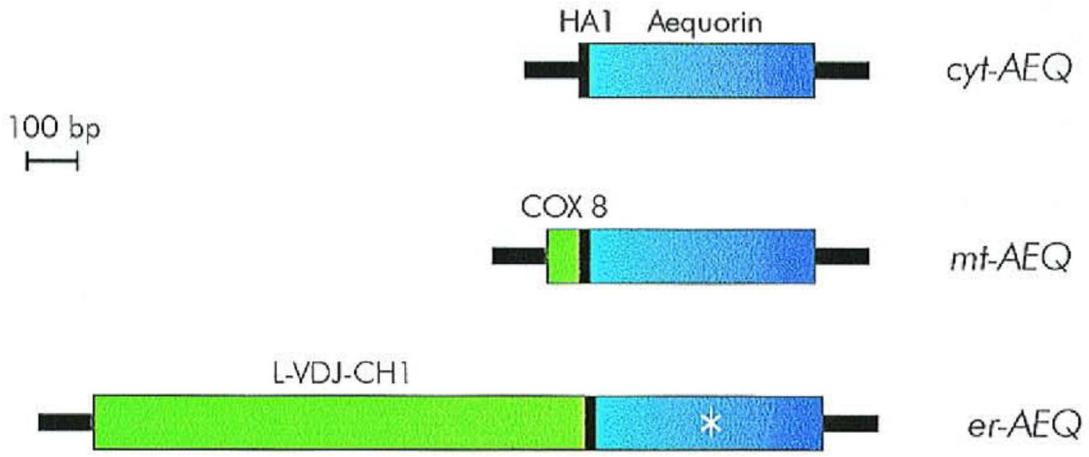

Fig. 3: Schematic representation of aequorin chimeras.

2.1.3 Luminescence detection

The aequorin detection system is derived from that described by Cobbold and Lee [47] and is based on the use of a low noise photomultiplier placed in close proximity (2-3 mm) of aequorin expressing cells. The cell chamber, which is on the top of a hollow cylinder, is adapted to fit 13-mm diameter coverslip. The volume of the perfusing chamber is kept to a minimum (about 200 µl). The chamber is sealed on the top with a coverslip, held in place with a thin layer of silicon. Cells are continuously perfused via a peristaltic pump with medium thermostated via a water jacket at 37°C. The photomultiplier (EMI 9789 with amplifier-discriminator) is kept in a dark box and cooled at 4°C. During manipulations on the cell chamber, the photomultiplier is protected from light by a shutter. During aequorin experiments, the shutter is opened and the chamber with cells is placed in close proximity of the photomultiplier. The output of the amplifier-discriminator is captured by an EMIC600 photon-counting board in an IBM compatible microcomputer and stored for further analysis. In order to calibrate the crude luminescent signal in terms of [Ca^{2+}] an algorithm has been developed that takes into account the instant rate of photon emission and the total number of photons that can be emitted by the aequorin of the sample13. In

order to obtain the latter parameter, at the end of each experiment the cells are lysed by perfusing them with a hyposmotic medium containing 10 mM $CaCl_2$ and a detergent (100 µM digitonin or 0,1% Triton X-100) in order to discharge all the aequorin that was not consumed during the experiment.

A schematic representation of custom-made luminometer used in my laboratory is shown in figure 4.

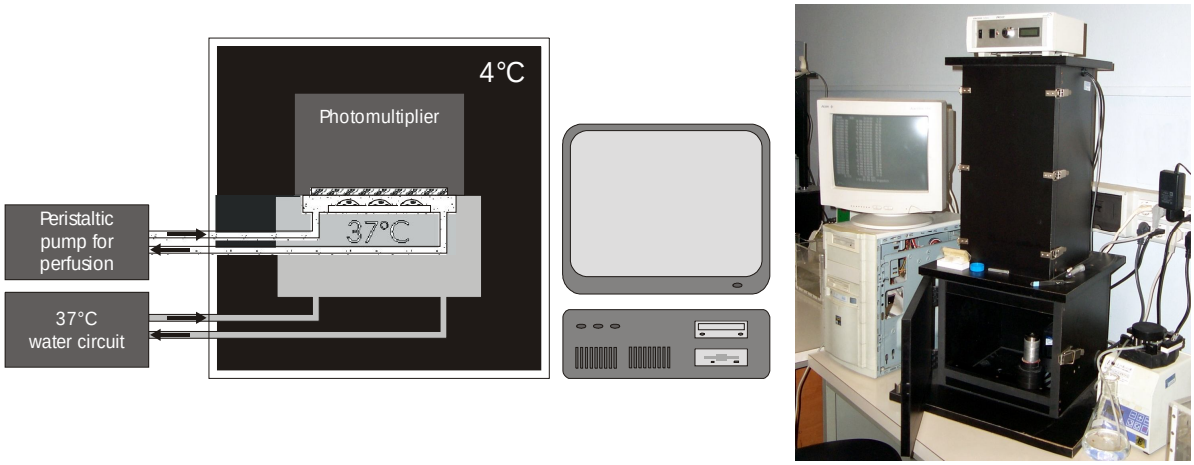

Fig. 4: Schematic representation of a custom-built luminometer. Cells loaded with functional aequorin probe are incubated in a perfusion chamber, at 37°C, in close proximity to a photon-counting tube. The complete assemblage is kept at 4°C, in the dark, to minimize extraneous signals. Acquisition of the data and subsequent calculations to transform light emission into $[Ca^{2+}]$ are performed by a dedicated computer algorithm.

2.1.4 Advantages and disadvantages of aequorin

In this section I will focus on the main characteristics that make aequorin such a flexible and powerful intracellular calcium sensor.

- *Advantages:*

1) Selective intracellular distribution. Whereas recombinantly expressed wild-type aequorin is exclusively cytosolic, the intracellular fate of the photoprotein can be modified by adding specific targeting sequences.

2) High signal-to-noise ratio. Due to the low luminescence background of cells and the steepness of the Ca^{2+} response curve of aequorin, minor variations in the amplitude of the agonist-induced $[Ca^{2+}]$ changes can be easily appreciated with aequorin.

3) Low Ca^{2+} buffering effect. Although the binding of Ca^{2+} by aequorin may, in principle, affect intracellular Ca^{2+} homeostasis, this undesired effect is less relevant than with

fluorescent indicators. In fact, thank to the excellent signal to noise ratio, aequorin is loaded at a concentration which is 2-3 orders of magnitude lower than dyes, i.e. usually from <0.1 μM (for the recombinantly expressed photoprotein) to ~1 μM (in the case of microinjection of the purified photoprotein for single cell studies).

4) Wide dynamic range. It is clearly evident from Fig. 2 that aequorin can accurately measure $[Ca^{2+}]$ ranging from 0.5 μM to 10 μM, i.e. reaching concentrations at which most fluorescent indicators are saturated. Indeed, thank to these properties and to the low buffering effect, it is possible to estimate the large $[Ca^{2+}]_c$ rises which occur, for example, in neurons [48]. Moreover, by introducing point-mutations in the Ca^{2+}-binding sites [49], using surrogate cations, such as Sr^{2+}, and/or modified prosthetic groups, the sensitivity of the recombinant photoprotein can be further reduced, and thus the $[Ca^{2+}]$ can be monitored also in intracellular compartments endowed with high $[Ca^{2+}]$ (e.g. the lumen of the ER).

5) Possibility of co-expression with proteins of interest. A powerful approach for investigating the role, and the properties, of the various molecular components of the Ca^{2+} signalling apparatus is either the overexpression of the heterologous protein, followed by the study of the molecularly modified cell. This can be accomplished in two ways, either by generating stably transfected cell clones, or by transiently expressing the protein of interest in a cell type.

- *Disadvantages:*

1) Overestimation of the average rise in cells (or compartments) with dishomogeneous behaviour. A disadvantages of the steepness of the Ca^{2+} response curve of aequorin is that, if the increase of the $[Ca^{2+}]$ is not homogeneous, the average estimate will be based towards the highest values. Indeed, by using targeted aequorin to monitor subplasmalemmal Ca^{2+} concentration, we measured a mean resting $[Ca^{2+}]$ of 1-2 μM, which most likely does not reflect the real average $[Ca^{2+}]_{pm}$ value, but, rather, the contribution of microdomains in the proximity of flickering Ca^{2+} channels [50].

2) Low light emission. In distinction to the fluorescent dyes (where up to 10^4 photons can be emitted by a single molecule, before photobleaching occurs), only 1 photon can be emitted by an aequorin molecule. Moreover, the principle of the use of aequorin for Ca^{2+} measurements is that only a small fraction of the total pool (varying, in a typical physiological experiment, from 10^{-7} to 10^{-2}) emits its photon every second. This is not a major limitation in population studies, as averaging over 10^3-10^4 cells. Conversely, single cell imaging requires very high expression and special apparatuses [51] and it is endowed with lower spatial and temporal resolution than that obtained with fluorescent indicators.

2.2 Green Fluorescent Protein (GFP)

In recent years, two decisive methodological advances have greatly improved optical microscopy and allowed to follow biological processes in living cells: the improvement of the instrumentation (with the development of confocal microscopes and of mathematical methods for image analysis) and the discovery of the "green fluorescent protein" (GFP), a protein derived from a jellyfish that can be utilized as a highly efficient intracellular probe in fluorescence microscopy. It is thus now possible to follow directly in intact, living cells cellular events of major biomedical relevance, such as the movement of proteins (including their mutated variants in genetic diseases) or intracellular organelle distribution. The possibility of directly identifying intracellular organelles in living cells has a major relevance in these cell biology studies. Indeed, key events, such as organelle distribution and dynamics, can be monitored in a variety of physiological phenomena (e.g. localized Ca^{2+} rises), and also the intracellular location (and the relative relations between the different organelle) can be unambiguously identified.

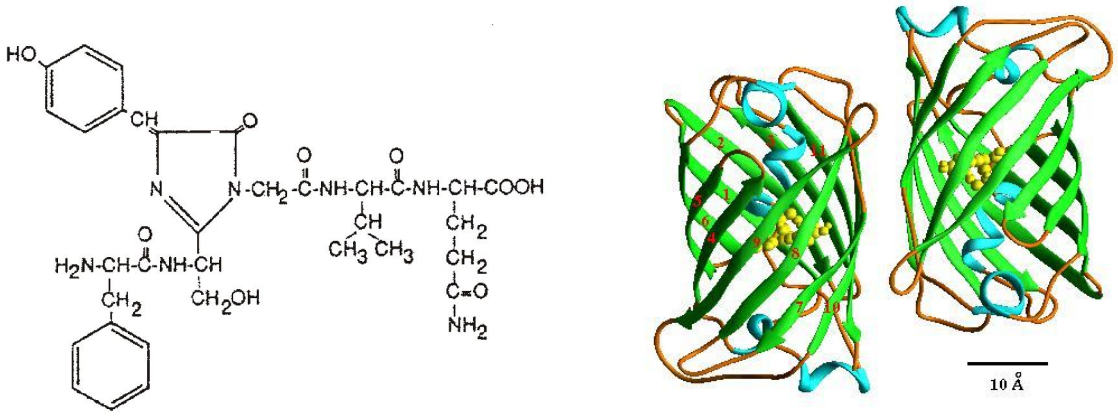

Fig. 5: The chemical structure of the chromophore in Aequorea GFP. Structural formula of GFP. GFP has a cylindrical fold. Two protomers associate together to form a dimer in the crystal and also in solution at low ionic strengths, <100 mM. Dimerization has an effect on the excitation spectra and energy transfer of GFP. The dimer is involved in physiological interactions with aequorin for efficient energy transfer. The structure is comprised of two regular beta-barrels.

Green fluorescent protein, GFP, is in nature the legitimate partner of aequorin. Indeed, it is produced by the same jellyfish (*Aequorea victoria*) and packed in close association to the photoprotein, acting as a natural fluorophore that absorbs the blue light emitted by the photoprotein and re-emits photons of a longer wavelength (thus accounting

for its own name and for the greenish hue of the jellyfish luminescence) [41, 52, 53]. In research applications, GFP retains its fluorescence properties, and thus can be added to the long list of probes of the cell biologist's toolbox [54]. Some of its unique properties account for its explosive success, and has made it, in relatively few years (the first report of GFP expression in heterologous systems dates back to 1994) [55], a powerful and versatile tool for investigating virtually all fields of cell biology (ranging from the study of gene expression to protein sorting, organelle structure, measurement of physiological parameters in living cells) [56, 57].

The main reason for the success of GFP is its own nature: the fluorescent moiety is a gene product (with no need for cofactors) that is open to molecular engineering and transient or stable expression in virtually every cell type. Moreover, its mutagenesis has allowed the adaptation of its fluorescent properties to different experimental needs (for a detailed description see reviews [54, 58]).

GFP mutants can be grouped in two major classes: the first are the "optimising" mutations, i.e. those that increase light emission by either altering the intrinsic properties of the fluorescent protein [59, 60] or increasing its production in mammalian cells [61]. The latter are the so called "humanised" versions of the cDNA, in which silent mutations are introduced in order to convert some of the codons into the most common and efficient for translation in mammalian cells.

As to the modification of GFP properties, mutations have been described that alter the stability of the protein and/or the quantum efficiency upon illumination with visible light (native GFP has a bimodal excitation peak, larger with UV than with blue light, while all currently employed green variants of GFP are best excited with blue light, thus minimising cytotoxicity and photobleaching). Among these mutations, the most useful appears to be the substitution of Ser^{65} into Thr (S65T), which causes the chromophore to be entirely in the anionic form: thus, when compared to wild-type GFP the quantum efficiency upon excitation with blue light is 6-fold increased, the rate of fluorophore formation is 4-fold faster and photobleaching is markedly reduced. The second class is represented by GFPs emitting light of a wavelength that can be clearly distinguished from the green colour of native GFP. This class includes some popular mutants commonly referred to as blue (Y66H, Y145F), cyan (Y66W) and yellow (T203Y) GFPs.

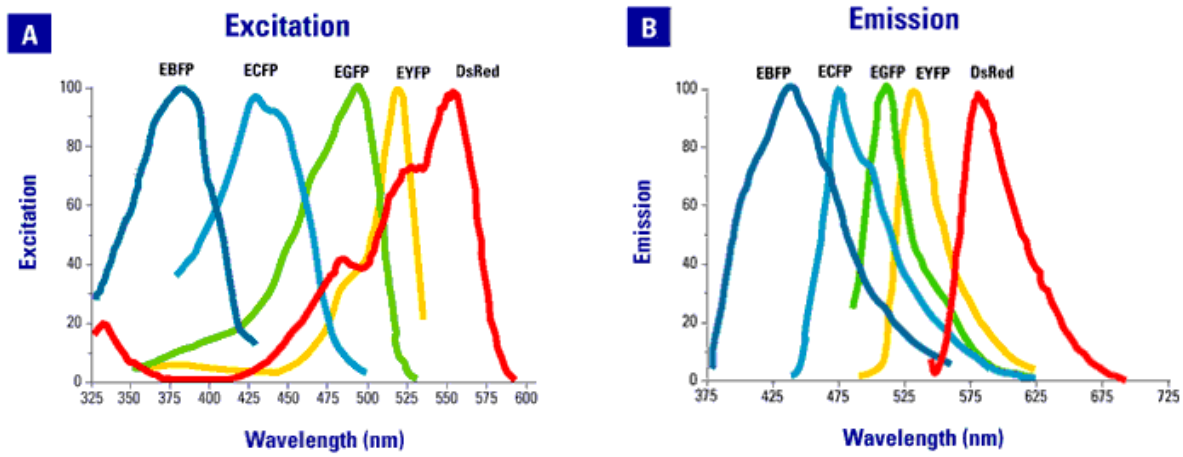

Fig. 6: Excitation (A) and emission (B) spectra of different GFP mutants.

Another green fluorescent protein, found in the sea pansy *Renilla*, has been biochemically characterised [62], while the cDNA has not been isolated yet. Although the chromophore of *Renilla* is similar to that of *Aequorea*, some of their biochemical properties differ. *Renilla* GFP has a much higher extinction coefficient, is an obligate dimer and is more resistant to pH-induced conformational changes, which could make it useful for some cell physiology studies.

Nowadays the most frequent application of the GFPs is to use them as a tag. In fact, fusing in frame the GFP cDNA to a cDNA coding for a protein of interest, it is possible to examine the function and fate of the resulting chimera in living cells. Moreover, chimeras with different spectral properties can be employed for visualising simultaneously two proteins of interest (e.g. two isoforms of a signalling molecule) or the morphology and spatial relationship between two intracellular compartments. The GFPs can also be used as a tool for analysing transfection efficiency or as sensors for physiological parameters. This approach stems from an interesting phenomenon, called fluorescence resonance energy transfer (FRET), occurring between two GFPs with different colours. FRET may occur only if the fluorescence emission spectrum of the “donor” GFP overlaps with the excitation spectrum of the “acceptor” GFP and if the two fluorophores are located within few nanometers in a favourable orientation.

As for aequorin I briefly describe the GFP constructs that were present in our laboratory and that I used for the thesis:

- ***mitochondrial GFP probe***: the previously employed mitochondrial presequence derived from subunit VIII of cytochrome c oxidase (encoding the 25 aa-long presequence and 6 aa of the mature polypeptide) to construct a mitochondrially targeted aequorin

chimera [45] was fused in frame with the GFP, in order to construct mitochondrially-targeted GFP (mtGFP) [63]. When expressed in mammalian cells, the chimeras show a typical mitochondrial distribution.

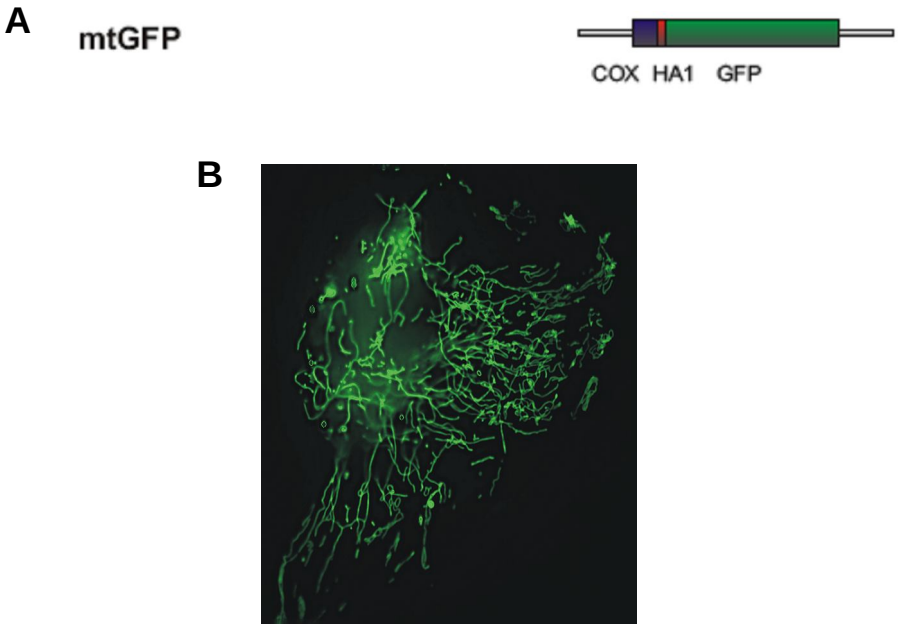

Fig. 7: The mitochondria-targeted GFP construct. The mitochondrial presequence of COX VIII protein was fused in frame with GFP at N-terminus (A). As aspected, this chimera shows a typical mitochondrial staining (B).

2.3 Experimental set-up: collecting and analysing the GFP images

The fluorophore of GFP is formed by the cyclization of three amino-acid residues of the primary sequence. This process directly follows, with few constraints (a relatively brief time lag), the synthesis of the protein, and thus GFP proved brightly fluorescent when expressed in a wide variety of cell types (mammalian cells, plants, fungi, bacteria, etc.) and intracellular locations (cytoplasm and virtually every organelle). Thus, also in our experiments the various GFP chimeras are transfected with the appropriate procedure (calcium phosphate, liposomes or particle gun, depending on the cell type), and directly visualised in living cells after allowing sufficient time for expression and chromophore formation (usually 24-36 hours). For this purpose, the coverslip with the transfected cells is fitted at the base of a thermostatted chamber, which is placed on the microscope stage.

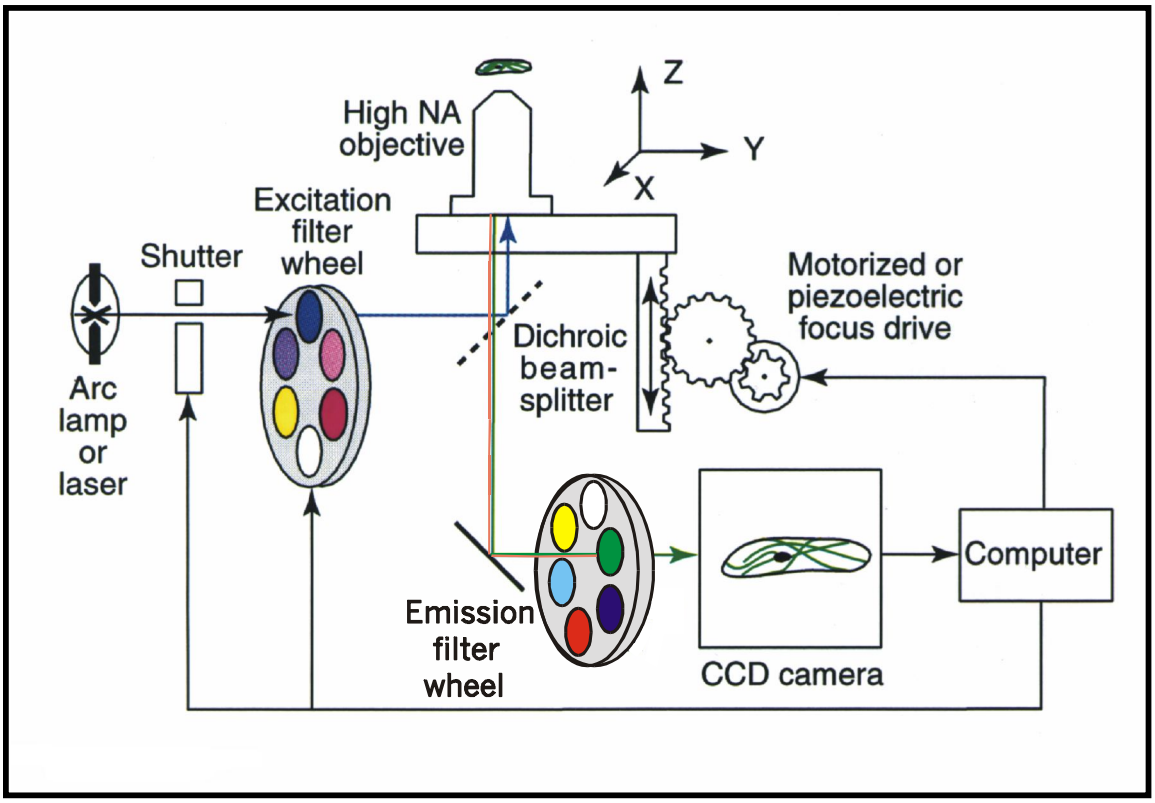

Fig. 8: Microscope setting. A digital imaging system, built on an epifluorescence microscope, is equipped with filter-wheels placed on the excitation and emission light paths, a piezoelectric motor and a CCD camera. The system is operated by a software that also permits to analyse and computationally deblur the images.

Our microscope set up is presented in figure 8. In brief, a traditional wide-field, epifluorescence microscope is equipped with filter-wheels located both in the incoming and in the out-coming light paths (thus allowing to rapidly alternate excitation and/or emission wavelength) and a piezoelectric transducer (or motor drive) for rapid focussing in the z plane. The fluorescence image is collected by a back-illuminated and cooled (-40°C), charge coupled device (CCD) camera having high quantum efficiency (>70% at 500nm) and low noise (<10e^- RMS at 1MHz) characteristics, and the image is stored as a digital file using the Metamorph/Metafluor program (Universal Imaging). This allows the direct monitoring of fluorescence intensity, important for some applications (e.g. the monitoring of FRET, or the pH measurements using the pH-sensitive GFP mutants, a topic that for reasons of brevity will not be discussed in this thesis).

A high-resolution, 3-D reconstruction of the distribution of a GFP chimera can be obtained with the technique of digital image restoration, also called deconvolution or deblurring. [64].

In situations where there may be significant intracellular motion of the GFP chimera, two approaches can be used to decrease the time for image acquisition. The area of the cell (i.e. the number of pixels in each optical section) imaged can be reduced, thus decreasing the time to transfer the image data to computer storage. A high-resolution image restoration of a limited volume of a cell has been obtained using a few as 5 to 7 optical sections [65], minimising the total acquisition time.

A high-speed version of this microscopy has been developed [66] that can acquire an entire through-focus image series of a GFP labelled cell in less than 1 second. This microscope system can be used to follow spatial and temporal intracellular dynamics (e.g. motor-protein based transport, signal transduction) too rapid for conventional fluorescence microscopy [66]. Conversely, if only the time course rather than the 3-D distribution of a fast process (e.g. Ca^{2+} signalling) needs to be assessed, single fluorescent images of the microscope field of interest can be acquired every 10-20 ms with no further image processing [67].

Finally, the filter-wheels allow the alternate imaging of two different fluorophores at different excitation and emission wavelengths, and thus the simultaneous visualisation of two different proteins of interest in the same cell, or the measurement of donor and acceptor fluorescence in FRET applications. When compared to laser scanning confocal microscopy, digital imaging is characterised by higher flexibility in the selection of excitation wavelengths, lower illumination intensity (thus reducing photobleaching and photodamage) and lower cost. Conversely, its disadvantages are the need for time-consuming off-line image processing and the unsuitability for the analysis of thick specimen (e. g. tissue slices).

2.4 Luciferase

Firefly luciferase was cloned in the late 1980s [68], and versions of the gene, optimised for thermostability and expression in mammalian cells, were generated. The enzyme uses an oxidisable substrate, termed luciferin, which is converted to an AMP adduct before final oxidation with molecular oxidation and the release of a photon of light (Fig. 9).

cDNA encoding luciferase can readily be introduced into most mammalian (and other) cell types by conventional transfection techniques. Whilst originally also intended for detection of the total luciferase amount in cell homogenates, luciferase light output can

also be readily measured from living cells, after the addition of the (reasonably cell-permeant) cofactor, luciferin. Under most conditions, O_2, and cofactors other than ATP, are not limiting. Further, it can be calculated that the contribution of ATP consumption by luciferase represents only a tiny fraction of total cellular ATP turnover (<0.1 %, even at relatively high levels of luciferase expression, e.g. 1 x 10^6 molecules/cell) and thus non-perturbing for normal cellular ATP homeostasis.

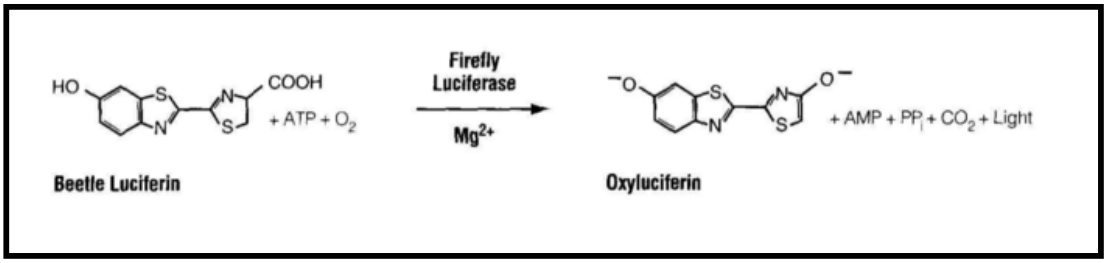

Fig. 9: The ATP-dependent luminescence reaction of Luciferase

The technology to the detection of changes in free intracellular ATP concentration require constantly high levels of luciferase expressed from strong viral promoters (e.g. the cytomegalovirus immediate early gene promoter, CMV-IE), so that small fluctuations in free ATP concentration can be monitored in cell populations, by detection of luciferase luminescence is possible with the photon-counting tube apparatus, as described above for the detection of aequorin luminescence.

Luciferase displays a K_m for ATP close to 1 mM when assayed in cell homogenates under approximate *in vivo* conditions of pH and physiological ionic strength [69] (compared to the low micromolar range under optimal in vitro conditions).

Confirming these values in living cells is complicated due to the distinct kinetics of the enzyme in the living cell ("glow" *versus* "flash" kinetics"). Although the basis for this difference is not fully understood, it may reflect a lack of the accumulation of inhibitory end product (oxyluciferin) in the cell, or a decreased sensitivity to this (or another inhibitor) mediated by other cellular cofactors (notably CoA). Whatever the mechanism, this makes monitoring [ATP] constantly in the living cell relatively straightforward, given sensitive photon detection equipment.

In order to measure [ATP] exclusively into the mitochondrial compartment ($[ATP]_{mt}$), our groups generated a mitochondrial-targeted luciferase, using the same strategies employed for creation of mtAEQ and mtGFP chimera (Fig. 10) [70]. Moreover, this paper

shown how stimulation with agonists evoking cytosolic and mitochondrial Ca^{2+} signals caused increases in $[ATP]_{mt}$ and $[ATP]_{cyt}$ [70].

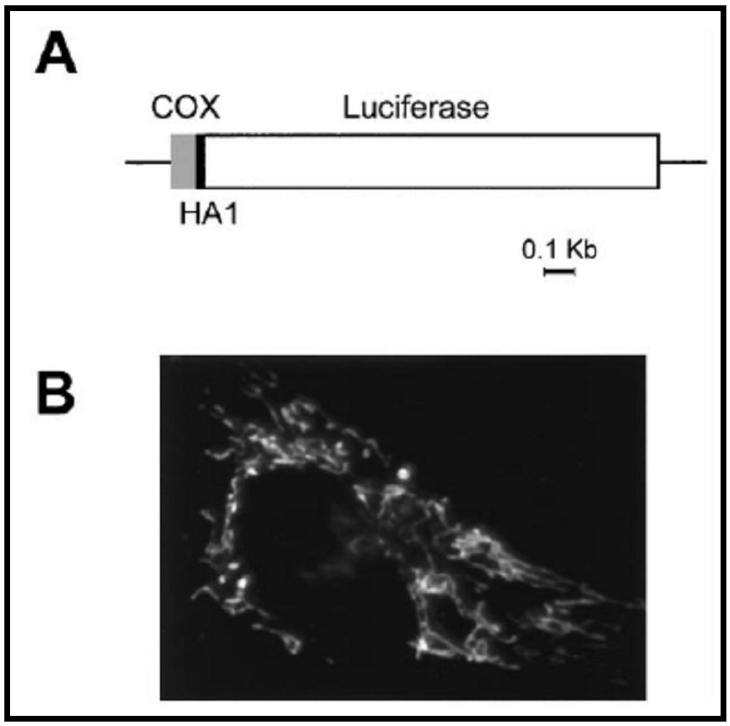

Fig. 10: Map and correct localization of mtLUC construct. A) Schematic map of the chimeric mitochondrial luciferase. Lines and bars indicate the noncoding and coding regions [gray, cytochrome *c* oxidase subunit VIII (COX8); black, HA1; white, luciferase], respectively. (B) Immunofluorescence image of HeLa cells transiently transfected with mtLuc and stained with the anti-HA1 mAb (figure from [70]).

3. Protein Kinase C β and Prolyl Isomerase Pin1 Regulate Mitochondrial Effects of the Life-Span Determinant p66Shc

3.1 Introduction

Many agents which induce apoptosis are either oxidants or stimulators of cellular oxidative metabolism. Conversely, many inhibitors of apoptosis have antioxidant activities or enhance cellular antioxidant defences. Mammalian cells exist in a state of oxidative siege in which survival requires an appropriate balance of oxidants and antioxidants, suggesting that eukaryotic cells may benefit from this perilous existence by invoking oxidative stress as a common mediator of apoptosis.

Apoptosis, the process that allows multicellular organisms to eliminate unnecessary, dangerous or damaged cells without evoking inflammation or tissue damage, occurs in both physiological and pathological contexts. Specific biochemical steps in the apoptotic pathway are inhibited by viruses and in tumors. On the other hand, excess apoptosis in non-proliferating cells has been proposed to be the basis of a number of degenerative disorders, as well as in progressive loss of organ function during ageing. The understanding of the control mechanisms of apoptosis is thus a major goal for the understanding of these pathophysiological events, and the development of novel therapeutic approaches.

Recently the mitochondrion has emerged as a key decoding station of the apoptotic process. Indeed, a large body of experimental evidence has unambiguously revealed that mitochondria trigger cell death, in addition to the well-established function of producing most of cellular ATP. Various apoptotic stimuli cause the release of specific mitochondrial proteins into the cytoplasm (including an essential component of the electron transfer chain, cytochrome *c*). Their assembly with cytosolic proteins forms a complex (the "apoptosome"), that recruits and activates effector caspases, which in turn trigger apoptotic death. The molecular mechanism of this release is still controversial, but may require the activity of a large-conductance channel, known as the permeability transition pore, PTP. Its opening induces the swelling of mitochondria, and this large-scale alteration of organelle morphology (with perturbation or rupture of the outer membrane) may allow the release of pro-apoptotic components into the cytosol.

There is no doubt that cell death belongs to the numerous cell functions on which Ca^{2+} exerts a complex regulatory role. As to the site of action of the "apoptotic" Ca^{2+} signal,

mitochondria again emerge as a critical site. Indeed, treatment with apoptotic stimuli, such as ceramide, causes a release of Ca^{2+} from the ER and induces dramatic changes of mitochondrial morphology [33]. If Ca^{2+} changes are prevented (e.g. by loading an intracellular Ca^{2+} buffer), mitochondrial morphology is preserved and the cells are protected from apoptosis. Much remains to be understood on the additional signals that converge on mitochondria and switch their function into apoptotic inducers. As much as Ca^{2+} appears to be involved, there is no doubt that coincident detection of other "pro-apoptotic" conditions needs to occur. Indeed, mitochondria can handle in physiological conditions large Ca^{2+} loads (e.g. in cardiac myocytes significant amounts of Ca^{2+} are accumulated at every heartbeat), with no deleterious effects. As to the additional "apoptotic signal", the most important is considered to be oxidative stress. However, on this topic the information is very scant, as its real significance in apoptosis and the mechanism of action are still largely unknown.

In 1999, the group of Pelicci and co-workers published a paper that became a crucial point in studies on the oxidative stress [71]. They proposed that mammalian life span can be controlled by p66Shc protein due to regulation of cellular response to oxidative stress. Ablation of the p66Shc gene causes life-span prolongation with no pathological consequence. In fact, mice lacking p66Shc gene had enhanced resistance to oxidative stress induced by paraquat (a potent inducer of oxidative stress *in vivo*).

3.1.1 p66Shc, an adaptor protein

The p66Shc protein is an alternatively spliced isoform of the growth factor adapter. Recently, three proteins from ShcA family have been identified (p66Shc, p52Shc and p46Shc). Each of them contains three functionally identical domains: the carboxy terminal Src homology 2 (SH2) domain, the central proline-rich domain (CH1), and the N-terminal phosphotyrosine-binding domain (PTB). PTB domain can bind to phospholipids and phosphotyrosine of the other proteins (Fig. 11).

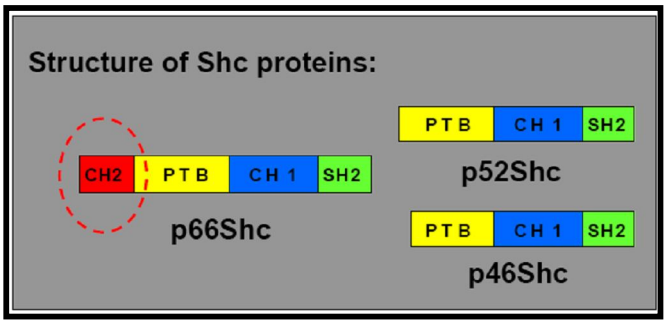

Fig. 11: Structure of Shc proteins.

P66Shc protein differs from p46Shc and p52Shc by the presence of an additional N-terminal proline-rich domain (CH2) with the serine phosphorylation site, Ser36. Phosphorylation of this residue plays an important role in the cellular response to the oxidative stress. Recently, it has been demonstrated that, in response to UV or H_2O_2 treatment, p66Shc is phosphorylated mainly at serine 36 in the N-terminal CH2 domain [71]. Also a p66Shc transfection with mutated Ser36 failed to restore apoptosis sensitivity in p66Shc lacking cells, what supports the importance of Ser36 in regulation of apoptosis.

The SH2 domain of Shc is important for certain receptor interactions, such as epidermal growth factor (EGF) receptor. Interaction between the SH2 domain and EGF receptor plays an important role in phosphorylation of tyrosines in the CH1 domain of p52Shc and p46Shc [72]. Tyrosine phosphorylation enables them to bind to the adaptor Grb2 protein–activator of Ras protein. Also p66Shc can be tyrosine phosphorylated, but there are no evidences about its ability to activate the Ras signalling pathway.

Further studies of the mechanism of lifespan-promoting activity of p66Shc deficiency, have suggested not only a role in ROS metabolism, but also in apoptosis. Steady-state ROS and p53-induced ROS are both decreased in p66Shc -/- Mouse Embryonic Fibroblasts (MEFs). Possibly as a consequence of this, hydrogen-peroxide-mediated release of cytochrome c is inhibited in p66Shc -/- MEFs, and transfection of p66Shc into these cells rescues the sensitivity. Furthermore, there is a reduction in the amount of oxidation-damaged DNA of p66Shc -/- mice, as well as for mitochondrial DNA [73].

P66Shc appears to sensitively detect oxidative stress, i.e. the pathophysiological condition that has been often associated to cellular ageing, and is known to sensitize to a number of apoptotic challenges. P66Shc thus appears as a very promising link between phenomenological observations of the ageing process and the identification of the molecular mechanism responsible for the cellular changes. This is a fundamental step as it highlights potential targets for pharmacological intervention.

In this scenario, the portion of p66Shc located into mitochondria seems to be fundamental for its role in oxidative stress. In fact, a fraction of p66Shc localizes to mitochondria [74, 75], where it binds to cytochrome *c* and acts as oxidoreductase, generating reactive oxygen species (ROS) and leading to organelle dysfunction and cell death [76] (Fig. 12). The route leading to p66Shc activation is still unclear.

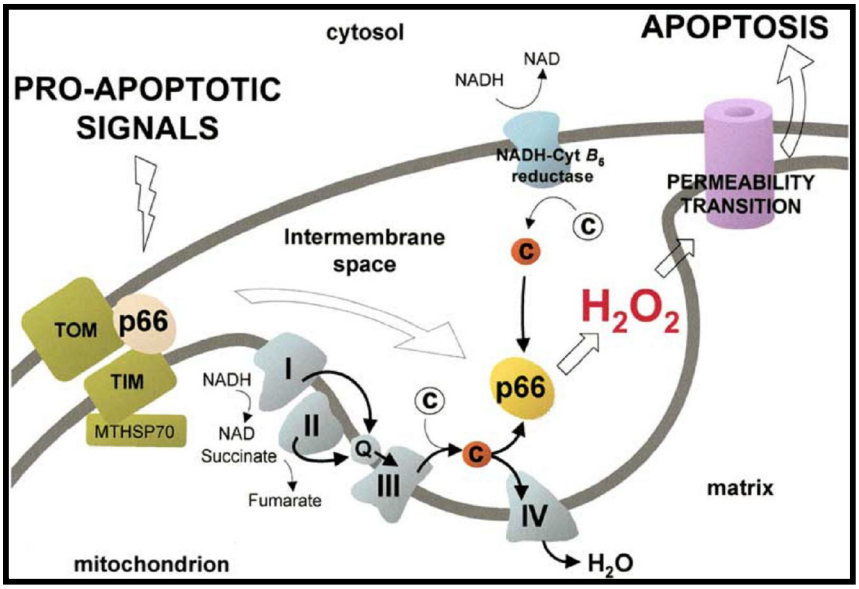

Fig. 12: Model of p66Shc redox activity during mitochondrial apoptosis. Proapoptotic signals induce release of p66Shc from a putative inhibitory complex. Active p66Shc then oxidizes reduced cyt c (red) and catalyzes the reduction of O_2 to H_2O_2. PTP opening by H_2O_2 then leads to swelling and apoptosis (figure from [76]).

In this work, we address this task, focusing on the Ca^{2+}-mediated signals in mitochondria. The rationale for this strategy stems from a number of experimental observations. Mitochondria receive, under stimulation by physiological agonists or toxic agents, Ca^{2+}-mediated inputs [34, 77, 78]. These Ca^{2+} signals are decoded within mitochondria into effects as diverse as stimulation of aerobic metabolism and alterations of organelle structure leading to release of caspase cofactors into the cytoplasm [79]. Recent works showed that the responsiveness of mitochondria to Ca^{2+} signals can be tuned by the cross-talk with other signalling pathways and the activation of regulatory proteins, such as kinases. Specifically, we could show that some PKC isoforms (i.e. the components of a wide molecular repertoire of kinases differing for biochemical properties and activation mechanisms) specifically affect mitochondrial Ca^{2+} responses to agonists (by reducing them, such as PKCβ, or enhancing them, such as PKCζ) [80]. Interestingly, PKCs were proposed to be activated directly in conditions of oxidative stress [81].

3.2 Results

3.2.1 Effect of oxidative stress and the aging protein p66Shc on the mitochondrial Ca^{2+} homeostasis

We used aequorin to monitor cellular concentrations of Ca^{2+}, a green fluorescent protein with mitochondrial presequence (mtGFP) to monitor organelle structure (well explained in section 2), and other molecular tools to clarify the signalling route linking the oxidative challenge to the activation of p66Shc proapoptotic effect within mitochondria in mouse embryonic fibroblasts (MEFs).

Using mtAEQ, we investigated organelle Ca^{2+} responses to adenosine triphosphate (ATP), an extracellular agonist that causes the release of Ca^{2+} from the endoplasmic reticulum. P66Shc −/− and wild-type MEFs showed similar responses of mitochondrial calcium ($[Ca^{2+}]_{mt}$) to ATP, both in amplitude and in kinetics (Fig. 13, A and B). This reflects a close similarity in the global Ca^{2+} signaling patterns. Indeed, the monitoring of concentration of free cytosolic Ca^{2+} ($[Ca^{2+}]_{cyt}$) showed that the $[Ca^{2+}]_{cyt}$ rises evoked by ATP in p66Shc −/− and wild-type MEFs were virtually superimposable (Fig. 13, A and B, insets).

To investigate the effect of an oxidative challenge, we treated cells for 30 minutes before the application of ATP with various concentrations of H_2O_2. Reduction of mitochondrial Ca^{2+} responses and fragmentation of the threedimensional mitochondrial network [33] was observed in wild-type MEFs (Fig. 13, A and a) several hours before signs of apoptosis (cell shrinkage and nuclear condensation, for example) were detected, whereas minor changes in the Ca^{2+} response and morphology were detected in p66Shc −/− MEFs (Fig. 13, B and b). This alteration in Ca^{2+} response was characteristically mitochondrial, because no difference in the ATP-dependent $[Ca^{2+}]_{cyt}$ rise was detected between p66Shc −/− and wild-type H_2O_2-treated MEFs (Fig. 13, A and B, insets). The reintroduction of p66Shc reestablished sensitivity to H_2O_2 in p66Shc −/− MEFs (Fig. 13, C and c).

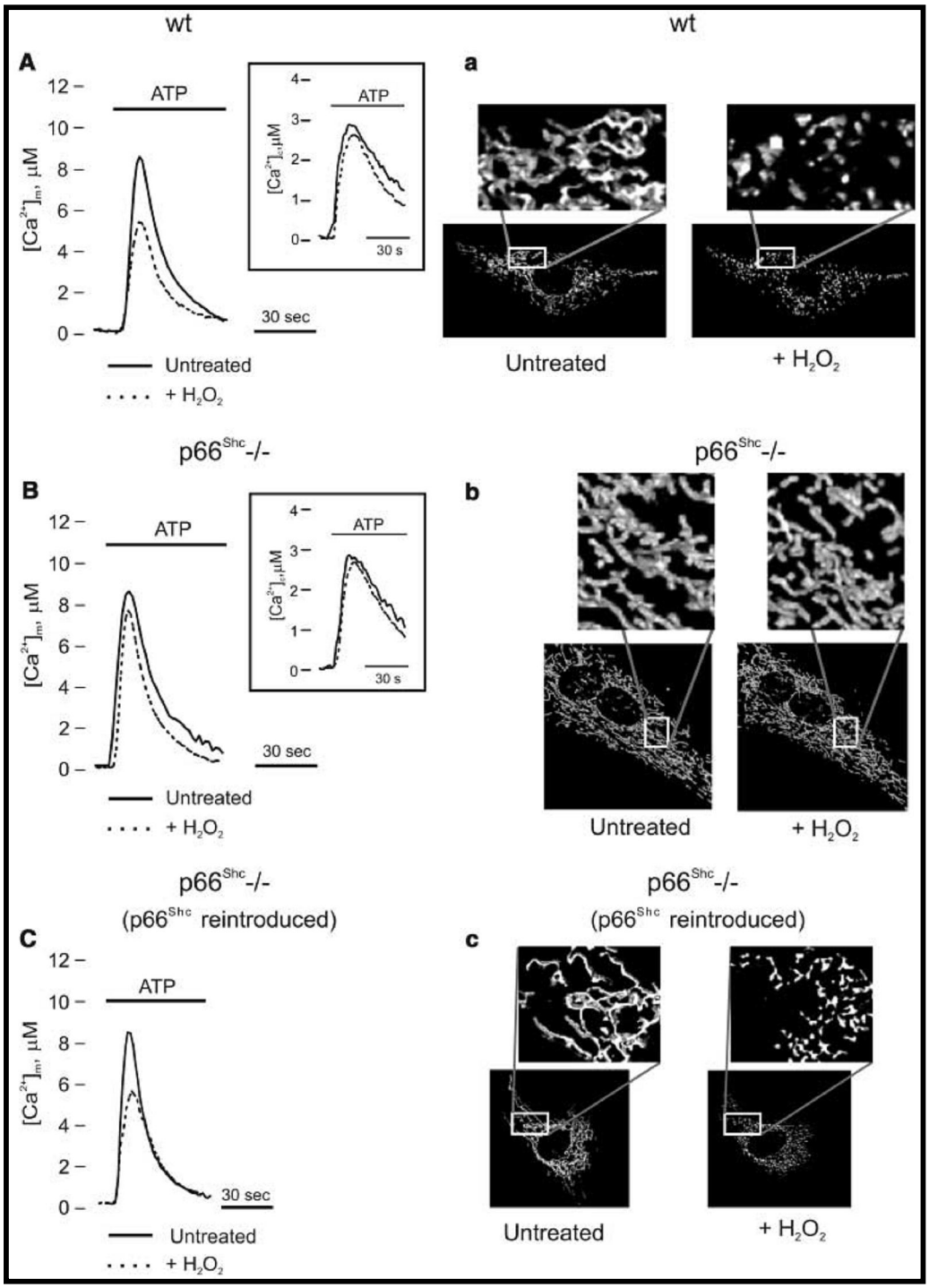

Fig. 13*: *Mitochondrial morphology and Ca^{2+} responses in p66Shc MEFs during oxidative stress.
Mitochondrial and cytosolic (inset) Ca^{2+} homeostasis in wild-type (wt) (A) and p66Shc −/− (B) MEFs. wt: $[Ca^{2+}]_{mt}$) peak, 8.64 ± 0.32 mM; $[Ca^{2+}]_{cyt}$) peak, 2.90 ± 0.11 mM. p66Shc −/−: $[Ca^{2+}]_{mt}$ peak, 8.71 ± 0.37 mM; $[Ca^{2+}]_{cyt}$ peak, 2.91 ± 0.15 mM. The dotted traces show the effect of treatment with H_2O_2 (1 mM, 30 min.) on the ATP-dependent responses. wt: $[Ca^{2+}]_{mt}$ peak, 5.84 ± 0.28 mM; $[Ca^{2+}]_{cyt}$ peak, 2.60 ± 0.07 mM. p66Shc −/−: $[Ca^{2+}]_{mt}$ peak, 7.87 ± 0.33 mM; $[Ca^{2+}]_{cyt}$ peak, 2.7 ± 0.09 mM. (a and b) Analysis of mitochondrial structure in cells treated with or without H_2O_2 (1 mM, 30 min). (C and c) Reintroduced p66Shc reestablishes the $[Ca^{2+}]_{mt}$ and morphology sensitivity to H_2O_2 in p66Shc −/− MEFs. $[Ca^{2+}]_{mt}$ peak, 8.69 ± 0.51 mM; after H_2O_2, $[Ca^{2+}]_{mt}$ peak, 5.76 ± 0.44 mM, $P < 0.01$. For all the experiments presented $n \geq 15$.

Production of ROS by p66Shc [76] influences the opening of the mitochondrial permeability transition pore (PTP) [82]. We thus investigated whether the Ca^{2+} and morphology changes triggered by H_2O_2 could be prevented by the PTP blocker cyclosporine A (CsA). In CsA-treated wild-type MEFs, the rise in $[Ca^{2+}]_{mt}$ evoked by ATP stimulation in the presence of H_2O_2 was largely restored (Fig. 14 A) and the integrity of the mitochondrial network was preserved (Fig. 14 a). On the contrary, no effect of CsA on p66Shc −/− (Fig. 14 A, inset). Mitochondrial Ca^{2+} responses and morphology were not modified by H_2O_2 application to p66Shc −/− MEFs in which either the p66ShcE132Q-E133Q mutant (p66Shcqq), incapable of binding cytochrome c [76] (Fig. 15, A and a), or the p66ShcS36A mutant [71] (Fig. 15, B and b) had been reintroduced, indicating that both the oxidoreductase activity of p66Shc and the phosphorylation of Ser36 are essential for the H_2O_2-induced proapoptotic changes.

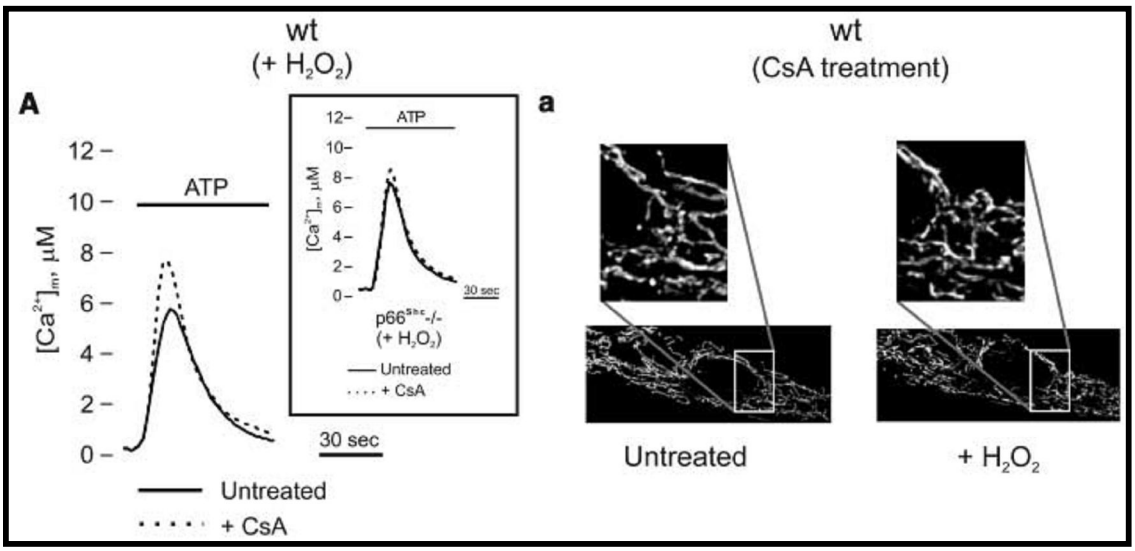

Fig. 14: Involvement of PTP in mitochondrial p66Shc action. Effect of treatment with CsA (4 mM, 10 min.) on H_2O_2-dependent reduction of $[Ca^{2+}]_{mt}$ responses in wt MEFs. $[Ca^{2+}]_{mt}$ peak, 5.84 ± 0.28 mM in cells treated only with H_2O_2; 7.58 ± 0.33 mM, $P < 0.01$, in cells pretreated with CsA, then treated with H_2O_2 (A). No effect of CsA on p66Shc −/− cells was detected. $[Ca^{2+}]_{mt}$ peak, 7.87 ± 0.33 mM in cells treated only with H_2O_2; 8.43 ± 0.54 mM in cells pretreated with CsA, then treated with H_2O_2 (inset). Morphology of H_2O_2-treated, CsA-pretreated cells (a).

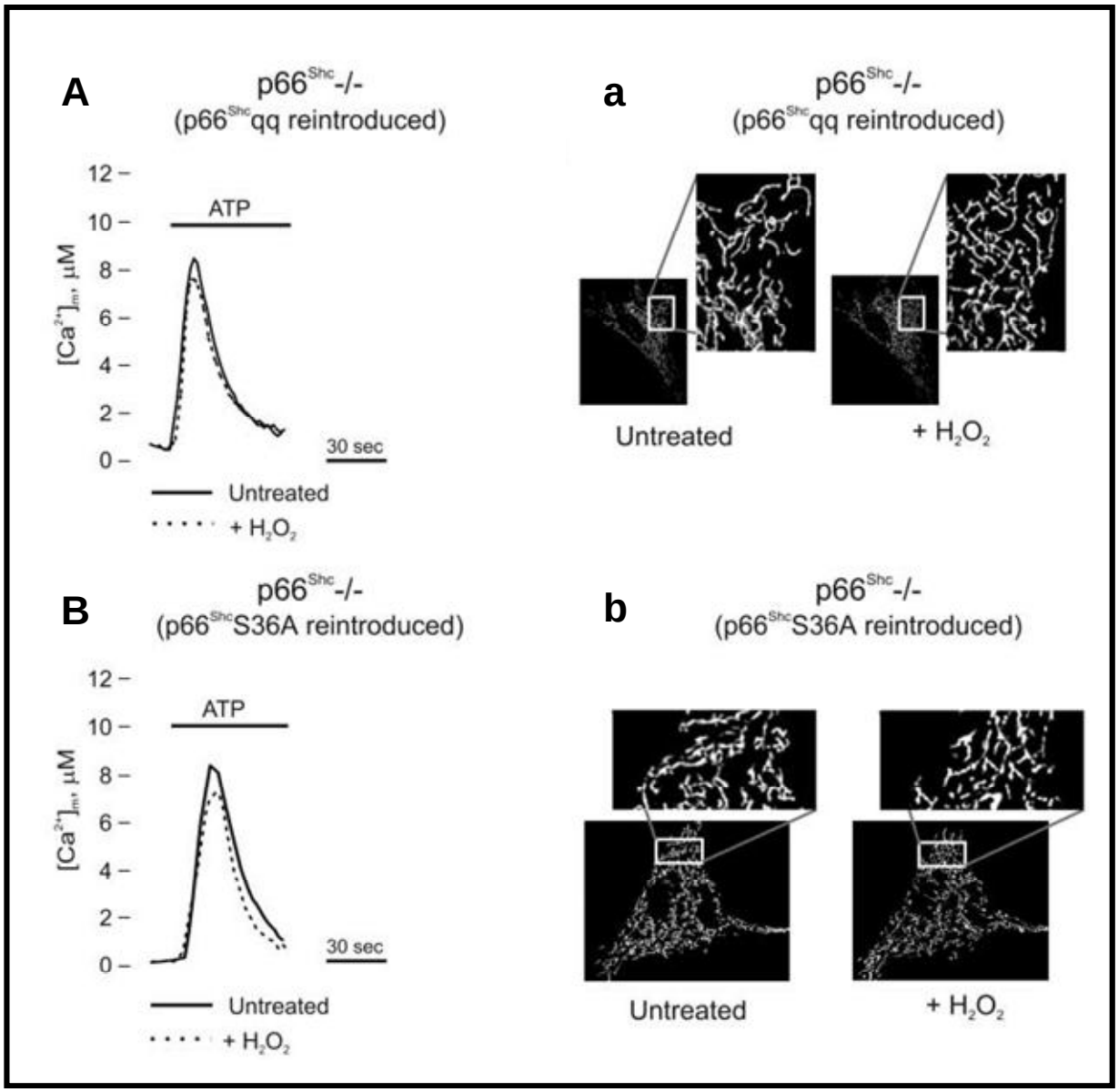

Fig.15: Involvement of p66Shc binding to cytochrome c, and p66Shc phosphorylation in mitochondrial p66Shc action. Failure of the p66Shcqq mutant ($[Ca^{2+}]_{mt}$ peak: control, 8.35 ± 0.71 mM; H_2O_2, 7.76 ± 0.35 mM) (A) or the p66ShcS36A mutant ($[Ca^{2+}]_{mt}$ peak control, 8.58 ± 0.61 mM; H_2O_2, 7.74 ± 0.64 mM) (B) to reestablish mitochondrial $[Ca^{2+}]$ sensitivity to H_2O_2 in p66Shc −/− MEFs. Morphology of H_2O_2-treated cells expressing the p66Shcqq (a) or p66ShcS36A mutants (b).

3.2.2 Effects of PKC β-dependent phosphorylation of p66Shc

We demonstrate that phosphorylation of p66Shc on Ser36 is fundamental in order to exert its activity on mitochondrial Ca^{2+} uptake. So we investigate about the putative effector of this phosphorylation.

Overexpression of the PKC isoform β reduces transient changes in $[Ca^{2+}]_{mt}$ in HeLa [80], PKC β is expressed in MEF cells (Fig. 16 A) and phosphorylated p66Shc was detected after treatment of cells with H_2O_2 or with 12-Otetradecanoylphorbol 13-acetate (TPA), a PKC activator (Fig. 16 C). After application of H_2O_2, membrane staining of GFP-tagged PKC β was detected by fluorescence microscopy (fig. 16 B), showing its activation [81]. Hispidin, a specific blocker of the PKC β isoform [83], inhibited p66Shc phosphorylation in both conditions (Fig. 16 C).

Overexpression of PKC β mimicked the activation of the endogenous kinase by oxidative challenges, causing a reduction in $[Ca^{2+}]_{mt}$ responses in wild-type MEFs (in which the putative downstream effector is present) but not in p66Shc −/− MEFs (Fig. 17 A). This effect was specific for PKC β. Moreover, when PKC β was inhibited pharmacologically with hispidin (Fig. 17 B) or its abundancewas decreased with RNA interference (RNAi) (Fig. 17 C), the $[Ca^{2+}]_{mt}$ peak was minimally affected by the application of H_2O_2. Similarly, hispidin treatment preserved mitochondrial morphology (Fig. 17 D).

We verified whether PKC β inhibition reduced the apoptotic efficacy of H_2O_2 treatment. We measured cell viability 8 hours after the addition of 1 mM H_2O_2 by counting surviving cells on the microscopy stage. Hispidin caused no change in cell viability in wild-type cells but increased the number of cells surviving oxidative stress (29% ± 2.1 in H_2O_2-treated cells versus 60% ± 4.75 in hispidin pretreated cells, expressed as a percentage of the cells counted on a coverslip not exposed to H_2O_2) (Fig. 18 A). To partially mimic an “aging” event, we analyzed mitochondrial Ca^{2+} responses in MEFs maintained in culture for 20 passages. In wild-type MEFs, the $[Ca^{2+}]_{mt}$ responses gradually decreased with time in culture, whereas no alteration was observed in p66Shc −/− MEFs or in wild-type MEFs if the culture medium was supplemented with hispidin (Fig. 18 B). We also analyzed the effect of PKC β on other mitochondrial parameters: mitochondrial membrane potential ($\Delta\Psi$) and production of ROS. PKC β activation by TPA caused a gradual reduction in $\Delta\Psi$ in wild-type but not in p66Shc−/− MEFs (Fig. 18 C). An increase in ROS production was observed shortly after infection of cells with an adenoviral vector driving PKC β expression: dihydroethidium fluorescence intensity (arbitrary units) 17.70 ± 1.2 versus 14.97 ± 1.3 in

nontransduced cells, supporting the view that PKC β triggers the oxidoreductase activity of p66Shc

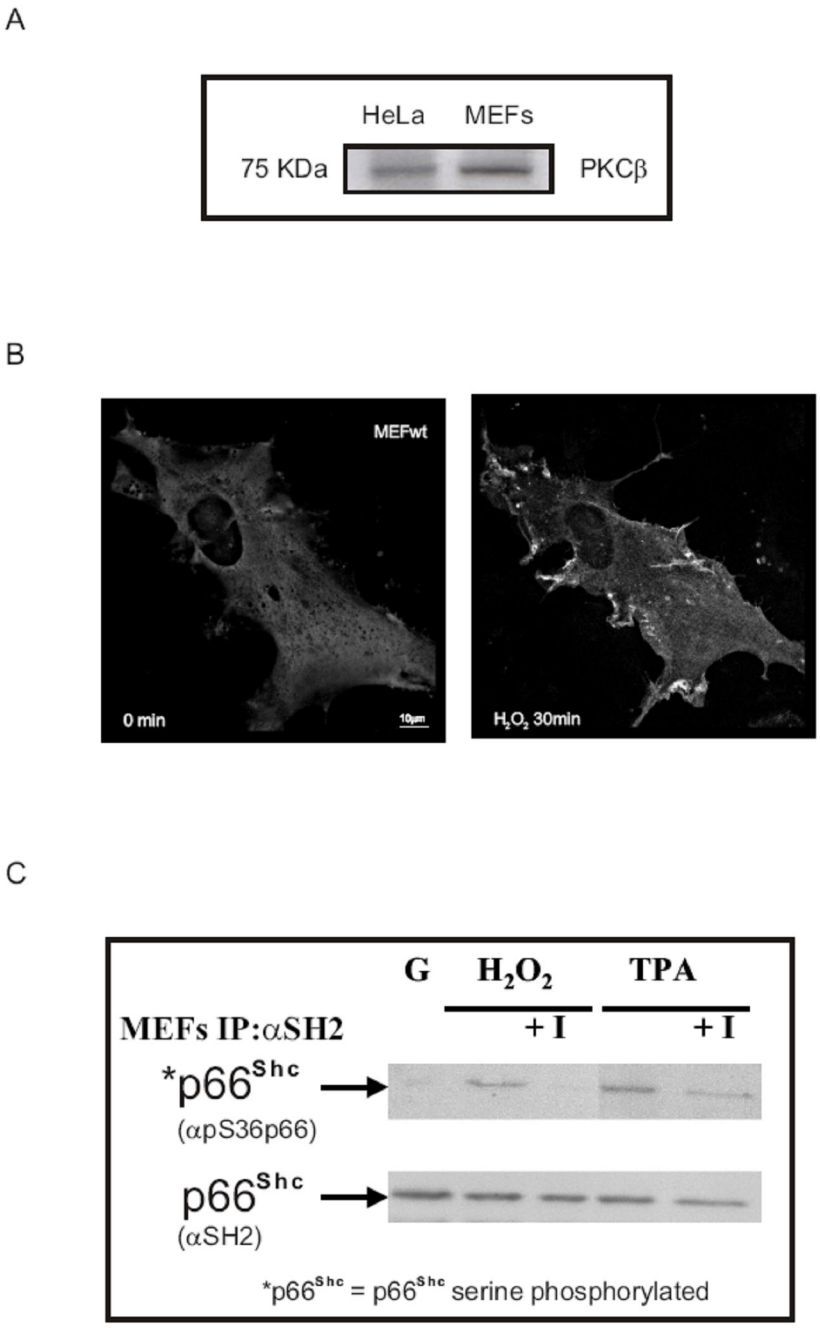

Fig. 16: Effects of PKC on p66^{Shc}. Expression of PKC β protein in HeLa and MEFs cells was visualized by Western blot analysis (A). Fluorescence image of PKC β̃-GFP before and after an oxidative challenge (H_2O_2 1mM, 30 min.) (B). Western blotting of control MEFs treated with H_2O_2 (500 μM, 10 minutes) or TPA (100ng/ml, 10 min.) using antibodies revealing phosphorylated (αpS36p66Shc) or non- phosphorylated (αSH2) p66Shc. **+ I**, the cells were pre-treated (24 hours) with the PKCβ specific inhibitor hispidin (5 μM) (C).

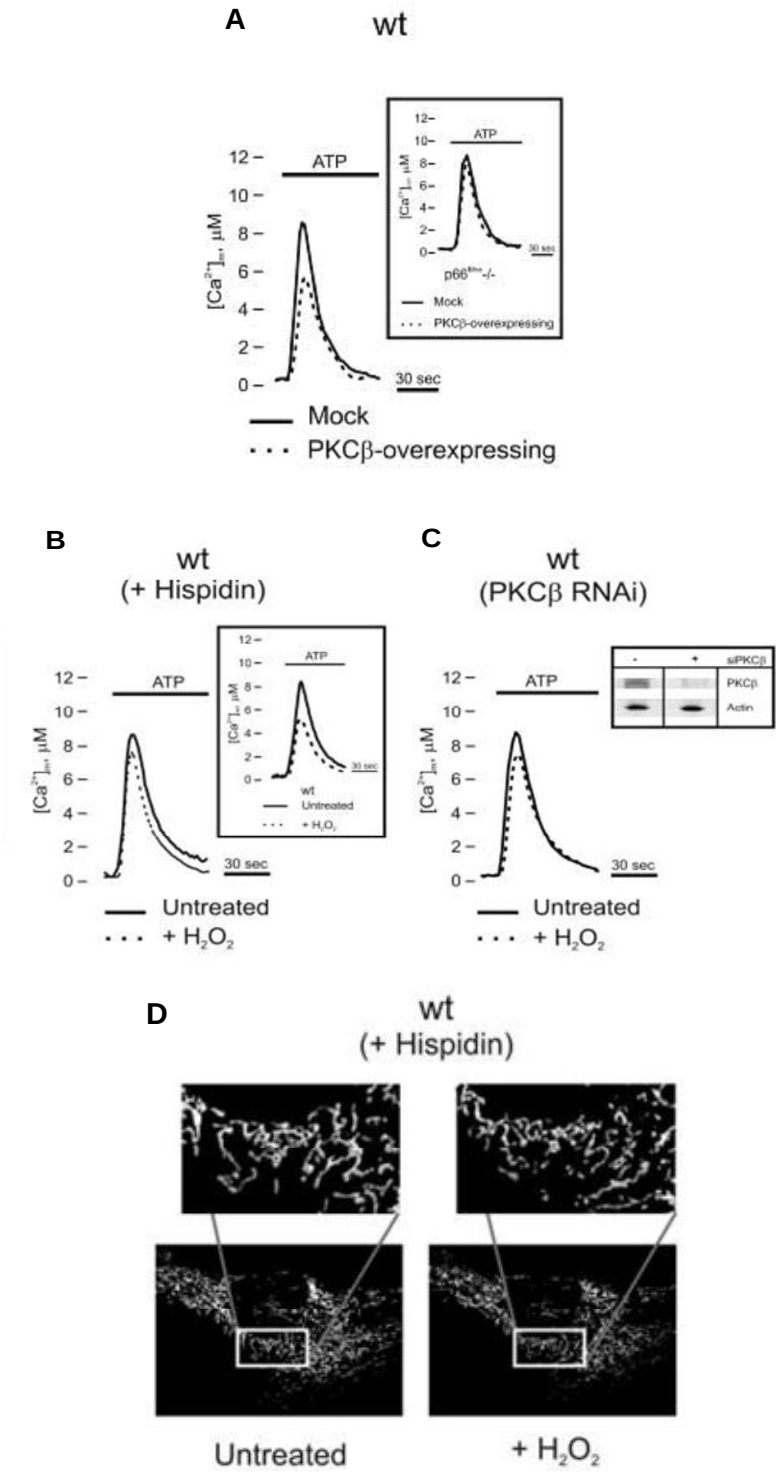

Fig. 17: Effects of PKC β-dependent phosphorylation of p66Shc. (A) Effect of PKC β overexpression on $[Ca^{2+}]_{mt}$ responses in wt ($[Ca^{2+}]_{mt}$ peak, 5.84 ± 0.18 mM versus 8.64 ± 0.32 mM in nontransduced cells, P<0.01) and (inset) p66Shc −/− MEFs ($[Ca^{2+}]_{mt}$ peak, 8.33 ± 0.37 mM versus 8.71 ± 0.37 mM in nontransduced cells). (B) Treatment of wt MEFs with hispidin (5 mM, 30 min.) prevents the H_2O_2-dependent reduction of $[Ca^{2+}]_{mt}$ responses ($[Ca^{2+}]_{mt}$ peak, 7.60 ± 0.46 mM versus 8.50 ± 0.43 mM in nontreated cells) and the alteration of mitochondrial structure (D). (C) Effects of depletion of PKC β with RNAi on H_2O_2-dependent reduction of $[Ca^{2+}]_{mt}$ responses ($[Ca^{2+}]_{mt}$ peak, 7.43 ± 0.49 mM versus 8.81 ± 0.56 mM in nontreated cells). Expression of PKC β after silencing is shown in the Western blot (inset).

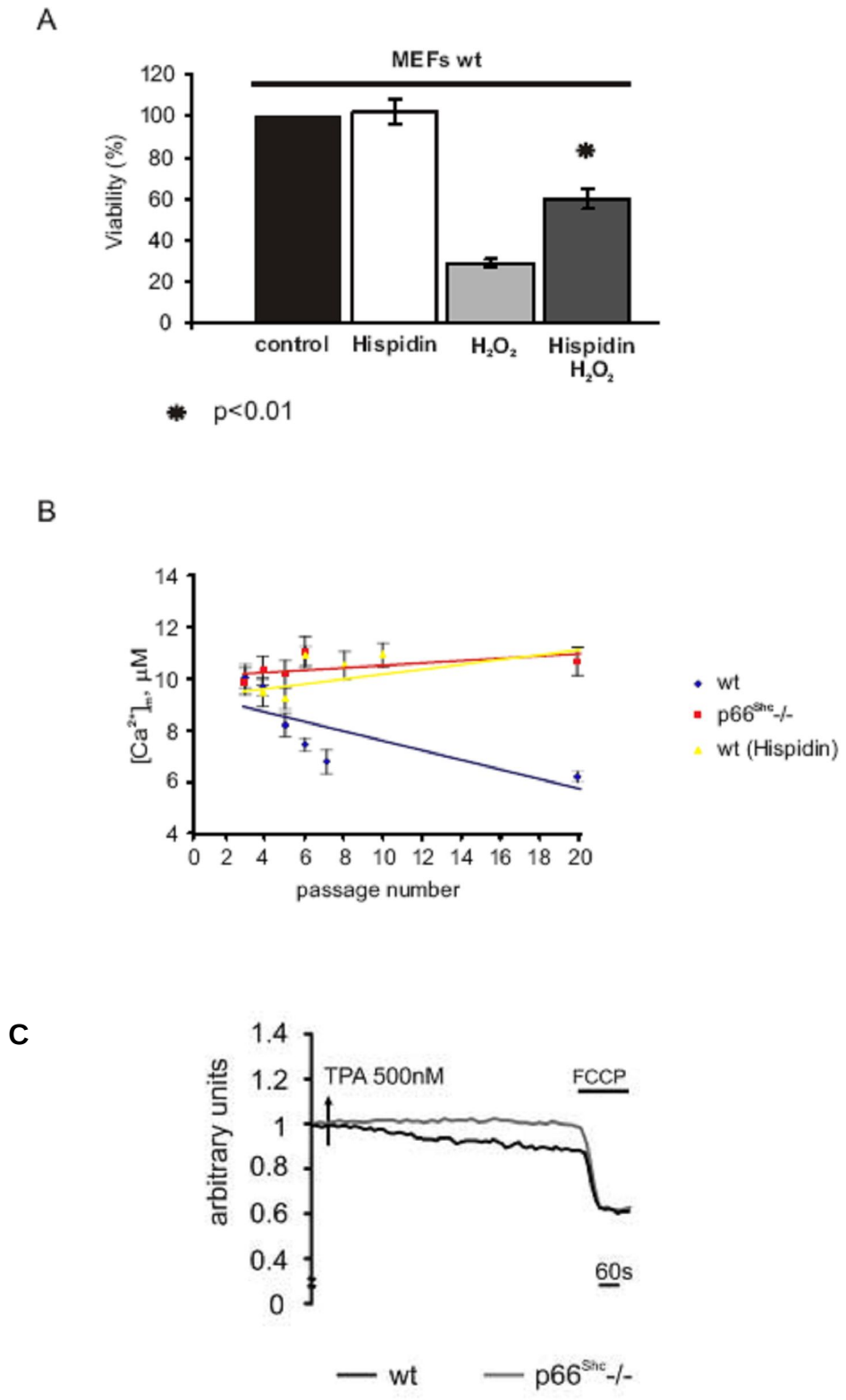

Fig. 18: Effects of hispidin on cell viability. (A) Cell viability after the addition of 1 mM H_2O_2 in wt and hispidin pretreated (5 µM, 2 hours) MEFs (B) Mitochondrial Ca^{2+} responses in wt and p66Shc -/- MEFs maintained in culture. Wt cells cultured in presence of hispidin were also monitored. (C) Kinetics of tetramethyl rhodamine methyl ester (TMRM) fluorescence of wt and p66Shc −/− cells treated with TPA. FCCP (carbonyl cyanide p-trifluoromethoxyphenylhydrazone), an uncoupler of oxidative phosphorylation, completely collapses the $\Delta\Psi$. The traces are representative of single cell responses.

3.2.3 Pin1 induces p66Shc mitochondrial translocation after Ser36 phosphorylation

We suspected that a possible link between PKC-dependent phosphorylation of p66Shc and its mitochondrial oxidoreductase activity was that phosphorylation mediated transfer of p66Shc from the cytosol to mitochondria. The prolyl isomerase Pin1 recognizes and induces cis-trans isomerization of pSer-Pro (or pThr-Pro) bonds, conferring phosphorylation-dependent conformational changes relevant for protein function [84, 85]. Moreover, Pin1 −/− MEFs are impaired in apoptosis after exposure to ultraviolet (UVc) radiation [86]. We identified a putative consensus for Pin1 binding (Ser36/Pro37) in p66Shc. Pulldown experiments with Pin1 linked to glutathione S-transferase (GST-Pin1) showed that Pin1 bound to p66Shc after exposure of cells to UVc radiation that caused phosphorylation of p66Shc. This interaction appeared to be phosphorylation dependent because it was reduced by treatment of cell extracts with calf intestinal phosphatase (CIP). Furthermore, the nonphosphorylatable mutant p66ShcS36A did not show detectable binding to Pin1 (Fig. 19 A).

We investigated the mitochondrial effects of H_2O_2 treatment in Pin1 −/− MEFs. In Pin1 −/− cells, the H_2O_2-dependent reduction of the $[Ca^{2+}]_{mt}$ peak was smaller than that of wild-type MEFs (Fig. 19 B). Overexpression of Pin1 sensitized cells to weaker oxidative stress. When wild-type MEFs were subjected to mild oxidative stress (100 μM H_2O_2 for 15 min. instead of 1 mM for 30 min.), no alteration in the agonist-dependent $[Ca^{2+}]_{mt}$ transient was detected, whereas in Pin1 overexpressing cells, the peak was reduced (Fig. 19 C). In certain substrates, the phosphoserine-proline (phosphoS-P) sites, once isomerized by Pin1, are recognized and dephosphorylated by PP2A [85]. In cells treated with okadaic acid (PP2A inhibitor), the reduction in agonist-dependent $[Ca^{2+}]_{mt}$ responses was markedly smaller (Fig. 19 D) than that in wild-type cells, which might suggest that dephosphorylation by PP2A follows Pin1 recognition and is necessary for the mitochondrial effects of p66Shc.

Finally, we tested the hypothesis that Pin1-dependent isomerization of p66Shc enhances the transfer of the protein to the organelle. We evaluated the mitochondrial pool of p66Shc in wild-type and Pin1 −/− MEFs by subcellular fractionation and immunoblotting (Fig. 19 E). In wild-type cells, oxidative stress increased the amount of p66Shc within mitochondria (~+100%). This effect appeared to depend on PKC activity, because a similar increase was evoked by treatment of cells with TPA, and hispidin inhibited the effects of H_2O_2 treatment. Blots of total homogenate showed only a small increase in the total amount of p66Shc (~+15%) [75], indicating that there was net translocation of p66Shc to the organelle. In Pin1 −/− MEFs, the mitochondrial fraction of p66Shc was smaller, either

at rest or after treatment with H_2O_2 or TPA. TPA had no detectable effect on localization of p66Shc in the Pin1 −/− cells.

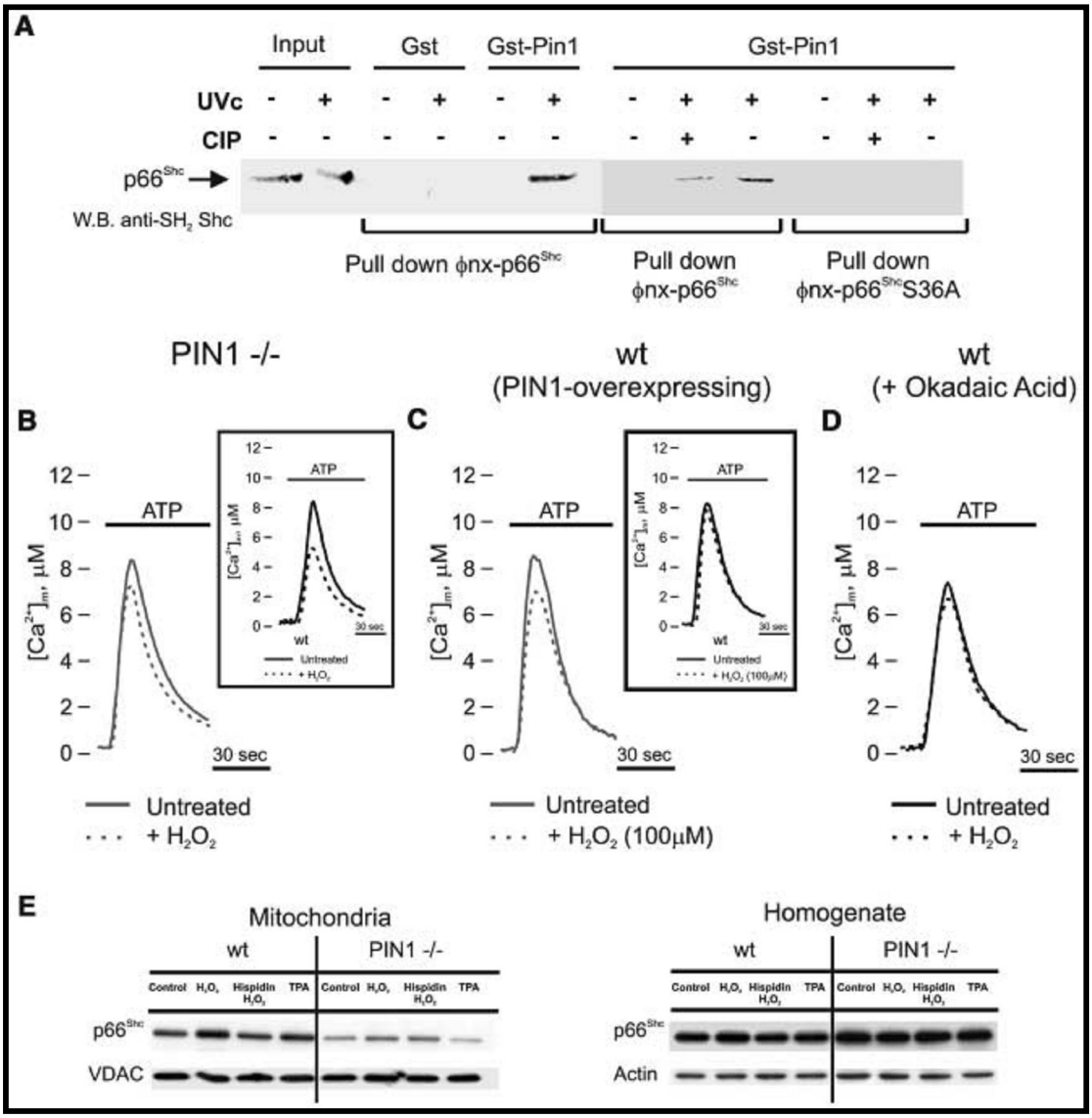

Fig. 19: Pin1 induces p66Shc mitochondrial translocation after Ser36 phosphorylation. (A) Total lysates from Phoenix cells (φnx) transfected with p66Shc or its S36A mutant, UV-irradiated and/or treated with CIP, were subjected to GST or GST-Pin1 pull-down followed by immunoblotting with antibody to Shc. (B) Effect of H_2O_2 on the ATP-dependent $[Ca^{2+}]_{mt}$ responses in Pin1 −/− ($[Ca^{2+}]_{mt}$ peak, 8.64 ± 0.49 mM in control versus 6.98 ± 0.46 mM in H_2O_2 treated) and (inset) wt ($[Ca^{2+}]_{mt}$ peak, 8.41 ± 0.22 mM in control versus 5.02 ± 0.39 mM, $P < 0.01$ in H_2O_2 treated) MEFs. (C) Effect of 100 mM H_2O_2 on $[Ca^{2+}]_{mt}$ responses in Pin1 overexpressing MEFs ($[Ca^{2+}]_{mt}$ peak, 8.60 ± 0.58 mM in control versus 7.26 ± 0.26 mM H_2O_2 treated, $P<0.05$) and (inset) in wt MEFs ($[Ca^{2+}]_{mt}$ peak, 8.64 ± 0.49 mM in control versus 8.56 ± 0.31 mM, H_2O_2 treated). (D) Effects of okadaic acid (1 mM, 1 hour) on H_2O_2-dependent reduction of $[Ca^{2+}]_{mt}$ responses ($[Ca^{2+}]_{mt}$ peak, 7.58 ± 0.33 mM versus 6.83 ± 0.24 mM, in okadaic acid pretreated cells before and after H_2O_2 treatment, respectively). (E) Western blot of p66Shc protein levels in the mitochondrial fraction and in the cell homogenate from wt and Pin1 −/− MEFs.

3.3 Discussion

The pathway emerging from these data is the following (Fig. 20): during oxidative stress PKC β is activated and induces p66Shc phosphorylation, thus allowing p66Shc to be recognized by Pin1, isomerised and imported into mitochondria after dephosphorylation by type 2 protein serine/threonine phosphatase (PP2A). At this point, the protein translocated into the appropriate cell domain, can exert the oxidoreductase activity, generating H_2O_2 and inducing the opening of PTP. This event in turn perturbs mitochondria structure and function (as revealed by the reduced Ca^{2+} responsiveness and the alteration of mitochondrial three-dimensional structure). Caspase cofactors, such as cytochrome c, are released and the cell progresses into apoptosis. By this way p66Shc may regulate the mitochondrial clock controlling the lifespan. Overall, these results thus identify and clarify a novel signalling mechanism, which is operative in the pathophysiological condition of oxidative stress, and may open new possibilities for pharmacologically addressing the process of organ deterioration during aging. In addition to this route, p66Shc appears to act through different pathways. Indeed, it has been shown that p66Shc enhances oxidative stress-induced apoptosis also by participating in the phosphorylation-induced repression of Forkhead transcription factors, which regulate expression of several antioxidant enzymes [87]. Consistent with this, p66Shc knockout mice exhibit higher catalase activity, and mice with extra catalase in their mitochondria lived about 20% more than controls and were less likely to develop cataracts, but they did not appear to age more slowly and their extended lifespan appeared to derive from a decrease in cardiac diseases throughout the entire lifespan [88] further emphasizing the mitochondrial role of p66Shc.

Finally, it should be remembered that the “aging” role of p66Shc appears in contrast with a recent publication showing that p66Shc is highly expressed in fibroblasts from centenarians [89]. An intriguing reconciling hypothesis could be the existence of some defects on the mitochondrial pathway of p66Shc (presented in Fig. 20) on centenarians that prevents the mitochondrial import of p66Shc and in turn its pro-aging properties, while leaving other biological functions (e.g., the production of low levels of ROS necessary in differentiation) unaffected.

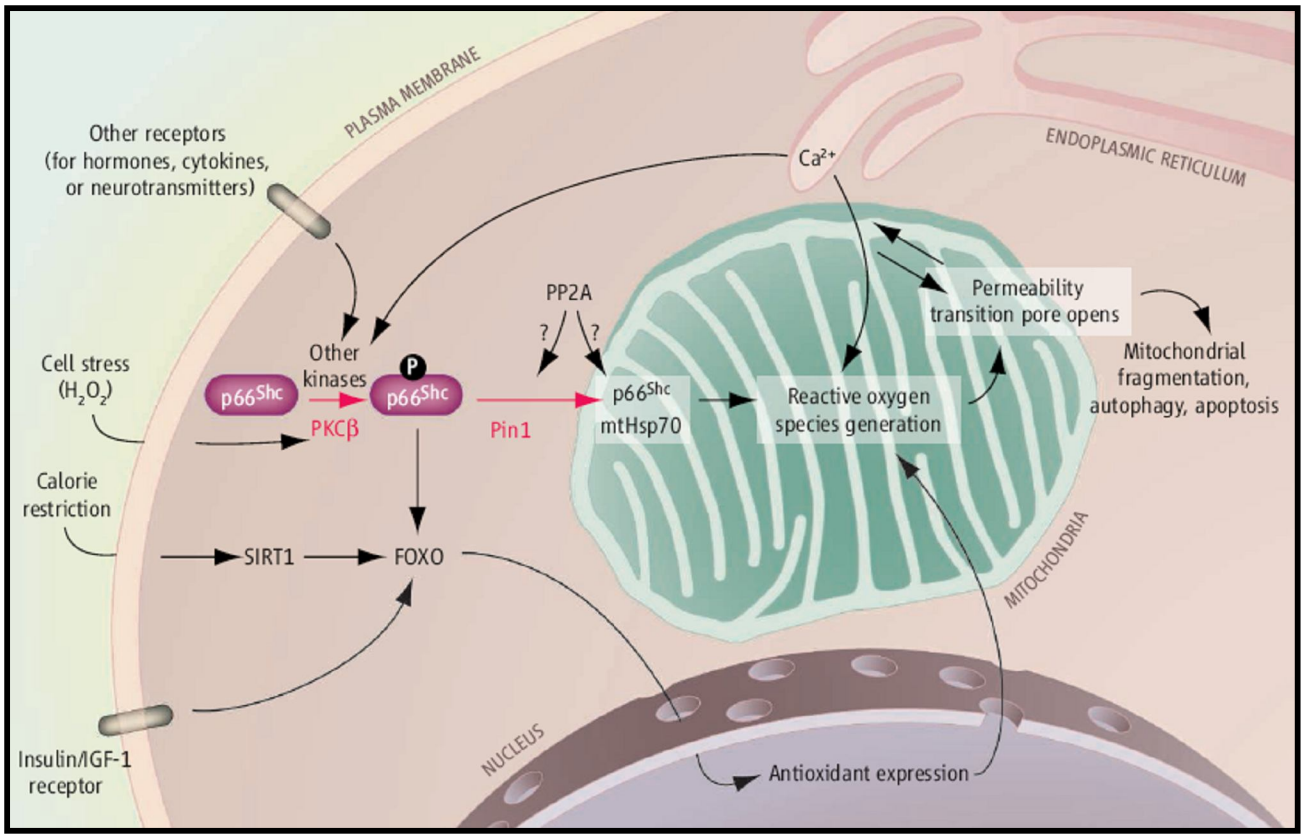

Fig. 20: Signal transduction pathway of p66Shc in oxidative condition. Phosphorylated p66Shc may serve as an integration point for many signaling pathways that affect mitochondrial function and longevity (figure from [90]).

4. Intramitochondrial calcium regulation by the FHIT gene product sensitizes to apoptosis

4.1 Introduction

The fragile histidine triad (*FHIT*) gene, isolated by positional cloning, encompasses the most common human fragile site FRA3B at 3p14.2. This chromosomal region is involved in hemizygous and homozygous deletions, and indeed mutations of *FHIT* were demonstrated in a large variety of human tumors [91-94]. *FHIT* encodes a 17-kDa protein (Fhit) that is abundantly expressed in normal human lung, stomach, kidney, and other epithelial tissues, whereas most tumors and tumor-derived cell lines do not express Fhit or show markedly reduced levels of the protein [95]. Fhit knock-out mice are more susceptible to cancer development than their wild-type counterparts [96], and *FHIT* gene therapy can prevent and reverse tumors in carcinogen-exposed Fhit-deficient mice [97]. However, the precise molecular mechanism involved in the antitumor function of *FHIT* remains largely unclear. Fhit is partly localized in mitochondria, and interaction with Hsp60/Hsp10 could be important for correct refolding after import and Fhit stability [98]. This compartmentalization of Fhit could reveal a transcription-independent regulation of cell fate. Indeed, mitochondria are at the crossroad of numerous apoptotic pathways that synergize in triggering the morphological transitions underlying the release of proapoptotic factors into the cytoplasm [29, 99, 100]. In most cases, Ca^{2+} acts as a fundamental sensitizing factor, and anti-apoptotic proteins, such as Bcl-2, have been shown to reduce ER Ca^{2+} levels, and agonist dependent release and mitochondrial loading [35, 101, 102].

Different agents induce Ca^{2+} release from the ER Ca^{2+} store through the IP_3R Ca^{2+} release channel [103]. Consequent mitochondrial Ca^{2+} uptake, via a yet unidentified Ca^{2+} channel of the inner mitochondrial membrane (the mitochondrial Ca^{2+} uniporter, MCU), regulates different processes: Aerobic metabolism [104], release of caspase cofactors [33], and feedback control of neighboring ER or plasma membrane Ca^{2+} channels [105, 106]. The ER and mitochondria are thus crucial nodes at which intracellular Ca^{2+} fluxes and functional outcomes are governed [107]. Their relevance to the control of cell survival is supported by several reports showing that modulation of mitochondrial Ca^{2+} accumulation (because of modification of the molecular repertoire of the cells) modifies cellular sensitivity to Ca^{2+}-mediated apoptotic stimuli [35, 101, 102].

We thus investigated whether Fhit has a role in the control of Ca^{2+} fluxes across the mitochondrial membranes. The results demonstrated that Fhit increases the affinity of the mitochondrial machinery for Ca^{2+} accumulation into the organelle, thus enhancing mitochondrial Ca^{2+} uptake triggered by physiological agonists and apoptotic challenges.

The increase in mitochondrial Ca^{2+} loading, by favoring the elimination of altered or damaged cells by apoptosis, may play a key role in the mechanism of action of this important tumor suppressor.

4.2 Results

4.2.1 Subcellular localization of Fhit and effect on Ca^{2+} homeostasis

The intracellular location (Fig. 21 A) and expression level (Fig. 21 B) of endogenous and overexpressed Fhit were first verified. Immunofluorescence experiments revealed a diffuse cytosolic and nuclear staining and a stronger labeling of filamentous structures corresponding to mitochondria (as confirmed by the merged image with cotransfected mitochondrial GFP, mtGFP) (Fig. 21 A). Upon overexpression, the fraction of nuclear Fhit appears increased, compared with the cytosol (compare Fig. 21 Ai and Aii). Moreover, the mitochondrial staining of Fhit was confirmed also after permeabilization of the plasma membrane using digitonin to remove the cytosolic pool of the protein (Fig. 21 C).

Then, calcium measurements were carried out, using aequorin-based recombinant probes [108]. Fig. 21 D shows the results of a typical experiment. Where indicated, HeLa cells were exposed to histamine (100 μM), causing the generation of inositol 1,4,5 trisphosphate (IP_3) and the consequent release of Ca^{2+} from the ER. No difference in cellular Ca^{2+} handling was observed between Fhit-overexpressing and control cells. Indeed, both groups of cells showed very similar luminal ER Ca^{2+} concentrations at rest ($[Ca^{2+}]_{er}$) (control 461.00 ± 22.90 μM vs. Fhit 471.50 ± 25.10 μM) and comparable release kinetics upon histamine addition. Accordingly, the transient rises of Ca^{2+} concentration in the cytosol ($[Ca^{2+}]_{cyt}$) and in the mitochondrial matrix ($[Ca^{2+}]_{mt}$) elicited by the agonist were very similar ($[Ca^{2+}]_{cyt}$, control 2.82 ± 0.05 μM vs. Fhit 2.92 ± 0.08 μM; $[Ca^{2+}]_{mt}$, control 82.20 ± 4.70 μM vs. Fhit 85.70 ± 3.79 μM).

The situation changed at a lower agonist dose (10 μM histamine). The aequorin probes showed very similar release kinetics from the ER, slower than with 100 μM histamine (control 3.21 ± 0.40 μM/sec. vs. Fhit 3.32 ± 0.29 μM/sec.), and superimposable

$[Ca^{2+}]_{cyt}$ peaks (control 2.67 ± 0.08 μM; Fhit 2.66 ± 0.08 μM) (Fig. 21 E). Conversely, in Fhit-overexpressing cells, the $[Ca^{2+}]_{mt}$ increase was approximately 30% greater (control 13.01 ± 0 75 μM vs. Fhit 16.74 ± 1.44 μM) (Fig. 21 E).

This effect was not cell type-specific, as the same results were obtained in A549 cells (Fig. 22 A), nor could it be related to overexpressed protein, as shRNA silencing of endogenous Fhit in HeLa cells caused the expected opposite effect (control 13.23 ± 1.92 μM vs. shRNA Fhit 10.93 ± 1.79 μM) (Fig. 22 B).

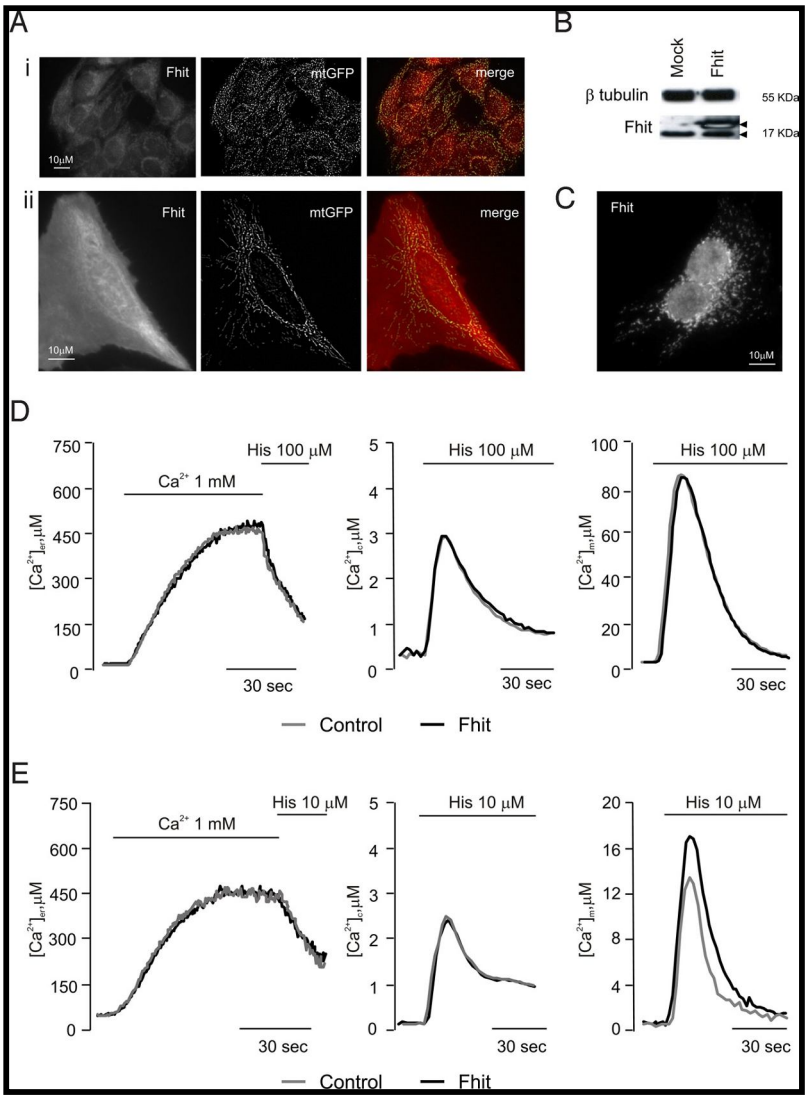

Fig. 21: Subcellular localization of Fhit and effect on Ca^{2+} homeostasis. (A) Immunofluorescence labeling of Fhit (*Left*), mtGFP visualization (*Middle*), and merged image (*Right*) in HeLa cells. (*I*) Control, (*II*) Fhit-overexpressing cells. (B) Western blotting of Fhit and β tubulin as reference. Arrowheads denote the position of endogenous (lower) and His-6-tagged (higher) Fhit bands in mock-transfected (Mock) and Fhit-overexpressing (Fhit) HeLa cells. The level of overexpression is typical of the results obtained in all of the experiments of this paper. (C) Immunofluorescencelabeling of overexpressed Fhit after plasma membrane permeabilization with digitonin. (D and E) $[Ca^{2+}]$ measurement in the ER (*Left*), cytosol (*Middle*), and mitochondria (*Right*) in controls (gray line) and Fhit-overexpressing cells upon 100 μM (D) and 10 μM (E) histamine.

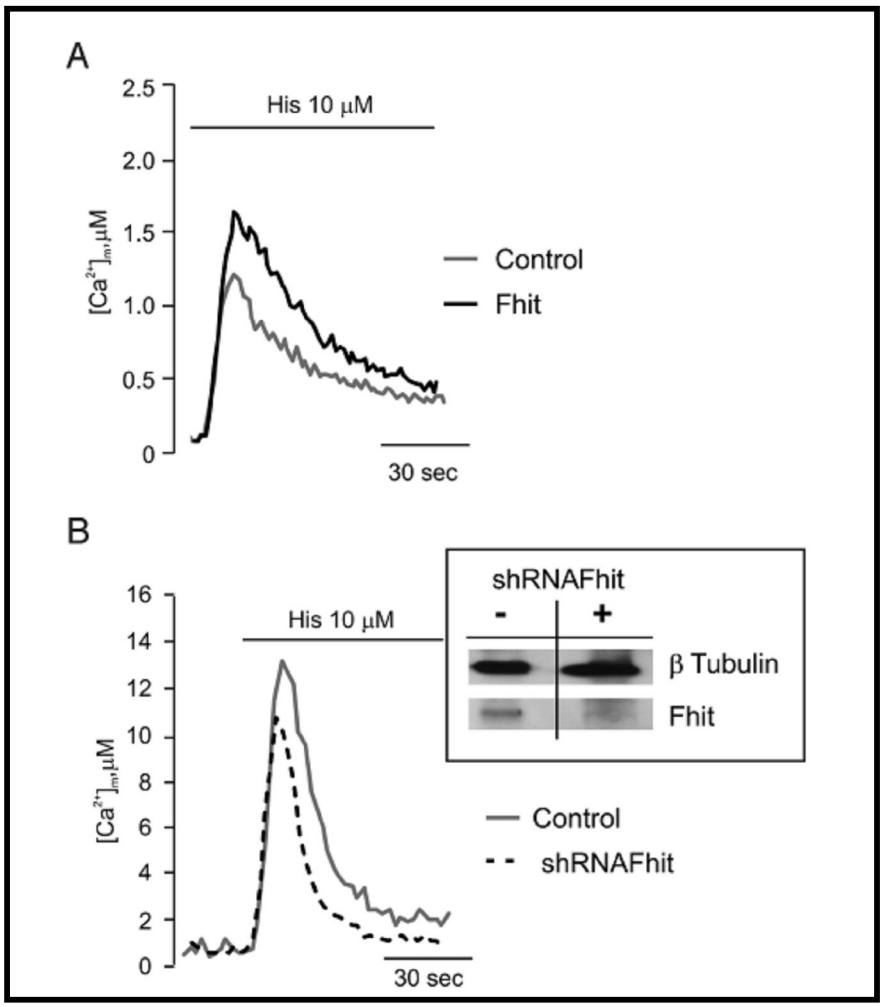

Fig. 22: Not cell type-specific role of Fhit and ShRNA Fhit effect on Ca^{2+} homeostasis. (A) $[Ca^{2+}]_{mt}$ measurements in control and in Fhit-transduced A549 cells after stimulation with histamine 10 μM. (B) $[Ca^{2+}]_{mt}$ measurements in control and shRNA-Fhit-transduced HeLa cells. *Inset*, Fhit immunoblotting to estimate the level of shRNA Fhit silencing.

4.2.2 Assessment of mitochondrial Ca^{2+}-uptake capacity in permeabilized and intact cells

We then investigated the possible mechanism of the increased uptake at submaximal agonist stimulation. Rapid uptake into mitochondria depends on close interactions with the ER [109, 110], as well as on the state of fusion/fission of the organelle network [111]. 3D reconstruction of mtGFP-labeled of mitochondria showed no difference in distribution and shape between Fhit-overexpressing and control cells (Fig. 23 A). As to the driving force for Ca^{2+} accumulation, loading of the potential-sensitive tetramethyl rhodamine methyl ester (TMRM) dye revealed no difference in the transmembrane potential ($\Delta\Psi$) (Fig. 23 B).

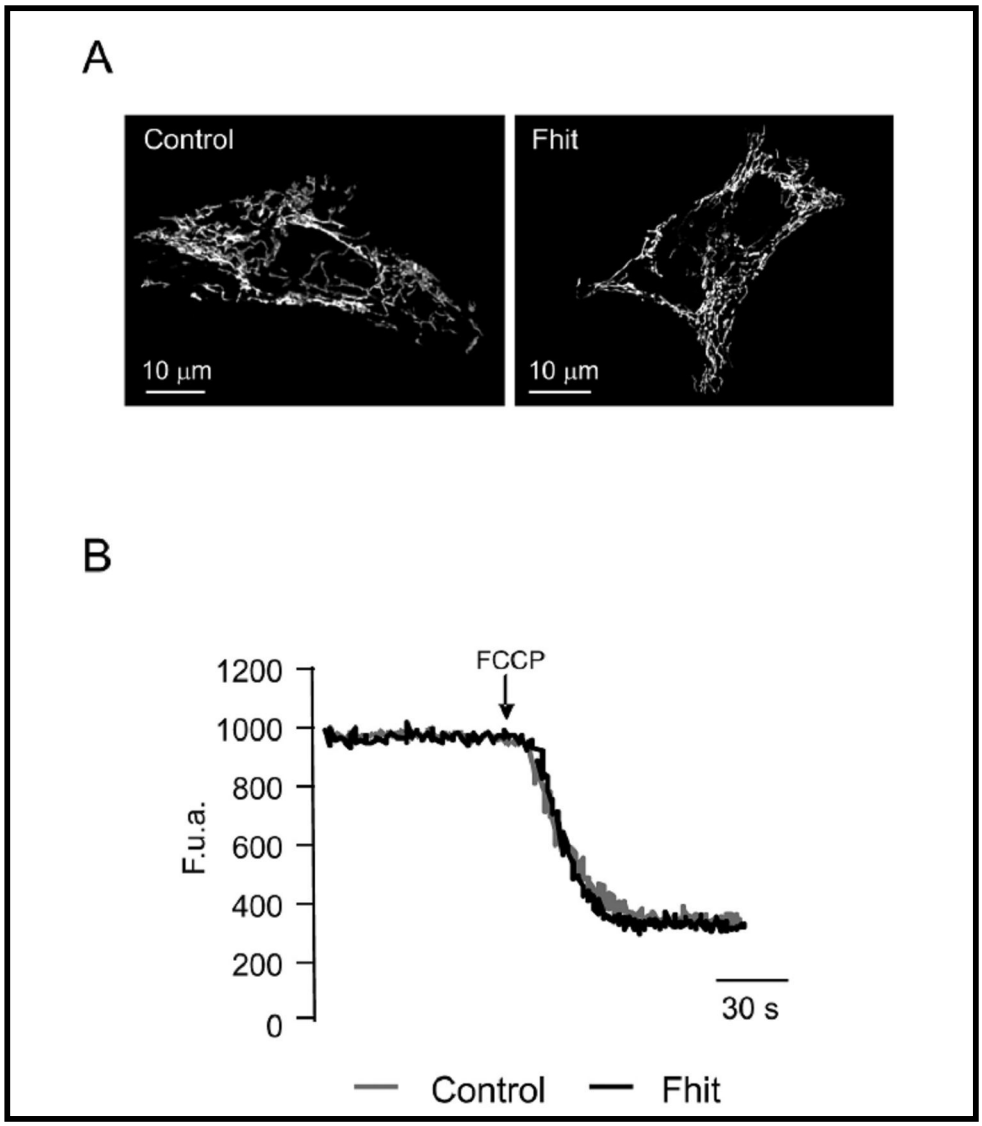

Fig. 23: Fhit-overexpression doesn't affect mitochondrial membrane potential and morphology. (A) Mitochondrial morphology in Fhit-transfected and control HeLa cells as revealed by mtGFP visualization. (B) TMRM fluorescence level of control and Fhit cells, before and after treatment with FCCP (carbonyl cyanide *p*-trifluoromethoxyphenylhydrazone), to collapses mitochondrial $\Delta\Psi$.

We thus concluded that the explanation of our results most likely resided in the increased affinity of the molecularly undefined transporter (the mitochondrial Ca^{2+} uniporter, MCU). We explored this possibility by measuring mitochondrial Ca^{2+} uptake in permeabilized cells and by visualizing the hotspots of rapid mitochondrial uptake in intact cells. In the former case, transfected HeLa cells were perfused with a solution mimicking the intracellular milieu (IB), supplemented with 2 mM EGTA, and permeabilized with 20 μM digitonin for 1 min.

Then, the perfusion buffer was changed to IB with an EGTA-buffered [Ca^{2+}] of 1 μM, eliciting a gradual rise in $[Ca^{2+}]_{mt}$ that reached a plateau value of approximately 30 μM (Fig. 24 A). In Fhit-overexpressing HeLa cells, the [Ca^{2+}] increase was larger and faster than in controls (V_m, mean of first 15 sec., control 0.53 ± 0.01 μM/sec. vs. Fhit 0.79 ± 0.01 μM/sec.) and reached an approximately 20% higher plateau. A coherent picture emerged from single-cell imaging experiments in HeLa cells with a GFP-based mitochondrial probe, 2 mtRP [112]. Time-lapse series of high resolution images were acquired at 5–10 frame/sec. and visualized as 2D image series of the whole mitochondrial network. These data allowed calculation of the number of localized $[Ca^{2+}]_{mt}$ increases (hotspots), visualized in a pseudocolor scale, and evaluation of their diffusion across mitochondria.

After application of 10 μM histamine, mitochondrial Ca^{2+} uptake initiated at preferential points of the mitochondrial network and the [Ca^{2+}] increase traveled along the mitochondrial profiles, saturating the relatively high-affinity probe. In Fhit-overexpressing cells, the number of hotspots was markedly greater than in controls (Fig. 24 B). This heterogeneity, and the increased number of hotspots in Fhit-overexpressing cells, was quantified by calculating the standard deviation of the relative fluorescence changes over individual mitochondrial objects (control 10.55 ± 0.95 vs. Fhit 16.06 ± 1.45, $P < 0.01$) (Fig. 24 C). Based on previous observations that stimulations with agonists evoking mitochondrial Ca^{2+} signals cause parallel increases in intracellular ATP [70], we also measured mitochondrial ATP levels ($[ATP]_{mt}$) in control and Fhit-overexpressing HeLa cells. For this purpose, the mitochondria-targeted ATP probe luciferase (mtLUC) was cotransfected, as previously reported (Fig. 24 D) [70].

Interestingly, overexpression of Fhit increases the $[ATP]_{mt}$ rise evoked by 10 μM histamine, thus demonstrating that (i) also at submaximal agonist challenges the $[Ca^{2+}]_{mt}$ rise is decoded into a stimulation of mitochondrial aerobic metabolism and (ii) Fhit plays a role in the metabolic effect of mitochondrial Ca^{2+} signals.

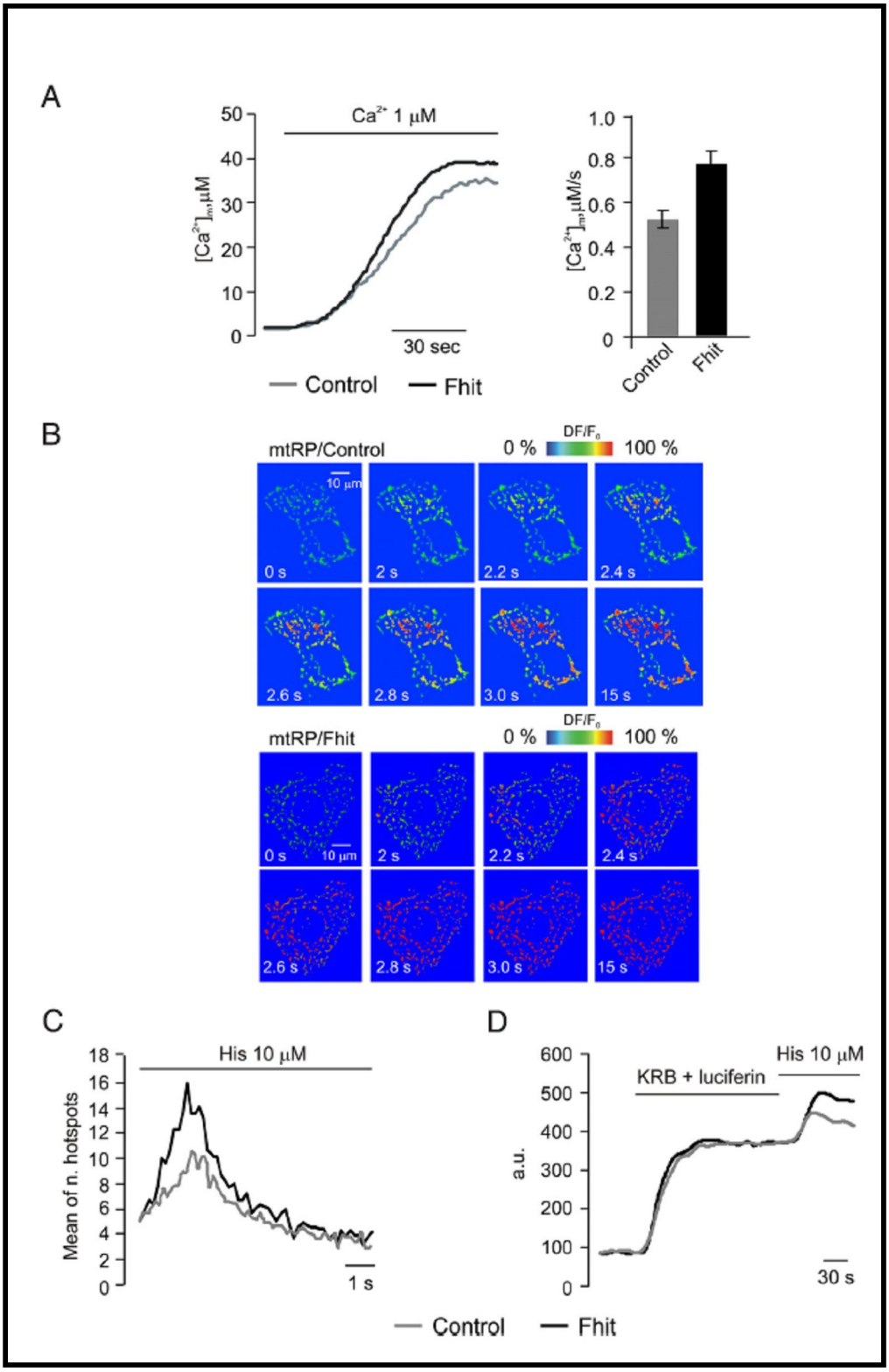

Fig. 24: Assessment of mitochondrial Ca^{2+}-uptake capacity in permeabilized and intact cells. (A) Mitochondrial Ca^{2+}-uptake in permeabilized cells: Representative traces (*Left*) and average speed (*Right*). Where indicated (Ca^{2+} 1 µM) the medium was switched from IB/EGTA to IB/1 µM [Ca^{2+}]. (B) Rapid imaging of the $[Ca^{2+}]_{mt}$ increase elicited by 10 µM histamine, in control (mtRP/Control) and Fhit-overexpressing (mtRP/Fhit) HeLa cells. The images in the panel show the fluorescence changes of the mtRP probe, expressed in a pseudocolor scale (warmer colors revealing the $[Ca^{2+}]_{mt}$ increases). (C) Total number of generated mitochondrial Ca^{2+} hotspots, plotted through time after stimulation. (D) Mitochondrial [ATP] changes in control and Fhit-overexpressing HeLa cells.

4.2.3 The $[Ca^{2+}]_{mt}$ is affected by a mitochondrial Fhit chimera

We then investigated whether the mitochondrial signaling alteration is caused by the fraction of Fhit protein localized to mitochondria. To fully sort Fhit to mitochondria, a mitochondrial targeting sequence was appended at its N terminus (mtFhit; Fig. 25 A). Indeed, immunofluorescence experiments showed only the typical filamentous structure of the mitochondrial network (Fig. 25 A). We then carried out mitochondrial Ca^{2+} measurements, using the mtAEQ, erAEQ, and cytAEQ probes, cotransfected with mtFhit (mtFhit). Upon submaximal histamine challenge (10 μM), mtFhit-overexpressing cells underwent a $[Ca^{2+}]_{mt}$ rise that was markedly greater than that of controls and comparable to that of Fhit-overexpressing cells (mtFhit 16.53 ± 1.85 μM), whereas the $[Ca^{2+}]_{er}$ and $[Ca^{2+}]_{cyt}$ values were comparable to those of control cells.

These data show that a Fhit variant with exclusive mitochondrial localization fully retains the effect on mitochondrial Ca^{2+} signaling of the wild-type protein (Fig. 25 B). We then labeled the ER and the mitochondria with a GFP-based probe (erGFP) and MitoTracker-Red to investigate organelle morphology in mtFhit-transfected and control cells. No alteration was observed in the morphology of the two organelles nor in the number and location of the contacts. Then $\Delta\Psi$ was measured with TMRM; also in this case, no difference was observed between mtFhit-expressing and control cells. We thus concluded that mtFhit does not exert damaging effects on mitochondrial morphology, on the functional interaction with the ER, and in the generation of the membrane potential across the inner membrane.

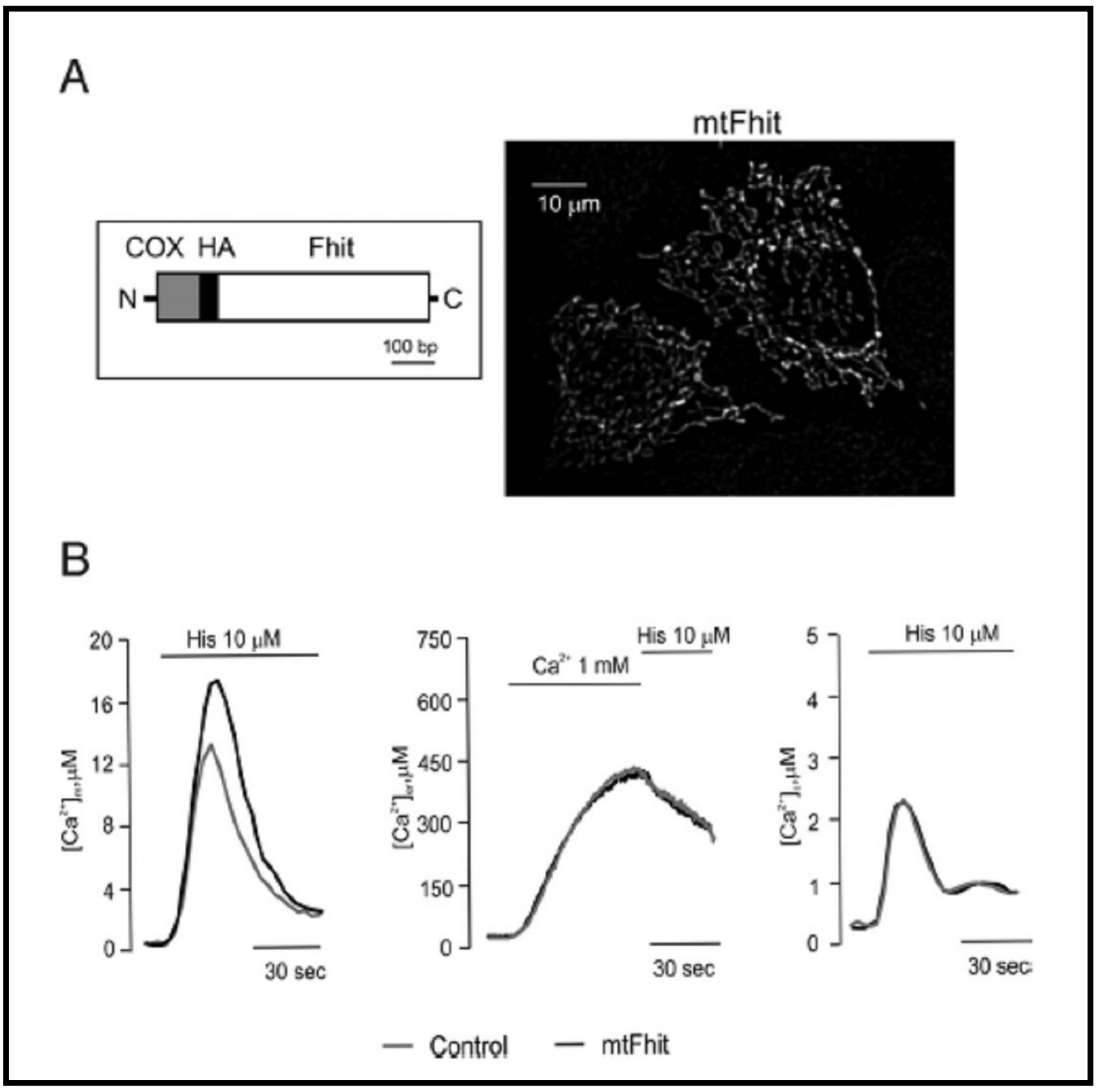

Fig. 25: Subcellular localization and effect on Ca^{2+} signaling of mtFhit. (A) Map of the mtFhit cDNA and immunolocalization of the expressed protein. (B) [Ca^{2+}] measurement in the mitochondria, ER (control 438 ± 26.90 μM vs. Fhit 411 ± 35.60 μM), and cytosol (control 2.48 ± 0.03 μM vs. Fhit 2.50 ± 0.03 μM) in controls (gray) and mtFhit-overexpressing cells (black) upon addition of 10 μM histamine.

4.2.4 The mitochondrial fraction of Fhit potentiates apoptotic effect of menadione

We then investigated the functional consequences of the signaling alteration. Various apoptotic challenges appear to use Ca^{2+} as a sensitizing cofactor, e.g., C2-ceramide, oxidative stress (menadione, H_2O_2) or arachidonic acid [105, 113-115]. These stimuli induce movement of Ca^{2+} from the ER to mitochondria, leading to Ca^{2+} overload, OMM permeabilization, and caspase-mediated cell death. To verify whether Fhit affects Ca^{2+} homeostasis and cell survival in apoptotic conditions, we investigated the effects of menadione. Treatment with menadione caused a small, transient $[Ca^{2+}]_{cyt}$ rise followed by

a lower, sustained plateau (Fig. 26 A). As expected, this low-amplitude $[Ca^{2+}]_{cyt}$ increase correlated with a marginal uptake of Ca^{2+} into mitochondria (Fig. 26 B).

Interestingly, also in the case of the apoptotic challenge the $[Ca^{2+}]_{mt}$, but not the $[Ca^{2+}]_{cyt}$ rise, was markedly greater in Fhit-overexpressing cells. We then correlated the Ca^{2+} data with the efficacy of the oxidizing agent in causing cell death, by 2 approaches: the microscopic assessment of cell survival (apoptotic counts), after coexpression of a fluorescent marker (mtGFP), and Annexin V-based measurement of apoptosis. In the first case, a decrease in the percentage of fluorescent cells correlates with a proapoptotic role of the expressed protein. As expected, after menadione treatment a substantial reduction in the number of Fhit-overexpressing cells was observed (control Δ% 1.94 $\pm$ 6.75 vs. Fhit -36.79 $\pm$ 7.25) (Fig. 26 C). Interestingly, the reduction was greater with mtFhit (Δ% -45.48 $\pm$ 7.39).

In Annexin V measurements, Fhit-overexpressing and control cells were labeled with Alexa Fluor 488 Annexin V, sorted by flow cytometry, and expressed as percentage of strongly fluorescent cells (Fig. 26 D). In basal conditions, higher levels of Annexin V labeling were detected in Fhit-overexpressing HeLa cells (21.1%) compared with controls (13%). After a 2-h treatment with menadione, the percentage of Annexin-positive cells increased to 38.3% (16.6% of nontransfected cells). With mtFhit, the percentage of Annexin V-positive cells was comparable to controls in basal conditions (12%), but was greatly measured after treatment with menadione (16.6%, 38.3%, and 52.5% for control, Fhit, and mtFhit-transfected cells, respectively). Overall, these data indicate that mitochondrially localized Fhit does not influence basal levels of apoptosis, but greatly sensitizes to apoptotic challenges, in good agreement with the view of a Ca^{2+}-mediated intramitochondrial potentiation of apoptotic routes.

Finally, we investigated whether other putative functions of Fhit, which have been proposed to cooperate in tumor suppression but are unlikely to be ascribed to a mitochondrial effect, are also shared by mtFhit. We focused on cell cycle control [116] and carried out FACS sorting of cells after DNA labeling with propidium iodide (Fig. 27). Fhit-overexpressing cells showed an increased number of cells in the G2 phase or at the S-G2 boundary, as reported in H460 cells [117]. Conversely, mtFhit does not share this property with Fhit, as the distribution of cells in G0/G1, S, and G2/M is very similar to that of control cells (G0/G1: 48.4%, 35.1%, 47.1%; S: 8.2%, 9.6%, 7.9%; G2/M: 36.8%, 42.7%, 36.4% for control, Fhit, and mtFhit-transfected cells, respectively).

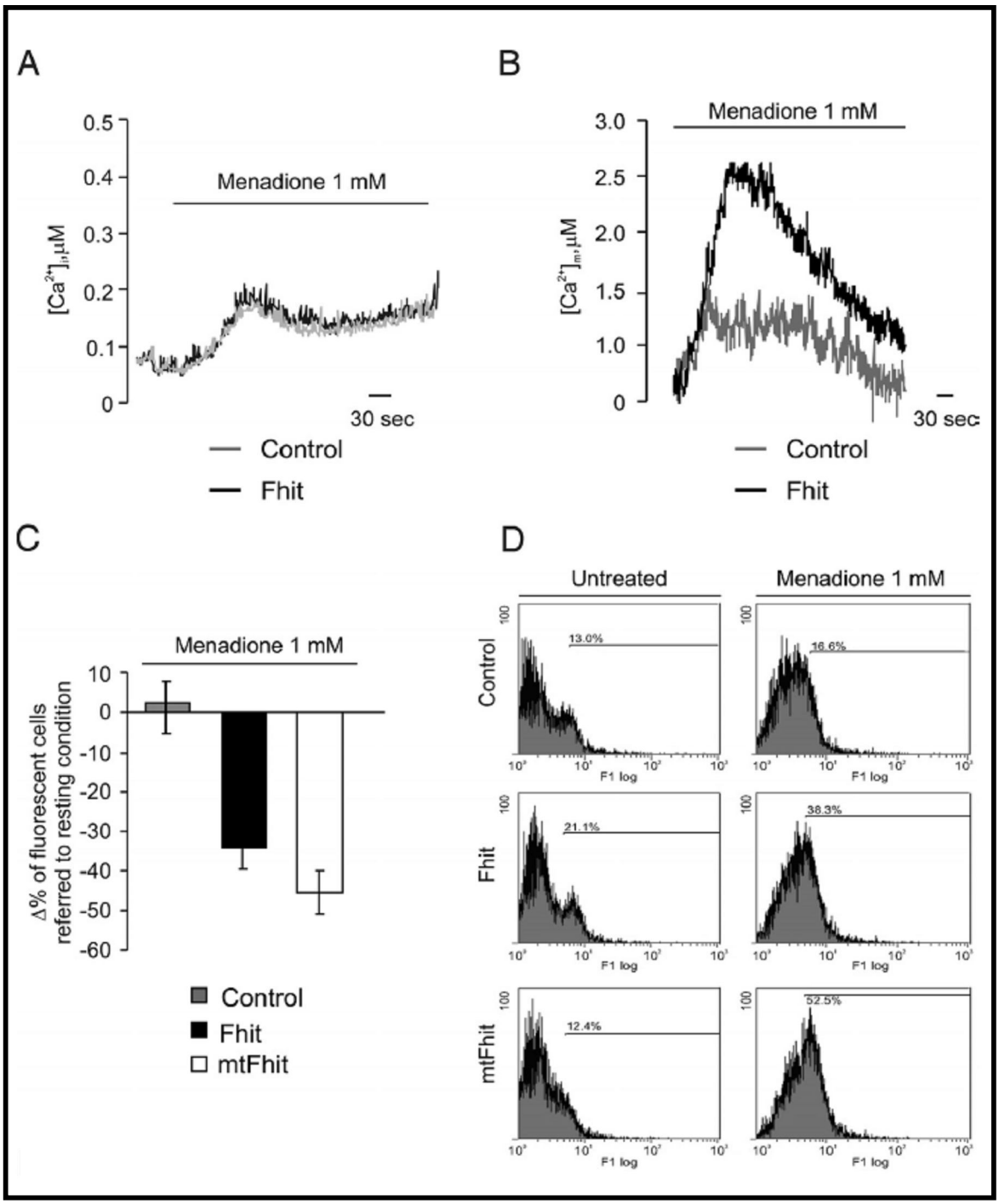

Fig. 26: The mitochondrial fraction of Fhit potentiates apoptotic challenges. (A) $[Ca^{2+}]_{cyt}$ and (B) $[Ca^{2+}]_{mt}$ increases elicited by 1mM menadione. (C and D) Assessment of cell viability via apoptotic counts (C) or Annexin V labeling (D) in controls, Fhit and mtFhit overexpressing cells, as indicated. In panel D, the percentage of cells over a common arbitrary level of fluorescence is indicated.

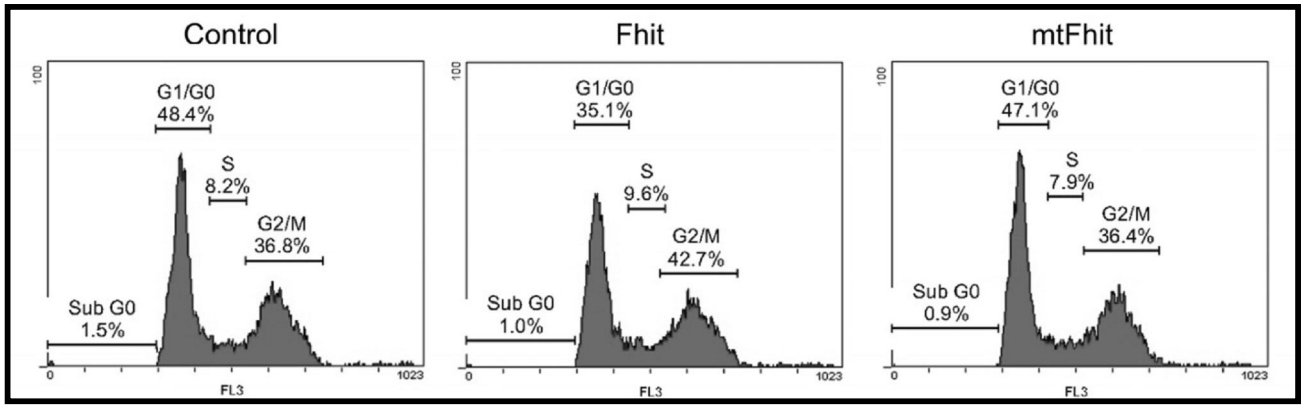

Fig. 27: Effect of Fhit and mtFhit overexpression on cell cycle. Distribution of HeLa cells in the cell cycle, as estimated by propidium iodide staining of DNA. The percentage of cells in G0/G1, S, and G2 is reported in each graph.

4.3 Discussion

Our previous observation that Fhit protein is localized within mitochondria and engages protein-protein interactions with resident proteins such as ferredoxin [98] highlighted the possibility that it could tune apoptotic signals reaching the mitochondrial checkpoint.

We pursued this hypothesis, focusing on Ca^{2+} signaling, based on a large body of experimental evidence by us and other groups that demonstrates the importance of mitochondrial Ca^{2+} loading for triggering the morphological transitions of apoptosis [29, 100, 118, 119]. The results were very striking, as not only they revealed a marked potentiation of the matrix [Ca^{2+}] transients elicited by physiological stimuli and apoptotic agents, but also identified a mechanism for this effect.

Fhit is an enigmatic protein, exerting an AP3Ahydrolase activity that is not required for its tumor suppression function [120]. To date, the exact mechanism by which Fhit exerts its antitumor activity remains obscure. A considerable body of evidence points to the role of Fhit in apoptosis induction and cell cycle regulation, including its role as modulator of DNA damage checkpoint response [96], but the molecular pathways of the apoptotic activity of Fhit remain elusive. Our results bring this tumor suppressor to the core mechanism of the intrinsic pathway of apoptosis, participating in the regulation of the critical mitochondrial steps. This effect is mediated by the fraction of Fhit localized in mitochondria [98], whereas other reported functions of Fhit, such as the putatively transcriptional control of the cell cycle are unaffected by an exclusively mitochondrial Fhit chimera. These data thus

suggest that the complex intracellular distribution of Fhit may underlie a synergistic effect of different protein pools (cell cycle block, induction of apoptosis) that cooperate in repairing or eventually clearing DNA-damaged cells. As to the mechanism itself, the data provide a radically different picture from the numerous previous examples of pro and anti-apoptotic proteins acting on calcium signaling. The $[Ca^{2+}]_{ER}$ levels were shown to be modulated by the Bcl-2 family members, with Bcl-2 itself reducing the state of filling of the Ca^{2+} store [35], and Bax and Bak counteracting this effect [114]. In turn, the partial emptying reduces mitochondrial Ca^{2+} loading and, hence, the efficacy of various apoptotic challenges [33, 114]. In the case of neurodegenerative signals and of the proapoptotic HBx protein, mitochondrial Ca^{2+} overload was shown to depend on the caspase-mediated cleavage of the plasma membrane Ca^{2+} ATPase (PMCA) that impairs the termination mechanism of the Ca^{2+} signal and amplifies and extends the cytosolic Ca^{2+} increases [36, 121].

Here, we report that Fhit does not alter cytoplasmic Ca^{2+} signals and acts specifically on mitochondria by modifying the affinity of the MCU. Accordingly, mitochondrial Ca^{2+} signals are minimally affected by supramaximal agonist stimulations, but are markedly increased at lower, more physiological agonist concentrations. This mechanism of action appears very effective in apoptosis for 2 reasons. The first reason is that apoptotic challenges, such as the lipid mediator C2-ceramide [33] and oxidative stress, such as that caused by menadione or H_2O_2 and used in this paper, have been shown to empty Ca^{2+} stores, but do so with a slow kinetics. Accordingly, mitochondrial uptake is relatively modest, because the low affinity of the MCU requires the generation of high $[Ca^{2+}]$ microdomains at the ER/ mitochondria contacts [109, 110]. If, however, the affinity of the MCU is increased by Fhit, also under those conditions mitochondria accumulate a large Ca^{2+} load, allowing the opening of the PTP and the induction of cell death, as directly shown in the experiment of Fig. 26. In addition, physiological Ca^{2+}-mediated signals may synergize with PTP sensitizers (e.g., ceramide or alcohol), initiating slow waves of depolarization and Ca^{2+} release propagating through the cell [113]. In this picture, Fhit, by sensitizing mitochondria, increases the possibility that any stimulatory input to the cell reaches the threshold for initiating the apoptotic Ca^{2+} wave. The observation of Fig. 24 that Fhit increases the number of hotspots (i.e., initial sites of Ca^{2+} uptake in mitochondria) strongly supports this scenario.

Finally, the identification of Fhit as a protein modulator of the MCU can open the way to proteomic approaches for solving the molecular enigma of mitochondrial Ca^{2+}

homeostasis. Indeed, despite the growing interest in this process, the MCU remains undefined at the molecular level, and all of the efforts for biochemically identifying it have been frustrated by the lack of specific tools for labeling the proteins (the best characterized inhibitor, Ruthenium Red, binds unspecifically to a wide array of proteins). The demonstration that Fhit binds, directly or indirectly, to the MCU gives the possibility of analyzing the mitochondrial complexes in which it is engaged, with the aim of identifying the molecular component(s) of the MCU.

Overall, understanding the mechanisms through which Ca^{2+} signals can be shifted from regulators of cellular functions to pathological effectors and the role of mitochondria as decisive checkpoints is an exciting task in biomedical research and a promising opportunity for developing drugs. The observation that Fhit is directly engaged in this process deepens our insight into the functioning of this important tumor suppressor and further stresses the relevance of mitochondrial Ca^{2+} homeostasis in cancer-related apoptosis.

5. Akt kinase reducing endoplasmic reticulum Ca^{2+} release protects cells from Ca^{2+}-dependent apoptotic stimuli

5.1 Introduction

Protein kinase B or Akt, is a serine/threonine kinase, which in mammals comprises three highly homologous members known as PKB α (Akt1), PKB β (Akt2), and PKB γ (Akt3) [122].

Key roles for this enzyme can be found in cellular processes such as glucose metabolism, cell proliferation, apoptosis, transcription and cell migration [123, 124]. Akt functions to promote cell survival through several pathways [123, 125, 126]. The precise mechanisms by which Akt prevents apoptosis are not completely understood.

The major structural features of the Akt proteins are illustrated in Fig. 28. Each isoform possesses an N-terminal pleckstrin homology (PH) domain of approximately 100 amino acids. Recent detailed structural examination of Akt PH domains reveals similarity to PH domains found in other signalling molecules that bind 3-phosphoinositides [127, 128]. This, together with evidence from earlier in vitro studies, indicates that the PH domain mediates binding of Akt to 3-phosphoinositides. The PH domain is followed by the kinase catalytic domain, which shows a high degree of similarity to those found in PKA and PKC [129, 130]. Also present in this region is a threonine residue (Thr308 in Akt1) whose phosphorylation is necessary for activation of Akt. Following the kinase domain is a hydrophobic C-terminal tail containing a second regulatory phosphorylation site (Ser473 in Akt1).

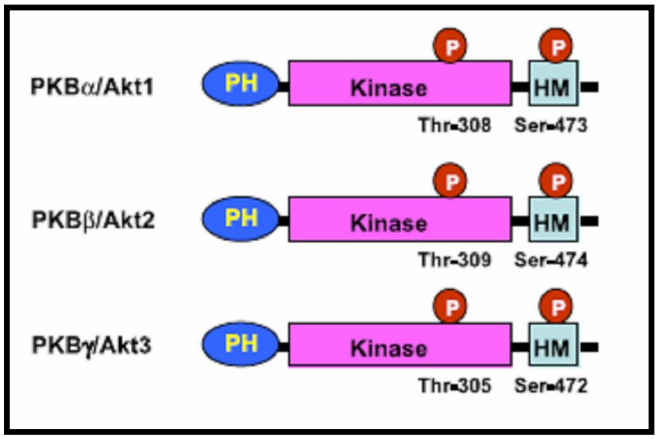

Fig. 28: Structure of different isoforms of Akt.

Phosphorylation at Thr308 and Ser473 occurs in response to growth factors and other extracellular stimuli and is essential for maximal Akt activation [131]. Akt may also be phosphorylated on Ser124 and Thr450 but neither of these sites appears to regulate Akt activity and their phosphorylation does not change following cell stimulation [131].

In particular, full activation of Akt is a multi-step process, and several proteins responsible for each step have been identified [132]. Some stimuli can promote the activation of Akt through the activation of receptor tyrosine kinases. One of the most significant findings in the early stages of Akt research was its PI3-kinase-dependent activation [133-135]. Akt is also activated by receptor tyrosine kinases such as platelet derived growth factor receptor (PDGF-R), insulin, epidermal growth factor (EGF), basic fibroblast growth factor (bFGF) and insulinlike growth factor I (IGF-I). Membrane-targeting processes are important for PI3-kinases to get access to their substrates, as they are anchored in the plasma membrane. At this level, Akt is phosphorylated in two different sites, Thr308 and Ser473 [131], by PDK1 [136, 137] and mTOR complex 2 [138], respectively. These two sites are necessary and sufficient for full activation of Akt, which can translocate to different organelles, such as the endoplasmic reticulum (ER), the nucleus and mitochondria. The model of Akt activation is showed in Fig. 29.

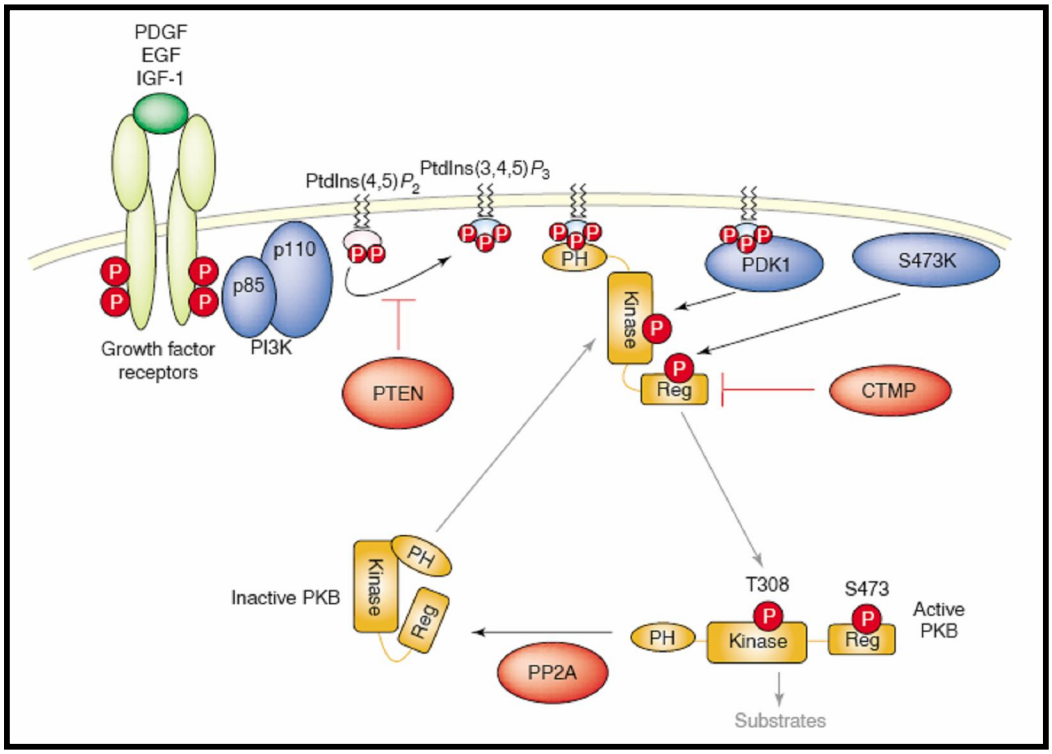

Fig. 29: Schematic model of Akt activation.

Forced membrane localization of Akt through its myristoylation/palmitylation is sufficient for maximal phosphorylation of key aminoacids and in turn for its full activation. The activity of this plasma membrane targeted Akt chimera (m/p-AKT1) is 60-fold higher compared with the unstimulated wild-type enzyme [139] and it is widely utilized in studying the effects of Akt in several signal transduction pathways [140-142].

Akt is a growth-factor-regulated protein kinase that phosphorylates in vitro and in vivo the inositol 1,4,5-trisphosphate (IP_3) receptor (IP_3R) (Fig. 30 B), thanks to the presence of a consensus substrate motif that is conserved in all three IP_3R isoforms (Fig. 30 A) [143]. The IP_3R is involved in Ca^{2+} mobilization from intracellular stores, where channel activity is largely under the control of the IP_3 binding. IP_3R is involved in fundamental processes such as fertilization, meiosis, and mitosis and it has been reported that several proteins interact with IP_3Rs [144]. Some of these have a modulatory role. Indeed, in addition to Akt mentioned above, the IP_3R is also a substrate for several other protein kinases including calmodulin dependent protein kinase II [145], protein kinase C [80, 146] and MAP kinases. As mentioned before, the main role of the IP_3R is releasing Ca^{2+} into the cytoplasm and to other effector systems (such as mitochondria). Ca^{2+} is recognized to be a fundamental second messenger involved in fertilization, proliferation, muscle contraction and secretion [103, 147]. As a second messenger, Ca^{2+} exerts its role inside the cell, where its concentration is highly controlled. The extent of Ca^{2+} signal is also a key determinant of the intrinsic apoptotic pathway, thus controlling cell fate under physiological and pathological conditions [31]. There is general agreement in the literature that Ca^{2+} efflux from the ER and Ca^{2+} accumulation into the mitochondria are linked to the effects of various apoptotic stimuli [31]. The task of this work was to evaluate the effect of the overexpression of a constitutively active AKT1 on subcellular Ca^{2+} homeostasis in transiently transfected HeLa cells, i.e. the same cell model in which the effects of Bcl-2 and Bax on Ca^{2+} signaling were previously detected and analyzed [33, 35, 36]. We then analyzed the effects of Akt overexpression on the cytosolic Ca^{2+} signal elicited by apoptotic stimuli such as oxidative stress and arachidonic acid, as they act through mitochondrial Ca^{2+} overload and activation of the intrinsic apoptotic pathway following to Ca^{2+} release from the ER. Altogether our data suggest that the alteration of Ca^{2+} fluxes through the IP_3R is a key component of the protective action of Akt against apoptosis induced by stimuli acting in a Ca^{2+}-sensitive manner.

A

type-I	2671	LDWFPRMRAMSLVSSDSEGE
type-II	2623	LDWFPRMRAMSLVSNEGDSE
type-III	2598	LDWFPRMRAMSLVSGEGEGE
Xenopus	2615	LDWFPRMRAMSLVSSDSEGE
Drosophila	2758	LEWFPRLRAMSLAAVDADGE
C.Elegans	2789	LDWFPRMQALSLQDSELDTD

B

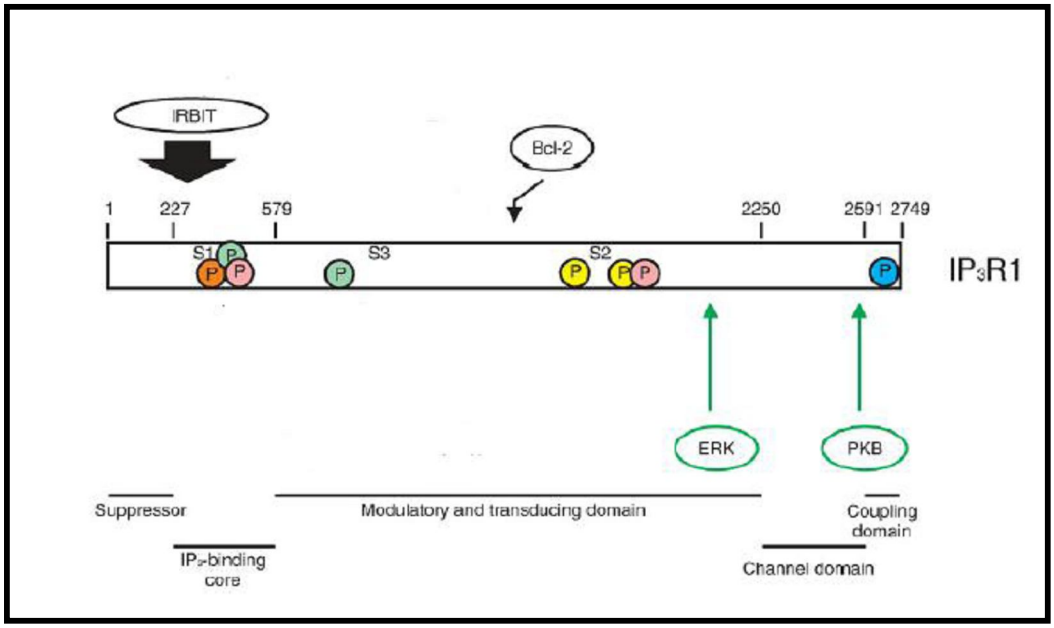

Fig. 30: Akt phosphorylates IP$_3$Rs. (A) All three isoforms of IP$_3$Rs present a conserved consensus sequence for Akt phosphorylation. (B) the residue of Serine phosphorylated by Akt is located at C-terminal of IP$_3$R, into the gatekeeper domain (figure A from [143], figure B from [148]).

5.2 Results

5.2.1 Akt drastically reduces ER Ca^{2+} release, while leaving ER Ca^{2+} levels unaffected

We measured the ER [Ca^{2+}] ([Ca^{2+}]$_{er}$) in HeLa cells transfected with ER-targeted aequorin . In these experiments, the ER Ca^{2+} store was first depleted of Ca^{2+}, during the phase of aequorin reconstitution, performed in Ca^{2+}-free medium (as described in Materials and methods, section 6). When Ca^{2+} was added back to the KRB perfusion

medium, $[Ca^{2+}]_{er}$ rose from <10 μM to a plateau value of ~400 μM. No significant difference was observed between m/p-AKT1 overexpressing and control cells (348 ± 20.08 μM and 357.16 ± 19.68 μM, n = 21; p > 0.1) (Fig. 31 A).

We then investigated the ER response to histamine, which acts on Gq-coupled plasma membrane receptors and causes the production of IP_3, thus releasing Ca^{2+} from the ER through the IP_3Rs, followed by sustained influx from the extracellular medium through plasma membrane Ca^{2+} channels (Fig. 31 B). When the $[Ca^{2+}]$ in the lumen of the ER reached a plateau value, the cells were treated with histamine. As expected, a decreases in the $[Ca^{2+}]$ of the ER compartment was observed both in control and m/p-AKT1 expressing cells (Fig. 31 B), but the decrease of $[Ca^{2+}]$ in control cells was extremely larger and faster (V_{max}: 23.03 ± 2.02 μM/sec. vs 3.87 ± 0.5 μM/sec.; mean of first 50 sec. of Ca^{2+} released: 3.67 ± 0.2 μM/sec. vs 1.56 ± 0.1 μM/sec., n = 21), thus reflecting a more rapid flow through the IP_3-gated channels, in controls compared to m/p-AKT1 expressing cells. Then we investigated if m/p-AKT1 overexpression could affect the IP_3Rs expression level: as shown in Fig. 31 C this was not the case. Indeed, both type 1 and type 3 IP_3R, are expressed at comparable levels in m/p-AKT1 transfected and control cells. We are unable to detect the type 2 IP_3R in HeLa cells, in according with previous reports showing that the amount of IP_3R II in HeLa cells is very low compared with other subtypes [149, 150].

Thus, we conclude that m/p-AKT1 is able to inhibit agonist-induced ER Ca^{2+} release into the cytoplasm.

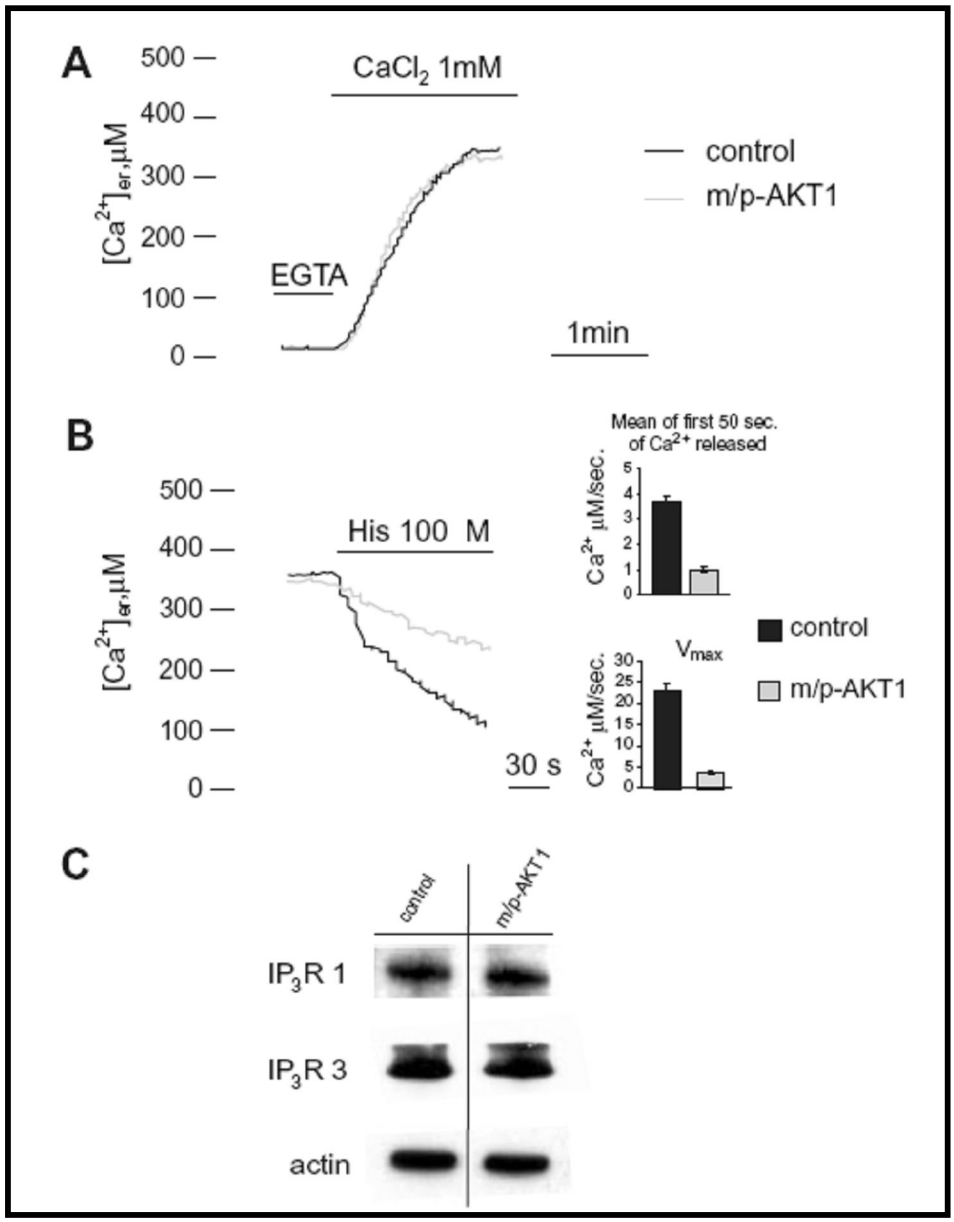

Fig. 31: Modifications of ER Ca^{2+} kinetic releases by overexpression of Akt in HeLa cells. (A) Effects of m/p-AKT1 on the ER Ca^{2+} concentration in control and in m/p-AKT1-overexpressing HeLa cells. (B) Reduced ER Ca^{2+} release in m/p-AKT1-overexpressing cells when stimulated with 100 µM histamine. To induce Ca^{2+} release from ER, the cells were challenged with an agonist that, trough interaction with G protein coupled receptors, evokes a rapid discharge from IP_3Rs. The bars in the graph show the extent of the reduction in the mean rate of Ca^{2+} released induced by overexpressing m/p-AKT1 after cell stimulation, both for the first 50 sec. (upper graph) and for the maximum rate (lower graph). (C) HeLa cells were transfected with m/p-AKT1 or mock transfected in control cells. Western blot analysis shows that overexpression of constitutively active Akt does not affect the expression of different types of IP_3 receptors.

5.2.2 Cytosolic and mitochondrial Ca^{2+} response to agonist stimulation is strongly impaired in m/p-AKT1 expressing cells

The effect of m/p-AKT1 expression on the cytosolic Ca^{2+} signal elicited by agonist stimulation was investigated using cytosolic aequorin. Both in control and m/p-AKT1-transfected cells, histamine stimulation causes a rapid rise in cytoplasmic $[Ca^{2+}]_{cyt}$, followed by a gradually declining sustained plateau. In m/p-AKT1-transfected cells, the $[Ca^{2+}]_{cyt}$ increases evoked by stimulation with histamine are significantly smaller than in controls (peak amplitude 1.07 ± 0.03 vs 2.72 ± 0.04 μM; n = 14) (Fig. 32 A). Then we evaluated whether m/p-AKT1 could affect Ca^{2+} handling in mitochondria, an important site for decoding cellular Ca^{2+} signals and in particular Ca^{2+} signals regulating apoptosis. Both in control and m/p-AKT1-transfected cells, histamine stimulation caused a large, rapid rise in $[Ca^{2+}]_{mt}$, that returned to almost basal levels in approx 1 min. However, in m/p-AKT1-transfected cells, the $[Ca^{2+}]_{mt}$ increases evoked by stimulation with histamine were drastically smaller than in controls (peak amplitude 76.82 ± 3.4 μM control, 22.84 ± 2.2 μM m/p-AKT1, n = 18) (Fig. 32 B).

Taken together, these data show that m/p-AKT1 globally affects cellular Ca^{2+} signaling probably acting on the ER Ca^{2+} release machinery.

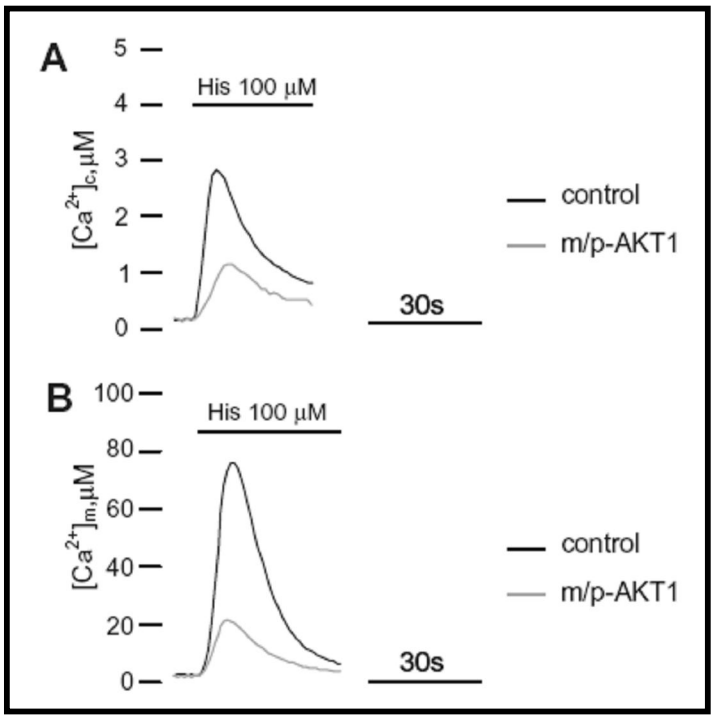

Fig. 32: Alteration of cytosolic and mitochondrial Ca^{2+} homeostasis in Akt-overexpressing cells. (A) Cytosolic Ca^{2+} homeostasis in control and m/p-AKT1-overexpressing HeLa cells. (B) Mitochondrial Ca^{2+} homeostasis in control and m/p-AKT1-overexpressing HeLa cells. Where indicated, the cells were stimulated with 100 μM histamine.

5.2.3 Akt overexpression protects against Ca^{2+}-mediated cell death

Mitochondrial Ca^{2+} uptake has been shown to be a fundamental factor in the activation of the intrinsic apoptotic pathway and in sensitizing the response to several apoptotic stimuli [33, 36, 151]. Reduction of mitochondrial Ca^{2+} accumulation by m/p-AKT1 thus might result in diminished cellular sensitivity to Ca^{2+}-mediated apoptosis. Therefore, we applied oxidative stress and arachidonic acid to induce apoptosis in HeLa cells, as they act through mitochondrial Ca^{2+} overload and ensuing activation of the intrinsic apoptotic pathway. HeLa cells were transiently transfected with mitochondrially targeted GFP alone (control) or in combination with m/p-AKT1 (m/p-AKT1), and 36 h after transfection the cells were treated with (1 mM) H_2O_2 or (80 μM) arachidonic acid. After 3 h incubation with the apoptotic stimulus of interest, and elimination of dead cells we observed a substantial increase in the proportion of m/p-AKT1-expressing cells after treatment (H_2O_2: 25.4 ± 5.11% increase in m/p-AKT1/mtGFP-overexpressing cells, n = 11; arachidonic acid: 19.67 ± 6.04% increase in m/p-AKT1/ mtGFP-overexpressing cells, n = 9. $p < 0.05$) (Fig. 33 A). In this experimental setup positive changes in the percentage of surviving transfected cells indicates protection against the apoptotic stimulus by the overexpressed protein, while reduction provides evidence for its proapoptotic effect, thus Akt protected a significant number of cells from H_2O_2 and arachidonic acid.

These data were confirmed by the direct measurement of caspase activity in H_2O_2 and arachidonic acid treated cells, showing a marked reduction of caspase-3 activity in m/p-AKT1 overexpressing cells (Fig. 33 B).

These results provided evidence that the m/p-AKT1-induced reduction of ER Ca^{2+} release increases the threshold for Ca^{2+}-mediated apoptosis.

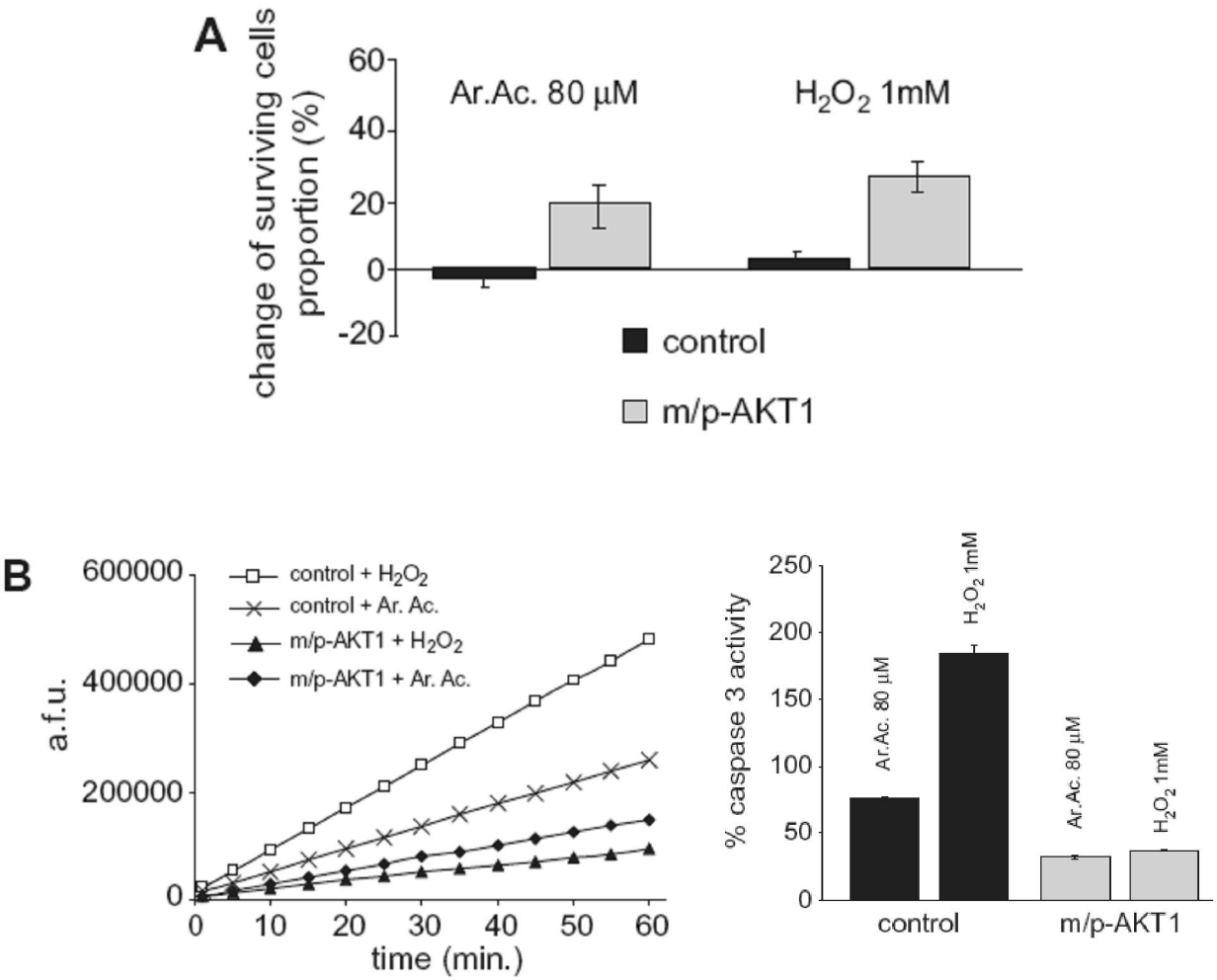

Fig. 33: Effect of Akt on cell death induced by Ca^{2+}-dependent apoptotic stimuli. (A) HeLa cells were co-transfected with mtGFP and m/p-AKT1 or mtGFP alone in control cells. At 36 h post-transfection, cells were treated with arachidonic acid (80 µM) and H_2O_2 (1 mM) for 4 h. The data show the change of percentage of GFP fluorescent cells among the whole cell population (determined by phase contrast microscopy), averaging values obtained by analyzing more than 50 fields. (B) HeLa cells were transfected and treated at the same manner of (A), and then aliquots of cells were centrifuged and lysates were assayed for caspase-3 activity as described in section 6. The left panel shows representative traces of a singular experiment. The data are the mean of different angular coefficients ± SE. of 5 independent experiments; the bars in the graph (right panel) show the change of percentage of caspase-3 activation compared to untreated cells.

5.2.4 Akt inhibits $[Ca^{2+}]_{cyt}$ increases induced by H_2O_2 and arachidonic acid

Apoptosis induced by H_2O_2 and arachidonic acid is triggered, or enhanced, by the release of Ca^{2+} from ER [152, 153]. Thus, we investigated whether m/p-AKT1, acting on

IP_3Rs, had a direct effect on cytosolic apoptotic Ca^{2+} signals triggered by these apoptotic stimuli.

Given that aequorin is not accurate enough to reveal small increases of $[Ca^{2+}]$, i.e. those expected in the cytosol after apoptotic stimulation, the $[Ca^{2+}]_{cyt}$ was measured with the fluorescent indicator Fura-2/AM [154]. In these experiments, in order to identify m/p-AKT1-overexpressing cells in single cell imaging experiments, the cells were co-transfected with mtGFP [57]. GFP-positive cells were distinguished from controls by the typical fluorescence emitted upon illumination with blue light. As shown in Fig. 33, treatment with 1 mM H_2O_2 (Fig. 34 A) or 80 μM arachidonic acid (Fig. 34 B) caused a $[Ca^{2+}]_{cyt}$ elevation, that gradually increased with time (Fig. 34). The simplest explanation for these results is that, as well as in the case of ceramide treatment, also these apoptotic stimuli caused a progressive release of Ca^{2+} from intracellular stores, thereby directly causing a $[Ca^{2+}]_{cyt}$ rise and activating capacitative Ca^{2+} influx, that in turn is responsible for maintaining a long lasting $[Ca^{2+}]_{cyt}$ plateau. Interestingly, in m/p-AKT1-transfected cells, the $[Ca^{2+}]_{cyt}$ increases evoked by stimulation with H_2O_2 and arachidonic acid were significantly smaller than in controls.

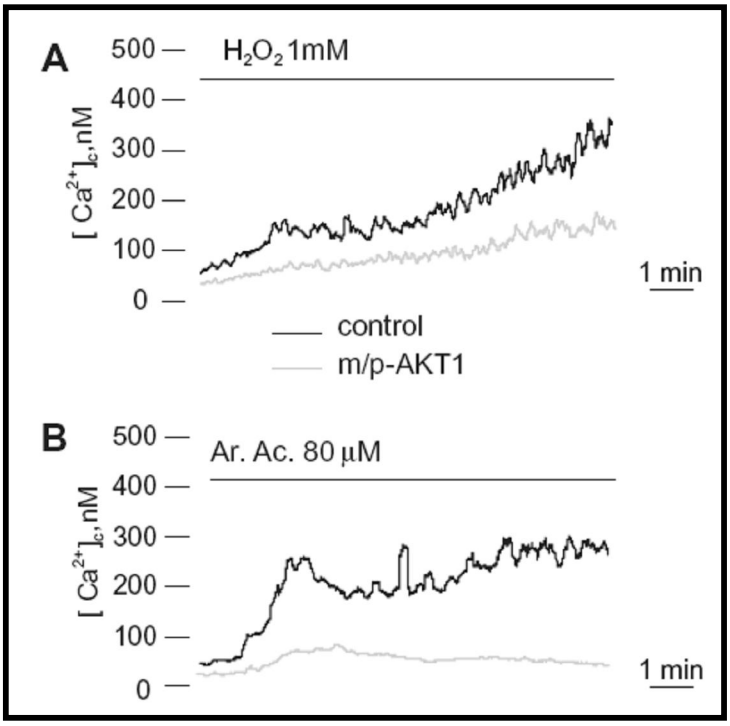

Fig. 34: Akt reduces $[Ca^{2+}]_{cyt}$ elevation generated by H_2O_2 and arachidonic acid. Effects of m/p-AKT1 on $[Ca^{2+}]_{cyt}$ increase induced by H_2O_2 (A) and Ar. Ac. (B). HeLa cells were loaded with the Ca^{2+} indicator Fura-2/AM and $[Ca^{2+}]_{cyt}$ changes were measured as details in section 6. The coverslips with the cells were maintained in 1 mM Ca^{2+}/KRB and, where indicated, the cells were challenged with 1mM H_2O_2 or 80 μM arachidonic acid. The traces show the calibrated $[Ca^{2+}]_{cyt}$ values. Experiments were repeated at least 5 times.

5.3 Discussion

Virtually in all eukaryotic cells the dynamic regulation of $[Ca^{2+}]_{cyt}$ is fundamental for cell life [1, 147]. In distinction to the other messengers, several organelles diffused throughout the cell can sequester Ca^{2+} and, in response to appropriate signals, release it back into the cytoplasm. Intracellular Ca^{2+} stores play an essential role in completing this regulation. The most important intracellular Ca^{2+} store is represented by the ER in non-muscle cells, and by its specialized counterpart, the sarcoplasmic reticulum, in muscle cells [40]. The Ca^{2+} channels responsible for the rapid release of Ca^{2+} from the ER in response to extracellular stimuli are the families of IP_3Rs [144]. Coordinated activation of these receptors is responsible for the generation of elementary and global (oscillating or persistent) Ca^{2+} signals observed in the cytosol [77, 155, 156].

Strong evidence has been also accumulated supporting a central role of Ca^{2+} in the regulation of cell death [120]. Recently it has been recognized, that modification of the ER Ca^{2+} pool may itself be involved in the initiation and regulation of the apoptotic process. As to ER Ca^{2+} release, it has been shown that owing to the efficient Ca^{2+} signal transmission between ER and mitochondria, ER Ca^{2+} release via IP_3R play a pivotal role in transmitting apoptotic Ca^{2+} signals into mitochondria [157, 158] and can sensitize to ceramide induced apoptosis [34, 151]. The involvement of IP_3Rs in sensitisation to apoptotic stimuli has been shown also by transgenic and anti-sense techniques. Thus, IP_3R-deficient lymphocytes are resistant to a large panel of apoptosis inducers [159] and anti-sense oligonucleotide-mediated downregulation of IP_3R decreases the cell death of glucocorticoid-treated T cells [160] and NGF-depleted neurons [157]. Akt has been found associated to ER membranes [161] and IP_3Rs can be phosphorylated by the well known apoptotic inhibitor Akt kinase [143].

The data presented here show that overexpression of m/p-AKT1 did not change the steady-state $[Ca^{2+}]_{er}$ level. In contrast, after stimulation with histamine we observed a dramatic reduction in the speed of Ca^{2+} release, without any changes of the IP_3R expression levels. Thus we can conclude that Akt was regulating IP_3R activity. This modulation of IP_3R activity resulted in an inhibition of agonist-induced Ca^{2+} release as we can observed measuring the cytosolic and mitochondrial Ca^{2+} responses.

More interestingly for an antiapoptotic protein such as Akt, its overexpression significantly blunted the $[Ca^{2+}]_{cyt}$ increases induced by H_2O_2 and arachidonic acid. This apoptotic protocol was chosen because shown to act through Ca^{2+} and, in our hands, Akt was highly efficient in protecting cells from death induced by these stimuli.

At this stage we can not ascribe the alterations of ER Ca^{2+} release to a direct Akt-dependent phosphorylation of the IP_3R. Indeed, in a recent work, Joseph and colleagues reported as the Ca^{2+} flux properties of IP_3R mutants in their Akt substrate motif did not reveal any modification of channel function under agonist stimulation [143]. A possibility is that m/p-AKT1 phosphorylates other proteins interacting with the IP_3Rs and in turn the phosphorylation state of these proteins regulates the IP_3-mediated Ca^{2+} channel activity of IP_3Rs. However, and probably more interestingly for a pro-survival protein, the Akt-dependent IP_3R phosphorylation appears functional to suppress the activation of cell death program triggered by apoptotic stimuli [143]. In agreement with this observation, our data clearly demonstrated that the overexpression of m/p-AKT1 chimera is efficient in reducing significantly the apoptotic Ca^{2+} signals induced by H_2O_2 and arachidonic acid.

Thus, these observations may provide one mechanism of Akt to restrain the apoptotic effects of Ca^{2+} (Fig. 35).

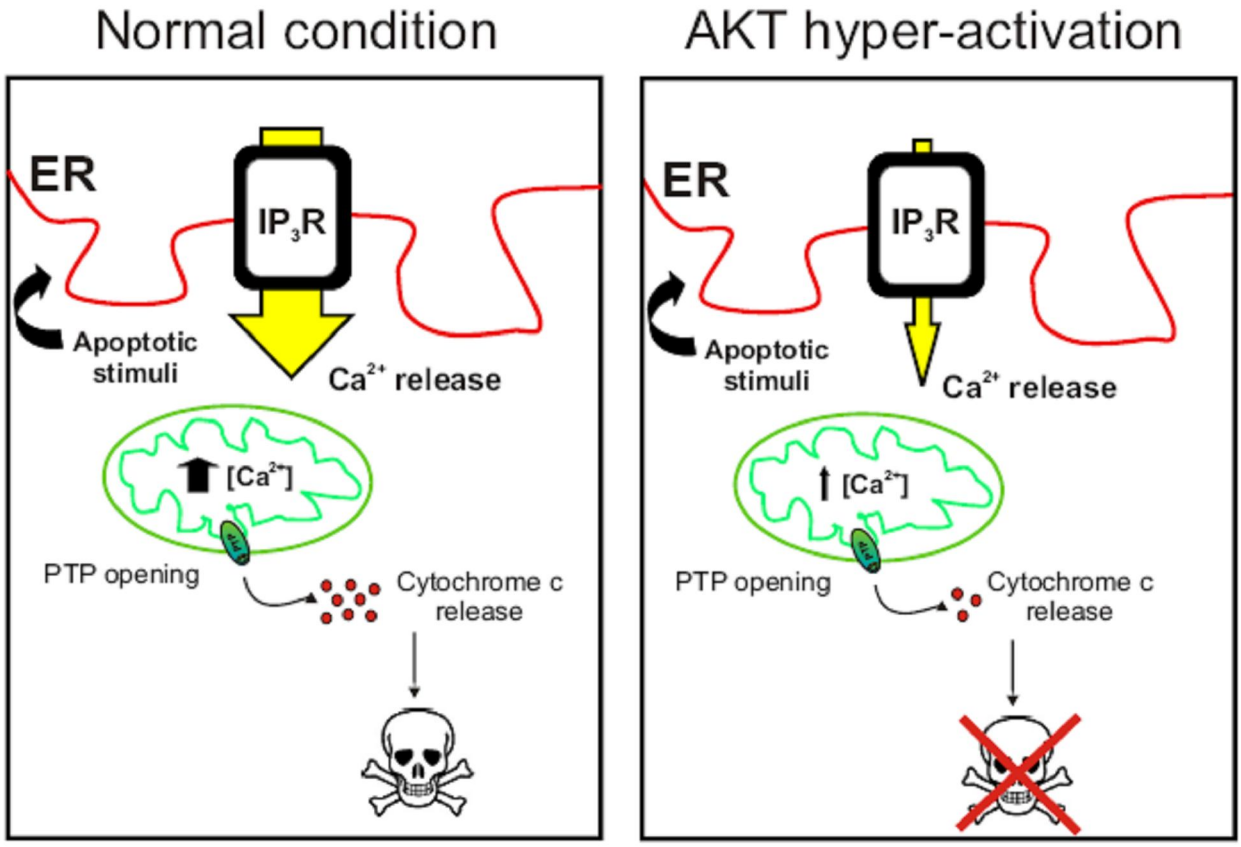

Fig. 35: Schematic model of Akt ability to protect cells from apoptosis through inhibition of Ca^{2+} release from IP_3R.

6. Materials and methods

6.1 Cell culture, infection and transfection

HeLa cells were cultured in Dulbecco's modified Eagle's medium (DMEM) supplemented with 10% fetal bovine serum (FBS), in 75-cm^2 Falcon flasks. For the aequorin experiments, the cells were seeded onto 13-mm glass coverslips and allowed to grow to 75% confluence. At this stage, transfection with 4 μg of total DNA (3 μg of indicated expression plasmids + 1 μg of AEQ) was carried out as previously described [63].

In order to measure $[ATP]_{mt}$ (Fig. 23), we worked similarly to aequorin experiments, using 4 μg of total DNA (3 μg of Fhit + 1 μg of mtLUC).

For experiments with Fura-2A/M (Fig. 23, 33), TMRM (Fig. 22), mitochondrial structure (Fig. 22) and apoptotic counts (Fig. 25, 32), cells were seeded on 24 mm coverslips and co-transfected 1:1 ratio with plasmid of interest and mtGFP, for a total amount of 8 μg of DNA.

For experiments with mtRP probe (Fig. 23 B), cells were seeded on 24 mm coverslips and co-transfected 3:1 (control: 6 μg empty vector + 2 μg mtRP; Fhit: 6 μg Fhit + 2 μg mtRP)

For Fhit shRNA silencing in HeLa cells, lentiviral (shRNA Fhit: shRNAFhit-pLKO.1) vectors were used, in association with adenoviral vectors for the expression of the aequorin probes (mtAEQ-pAdEasy).

All measurements were performed 36 h after transfection.

MEFs derived from wild-type p66Shc -/- and Pin1 -/- mice were grown in Dulbecco's modified Eagle's medium (DMEM), supplemented with 10% fetal bovine serum (FBS), in 75cm^2 Falcon flasks. For aequorin measurements, the cells were seeded before transfection onto 13 mm glass coverslips and allowed to grow to 50% confluence. At this stage, the cells were infected with the adenovirus expressing the appropriate chimera, as previously described [162]. For analyzing mitochondrial structure and PKC β translocation, the cells (seeded onto 24 mm coverslips) were transfected with mtGFP using lipofectamine (Invitrogen) or infected with an adenoviral vector driving PKCβ-GFP expression.

Pin1 over-expression in MEFs wt was performed with lipofectamine (Invitrogen).

For retrieval infections, we used a PINCO vector expressing the p66Shc moiety of interest and GFP from an internal CMV promoter. MEFs derived from p66Shc- /- mice were infected with vector alone, p66Shc wt, the non-phosphorylatable mutant p66ShcS36A

or the p66ShcE132Q-E133Q mutant (p66Shcqq), incapable of binding cytochrome c, as described previously [71, 76].

The efficiency of infection (90%) was determined by FACS analysis of GFP positive cells 48 h after infection.

A549 cells were maintained in RPMI-1640 medium plus 10% FBS.

For Fhit overexpression in A549, adenoviral (AdFhit: Fhit-His-6pAdenoVator-CMV5-IRESGFP, AdmtGFP: mtGFP-pAdEasy) vectors were used, in association with adenoviral vectors for the expression of the aequorin probes (AdmtAEQ).

6.2 Construction of mtFhit chimera

For constructing mtFhit, an in frame *Hin*dIII site and the HA1 tag were added via suitable PCR primers, then the HA-Fhit coding sequence was ligated to the mitochondrial targeting sequence (derived from subunit VIII of COX) excised from mtAEQ [45]. The final construct was cloned into the pcDNA3.1 expression vector.

6.3 Aequorin measurements

For cytAEQ and mtAEQ 24 hours after transfection, transfected aequorin was reconstituted by incubating the cells for 1 to 3h with 5 μM coelenterazine in DMEM supplemented with 1% fetal calf serum in a 5% CO_2 atmosphere.

For erAEQ, before the reconstitution it is necessary to drastically reduce the Ca^{2+} content of the endoplasmic reticulum. To this end, the cells were incubated for 1 h at 4 ^{o}C (in order to preserve membranes integrity), in KRB (Krebs-Ringer modified buffer: 125 mM NaCl, 5 mM KCl, 1 mM Na_3PO_4, 1 mM $MgSO_4$, 5.5 mM glucose, 20 mM HEPES, pH 7.4, 37^{o}C) supplemented with coelenterazine 5 μM, the Ca^{2+} ionophore ionomycin (5 μM) and 600μM EGTA. After this incubation the cells were extensively washed with KRB supplemented with 2% BSA (bovine serum albumin) and 1mM EGTA. During the experiments, the cells were perfused with modified Krebs-Ringer buffer (KRB) (125 mM NaCl, 5 mM KCl, 1mM Na_3PO_4, 1 mM $MgSO_4$, 5.5 mM glucose, 20 mM HEPES, pH 7.4 at 37°C), supplemented with 1 mM $CaCl_2$ (KRB/Ca^{2+}) and challenged with agonists and drugs added to the same medium.

In the experiments with permeabilized cells, a buffer mimicking the cytosolic ionic composition, ("intracellular buffer", IB) was employed: 140 mM KCl, 10 mM NaCl, 1 mM K_3PO_4, 5.5 mM glucose, 2 mM $MgSO_4$, 1 mM ATP, 2 mM sodium succinate, 20 mM Hepes (pH 7.05 at 37°C). The experiments were terminated by lysing the cells with 100μM digitonin in a hypotonic Ca^{2+}-rich solution (10 mM $CaCl_2$ in H_2O), thus discharging the remaining aequorin pool. After transfer to the luminometer chamber, Ca^{2+} uptake into mitochondria was initiated by replacing IB/EGTA with IB containing a 2 mM EGTA-buffered [Ca^{2+}] of 1 μM, prepared as elsewhere described [163]. The light signal was collected and calibrated into [Ca^{2+}] values as previously described [46, 48, 63].

In brief, a 13 mm-round coverslip with the transfected cells was placed in a perfused, thermostatted chamber, placed in the close proximity of a low-noise photomultiplier, with built-in amplifier-discriminetor. The output of the discriminator was captured by a Thorn-EMI photon counting board and stored in an IBM-compatible computer for further analyses. The aequorin luminescence data werte calibrated off-line into [Ca^{2+}] values, using a computer algorithm based on the Ca^{2+} response curve of wild-type and mutant aequorins, as previously described [46, 48].

6.4 Luciferase measurements

Cell luminescence was measured in the same purpose-built luminometer used for the aequorin measurements. Cells were constantly perfused with KRB, supplemented with 1 mM $CaCl_2$ and 20 μM luciferin. All additions were made to this medium, as specified in the figure legend. The light output of a coverslip of transient trasfected cells was in the range of 1,000 - 10,000 counts per second (cps) versus a background lower than 10 cps. All compounds employed in the experiments were tested for non-specific effects on the luminescence and none were observed.

6.5 Fura-2/AM measurements

Cytosolic free Ca^{2+} concentration was evaluated using fluorescent Ca^{2+} indicator Fura-2/AM (Molecular Probes, Inc.). Briefly, cells were incubated in medium supplemented with 2.5 μM Fura-2/AM for 30 min, washed with KRB to remove extracellular probe, supplied with preheated KRB (supplemented with 1 mM $CaCl_2$), and placed in a thermostated incubation chamber at 37 °C on the stage of an inverted fluorescence microscope (Zeiss Axiovert 200). Dynamic video imaging was performed using MetaFluor software (Universal Imaging Corp.). Fluorescence was measured every 100 ms with the excitation wavelength alternating between 340 and 380 nm and the emission fluorescence being recorded at 510 nm. At the end of the experiment, a region free of cells was selected, and one averaged background frame was collected at each excitation wavelength for background correction. The $[Ca^{2+}]_c$ was calculated by the ratio method using the equation: $[Ca^{2+}]_c = Kd\ (R - R_{min}) / (R - R_{max}) \times Sf2 / Sf1$ where Kd is dissociation constant of Fura-2/AM for (Ca^{2+}) taken as 240 nM at 37 °C, R is ratio of fluorescence for Fura-2/AM at the two excitation wavelengths, F340/F380, R_{max} is ratio of fluorescence in the presence of excess of calcium obtained by lysing the cells with 10 μM ionomycin (Sigma Aldrich), R_{min} is ratio of fluorescence in the presence of minimal calcium obtained by lysing the cells and then chelating all the Ca^{2+} with 0.5 M EGTA, Sf2 is fluorescence of Ca^{2+} free form of Fura-2/AM at 380nm excitation wavelength and Sf1 is fluorescence of Ca^{2+} bound form of Fura-2/AM at 380 nm excitation wavelength.

6.6 Caspase 3 assay

Cells were centrifuged (1000 g for 5 min.) and washed once in phosphate-buffered saline. The enzcheck® caspase-3 assay kit # 2 by Molecular Probes was used for determination of caspase-3 activity. Lysate (20 μg), resuspended in a final volume of 100 μl, was assayed using Wallac 1420 Victor 3 multitask plate reader (Perkin Elmer, Inc.).

6.7 Apoptotic counts

The mtGFP fluorescent marker was coexpressed with plasmid of interest, and effect on cell survival was estimated by calculating the fraction of fluorescent cells in the

surviving population after an apoptotic challenge. Ten different fields per coverslip (taken with an objective 20 X) were analyzed, and a mean per condition was extracted.

The results were obtained from at least 3 coverslips per condition and expressed as variation in the percentage of fluorescent cells.

6.8 Annexin V assay

After treatment with apoptotic stimulus, control cells or cells overexpressing the protein of interest, were incubated with the Alexa Fluor 488 Annexin V antibody kit, according to the instruction of the producer (Molecular Probes), and then sorted with a FACStar flow cytometer (Becton Dickinson).

6.9 Cell cycle analysis

For cell cycle analyses, control or transfected cells were washed twice with cold ethanol, then resuspended in 0.1 mg/mL propidium iodide/Triton X-100 staining solution (0.1% Triton X-100, 20 mg/ml DNase-free RNase A), and analyzed by flow cytometry, as described above.

6.10 Microscopic analysis of mitochondrial structure and PKC β translocation

Images of mitochondrial structure and PKC translocation were obtained by visualizing mtGFP or PKC β-GFP chimera, using a digital imaging system based on a Zeiss Axiovert 200 fluorescence microscope equipped with a back-illuminated CCD camera (Roper Scientific, USA), excitation and emission filterwheels (Sutter Instrument Company, USA) and piezoelectric motoring of the z stage (Physik Instrumente, GmbH & Co., Germany). The data were acquired and processed using the MetaMorph analysis program (Universal Imaging Corporation, USA). For computational deblurring, a stack of images through the z plane was acquired (200 ms/image; 20 plans 0.5 µm apart) and processed using the EPR software developed by the Biomedical Imaging Group of the University of Massachusetts Medical School (Worcester, MA, USA) [66].

6.11 Mitochondrial membrane potential measurements

Mitochondrial membrane potential ($\Delta\Psi_m$) was measured using 10 nM tetramethyl rhodamine methyl ester (TMRM) on a confocal microscope (model LSM 510; Carl Zeiss MicroImaging, Inc.). FCCP (carbonyl cyanide *p*-trifluoromethoxyphenylhydrazone), to collapses mitochondrial $\Delta\Psi$. The signal was collected as total emission >570 nm.

6.12 mtRP measurements

Mitochondrial Hot Spots was measured used mtRP probe (transfected as indicated in section 6.1) on a digital imaging system based on a Zeiss Axiovert 200 fluorescence microscope. Excitation λ is at 410/490 nm. Specifically, for the images of Fig. 24 B, the first deconvoluted image in the series was used as threshold to create a binary mask, allowing visualization of only the mitochondrial network. ΔF/F images were calculated from the original images and were multiplied by the binary mask with the image arithmetic functions of the MetaMorph software. Image scaling and pseudocolors were applied with the MetaFluor Analyst software of the Meta Imaging software package.

6.13 Immunofluorescence

Cells were fixed with 4% formaldehyde for 10 min at RT. After washing twice with phosphate-buffered saline (PBS), cells were permeabilized with 0.2% Triton X-100 in PBS (PBST) at RT for 10 min and treated with PBST containing 5% skim milk (PBSTM) at RT for 1 h. Cells were incubated with a monoclonal antibody to Fhit (Zymed Laboratories, 1 μg/ml, Fig. 21) or with monoclonal antibody to HA1 (Santa Cruz Biotechnology, 5 μg/ml, Fig. 25) in PBSTM overnight at 4 °C, washed three times with PBS, and then incubated with Alexa-546-conjugated anti-rabbit IgG (Molecular Probes) at RT for 1 h. After washing five times with PBS, slides were mounted in Vectashield (Vector Laboratories). Fluorescent images were taken through an inverted microscope with a 63 X Carl Zeiss objective.

6.14 Isolation of mitochondria

Cells were washed twice with PBS, resuspended and homogenized in a buffer containing 250 mM sucrose, 1 mM EGTA, 50 mM Tris-HCl, 1mM DTT, protease inhibitor cocktail, pH 7.4 with 40 μg of digitonin per ml in a glass homogenizer. Homogenate was centrifuged at 1,500 x g for 5 min twice. The final supernatant was collected and centrifuged at 10,000 x g for 10 min, the mitochondrial pellets were resuspended with homogenization buffer (without digitonin) and centrifuged again at 10,000 x g for 10 min. Mitochondrial pellets were disrupted in 100 μl lysis buffer at 4 °C, incubated 30 min. on ice and then centrifuged at 17,000 x g for 30 min. Protein concentration in the supernatant was determined by the Bio-Rad protein estimation kit.

6.15 In vitro binding (Fig.19 A)

In *GST-pull-down* assays ΦNX cells overexpressing p66Shc cDNA and p66ShcS36A mutant non irradiated or UVc-irradiated (50 J/m^2 for 10 min), were lysed in JS buffer (20 mMTris-HCl pH 7.8, 50 mM NaF, 50 mM NaCl, 30 mM $Na_4P_2O_7$, 1% Triton X-100) containing freshly added protease inhibitors (1 mM phenylmethylsulfonylfluoride, 10 μg/ml leupeptin and 5 mg/ml aprotinin). Lysates were clarified by centrifugation at 4 °C and incubated (1 mg) with 10 μl of agarose beads containing GST-Pin1 proteins or control GST for 2 hours at 4 °C. In the case of phosphatase treatment, 20 U/ml of CIP (New England Biolabs) were added to the lysates and the reaction was continued for 30 min. at 30 °C.

The precipitated proteins were washed five times in the same buffer and subjected to immunoblotting analysis with anti-Shc antibodies.

6.16 Immunoprecipitation (Fig. 16 C)

MEFs maintained in growth conditions (10% FCS) after 24 hours pre-incubation with 5 μM hispidin (where indicated) were challenged for 10 min with 500 μM H_2O_2 or 100 ng/ml TPA. Cellular extracts were lysed in JS buffer (20 mM Tris-HCl ph 7.8, 50 mM NaF, 50 mM NaCl, 30 mM $Na_4P_2O_7$, 5 mM Sodium Orthovanadate, 1% Triton X-100) containing protease inhibitors (PMSF, leupeptin and aprotinin), immunoprecipitated with polyclonal anti-Shc antibodies (Transduction Laboratories), and analyzed by immunoblotting with a

specific monoclonal antiphospho-(Ser36) p66Shc antibodies (Alexis) or with anti-Shc antibodies (Tansduction Laboratories).

6.17 Immunoblot

Lysates were centrifuged at 11,000 × g for 20 min, and then the supernatants were collected and conserved at -80 °C. The proteins (5-30 μg) were separated on 7-12% polyacrylamide gel and transferred to Nitrocellulose membrane.

Different antibodies used in this thesis are:

- PKCβ (BD Biosciences), dilution 1:500
- (αSH2)p66Shc (Santa Cruz Biotechnology), dilution 1:500
- αpS36p66Shc (Calbiochem), dilution 1:1000
- Actin (Cell Signalling), dilution 1:1000
- VDAC (Cell Signalling), dilution 1:1000
- Fhit (Zymed Laboratories), dilution 1:5000
- β-tubulin (Santa Cruz Biotechnology), dilution 1:1000
- IP_3R I (Santa Cruz Biotechnology), dilution 1:200
- IP_3R III (BD Biosciences), dilution 1:1000

7. Reference list

1. Berridge, M.J., P. Lipp, and M.D. Bootman, *The versatility and universality of calcium signalling.* Nat Rev Mol Cell Biol, 2000. **1**(1): p. 11-21.
2. Clapham, D.E., *Intracellular calcium. Replenishing the stores.* Nature, 1995. **375**(6533): p. 634-5.
3. Morgan, A.J. and A.P. Thomas, *Single cell and subcellular measurement of intracellular Ca2+ concentration ([Ca2+]i).* Methods Mol Biol, 1999. **114**: p. 93-123.
4. Jaffe, L.F. and R. Creton, *On the conservation of calcium wave speeds.* Cell Calcium, 1998. **24**(1): p. 1-8.
5. Petersen, O.H., D. Burdakov, and A.V. Tepikin, *Regulation of store-operated calcium entry: lessons from a polarized cell.* Eur J Cell Biol, 1999. **78**(4): p. 221-3.
6. Bennett, D.L., et al., *Expression and function of ryanodine receptors in nonexcitable cells.* J Biol Chem, 1996. **271**(11): p. 6356-62.
7. Giannini, G., et al., *The ryanodine receptor/calcium channel genes are widely and differentially expressed in murine brain and peripheral tissues.* J Cell Biol, 1995. **128**(5): p. 893-904.
8. Brini, M., *Plasma membrane Ca(2+)-ATPase: from a housekeeping function to a versatile signaling role.* Pflugers Arch, 2009. **457**(3): p. 657-64.
9. Brini, M. and E. Carafoli, *Calcium pumps in health and disease.* Physiol Rev, 2009. **89**(4): p. 1341-78.
10. Korczak, B., et al., *Structure of the rabbit fast-twitch skeletal muscle Ca2+-ATPase gene.* J Biol Chem, 1988. **263**(10): p. 4813-9.
11. MacLennan, D.H., et al., *Fast-twitch and slow-twitch/cardiac Ca2+ ATPase genes map to human chromosomes 16 and 12.* Somat Cell Mol Genet, 1987. **13**(4): p. 341-6.
12. Zhang, Y., et al., *Characterization of cDNA and genomic DNA encoding SERCA1, the Ca(2+)-ATPase of human fast-twitch skeletal muscle sarcoplasmic reticulum, and its elimination as a candidate gene for Brody disease.* Genomics, 1995. **30**(3): p. 415-24.
13. Van den Bosch, L., et al., *Regulation of splicing is responsible for the expression of the muscle-specific 2a isoform of the sarco/endoplasmic-reticulum Ca(2+)-ATPase.* Biochem J, 1994. **302 (Pt 2)**: p. 559-66.

14. Zarain-Herzberg, A., D.H. MacLennan, and M. Periasamy, *Characterization of rabbit cardiac sarco(endo)plasmic reticulum Ca2(+)-ATPase gene.* J Biol Chem, 1990. **265**(8): p. 4670-7.
15. Burk, S.E., et al., *cDNA cloning, functional expression, and mRNA tissue distribution of a third organellar Ca2+ pump.* J Biol Chem, 1989. **264**(31): p. 18561-8.
16. Odermatt, A., et al., *Sarcolipin regulates the activity of SERCA1, the fast-twitch skeletal muscle sarcoplasmic reticulum Ca2+-ATPase.* J Biol Chem, 1998. **273**(20): p. 12360-9.
17. Simmerman, H.K. and L.R. Jones, *Phospholamban: protein structure, mechanism of action, and role in cardiac function.* Physiol Rev, 1998. **78**(4): p. 921-47.
18. Carafoli, E., *Biogenesis: plasma membrane calcium ATPase: 15 years of work on the purified enzyme.* Faseb J, 1994. **8**(13): p. 993-1002.
19. Philipson, K.D. and D.A. Nicoll, *Sodium-calcium exchange.* Curr Opin Cell Biol, 1992. **4**(4): p. 678-83.
20. Hilgemann, D.W., D.A. Nicoll, and K.D. Philipson, *Charge movement during Na+ translocation by native and cloned cardiac Na+/Ca2+ exchanger.* Nature, 1991. **352**(6337): p. 715-8.
21. Cervetto, L., et al., *Extrusion of calcium from rod outer segments is driven by both sodium and potassium gradients.* Nature, 1989. **337**(6209): p. 740-3.
22. Rizzuto, R., et al., *Ca(2+) transfer from the ER to mitochondria: when, how and why.* Biochim Biophys Acta, 2009. **1787**(11): p. 1342-51.
23. Moore, C.L., *Specific inhibition of mitochondrial Ca++ transport by ruthenium red.* Biochem Biophys Res Commun, 1971. **42**(2): p. 298-305.
24. Griffiths, E.J., *Mitochondrial calcium transport in the heart: physiological and pathological roles.* J Mol Cell Cardiol, 2009. **46**(6): p. 789-803.
25. Moreau, B., C. Nelson, and A.B. Parekh, *Biphasic regulation of mitochondrial Ca2+ uptake by cytosolic Ca2+ concentration.* Curr Biol, 2006. **16**(16): p. 1672-7.
26. Green, D.R. and G. Kroemer, *The pathophysiology of mitochondrial cell death.* Science, 2004. **305**(5684): p. 626-9.
27. Danial, N.N. and S.J. Korsmeyer, *Cell death: critical control points.* Cell, 2004. **116**(2): p. 205-19.
28. Giacomello, M., et al., *Mitochondrial Ca2+ as a key regulator of cell life and death.* Cell Death Differ, 2007. **14**(7): p. 1267-74.

29. Hajnoczky, G., E. Davies, and M. Madesh, *Calcium signaling and apoptosis.* Biochem Biophys Res Commun, 2003. **304**(3): p. 445-54.
30. Nicotera, P. and S. Orrenius, *Ca2+ and cell death.* Ann N Y Acad Sci, 1992. **648**: p. 17-27.
31. Pinton, P. and R. Rizzuto, *Bcl-2 and Ca2+ homeostasis in the endoplasmic reticulum.* Cell Death Differ, 2006. **13**(8): p. 1409-18.
32. Biagioli, M., et al., *Endoplasmic reticulum stress and alteration in calcium homeostasis are involved in cadmium-induced apoptosis.* Cell Calcium, 2008. **43**(2): p. 184-95.
33. Pinton, P., et al., *The Ca2+ concentration of the endoplasmic reticulum is a key determinant of ceramide-induced apoptosis: significance for the molecular mechanism of Bcl-2 action.* Embo J, 2001. **20**(11): p. 2690-701.
34. Szalai, G., R. Krishnamurthy, and G. Hajnoczky, *Apoptosis driven by IP(3)-linked mitochondrial calcium signals.* Embo J, 1999. **18**(22): p. 6349-61.
35. Pinton, P., et al., *Reduced loading of intracellular Ca(2+) stores and downregulation of capacitative Ca(2+) influx in Bcl-2-overexpressing cells.* J Cell Biol, 2000. **148**(5): p. 857-62.
36. Chami, M., et al., *Caspase-dependent alterations of Ca2+ signaling in the induction of apoptosis by hepatitis B virus X protein.* J Biol Chem, 2003. **278**(34): p. 31745-55.
37. Schwab, B.L., et al., *Cleavage of plasma membrane calcium pumps by caspases: a link between apoptosis and necrosis.* Cell Death Differ, 2002. **9**(8): p. 818-31.
38. McCormack, J.G., A.P. Halestrap, and R.M. Denton, *Role of calcium ions in regulation of mammalian intramitochondrial metabolism.* Physiol Rev, 1990. **70**(2): p. 391-425.
39. Robb-Gaspers, L.D., et al., *Coupling between cytosolic and mitochondrial calcium oscillations: role in the regulation of hepatic metabolism.* Biochim Biophys Acta, 1998. **1366**(1-2): p. 17-32.
40. Rizzuto, R. and T. Pozzan, *Microdomains of intracellular Ca2+: molecular determinants and functional consequences.* Physiol Rev, 2006. **86**(1): p. 369-408.
41. Shimomura, O., F.H. Johnson, and Y. Saiga, *Extraction, purification and properties of aequorin, a bioluminescent protein from the luminous hydromedusan, Aequorea.* J Cell Comp Physiol, 1962. **59**: p. 223-39.
42. Inouye, S., et al., *Cloning and sequence analysis of cDNA for the luminescent protein aequorin.* Proc Natl Acad Sci U S A, 1985. **82**(10): p. 3154-8.

43. Nomura, M., et al., *A C-terminal proline is required for bioluminescence of the Ca(2+)-binding photoprotein, aequorin.* FEBS Lett, 1991. **295**(1-3): p. 63-6.
44. Watkins, N.J. and A.K. Campbell, *Requirement of the C-terminal proline residue for stability of the Ca(2+)-activated photoprotein aequorin.* Biochem J, 1993. **293 (Pt 1)**: p. 181-5.
45. Rizzuto, R., et al., *Rapid changes of mitochondrial Ca2+ revealed by specifically targeted recombinant aequorin.* Nature, 1992. **358**(6384): p. 325-7.
46. Montero, M., et al., *Monitoring dynamic changes in free Ca2+ concentration in the endoplasmic reticulum of intact cells.* Embo J, 1995. **14**(22): p. 5467-75.
47. Brini, M., et al., *Targeting of aequorin for calcium monitoring in intracellular compartments.* J Biolumin Chemilumin, 1994. **9**(3): p. 177-84.
48. Brini, M., et al., *Transfected aequorin in the measurement of cytosolic Ca2+ concentration ([Ca2+]c). A critical evaluation.* J Biol Chem, 1995. **270**(17): p. 9896-903.
49. Kendall, J.M., et al., *Engineering the CA(2+)-activated photoprotein aequorin with reduced affinity for calcium.* Biochem Biophys Res Commun, 1992. **187**(2): p. 1091-7.
50. Marsault, R., et al., *Domains of high Ca2+ beneath the plasma membrane of living A7r5 cells.* Embo J, 1997. **16**(7): p. 1575-81.
51. Rutter, G.A., et al., *Subcellular imaging of intramitochondrial Ca2+ with recombinant targeted aequorin: significance for the regulation of pyruvate dehydrogenase activity.* Proc Natl Acad Sci U S A, 1996. **93**(11): p. 5489-94.
52. Cody, C.W., et al., *Chemical structure of the hexapeptide chromophore of the Aequorea green-fluorescent protein.* Biochemistry, 1993. **32**(5): p. 1212-8.
53. Prasher, D.C., et al., *Primary structure of the Aequorea victoria green-fluorescent protein.* Gene, 1992. **111**(2): p. 229-33.
54. Tsien, R.Y., *The green fluorescent protein.* Annu Rev Biochem, 1998. **67**: p. 509-44.
55. Chalfie, M., et al., *Green fluorescent protein as a marker for gene expression.* Science, 1994. **263**(5148): p. 802-5.
56. Cubitt, A.B., et al., *Understanding, improving and using green fluorescent proteins.* Trends Biochem Sci, 1995. **20**(11): p. 448-55.
57. De Giorgi, F., et al., *Targeting aequorin and green fluorescent protein to intracellular organelles.* Gene, 1996. **173**(1 Spec No): p. 113-7.

58. Pollok, B.A. and R. Heim, *Using GFP in FRET-based applications.* Trends Cell Biol, 1999. **9**(2): p. 57-60.
59. Heim, R., A.B. Cubitt, and R.Y. Tsien, *Improved green fluorescence.* Nature, 1995. **373**(6516): p. 663-4.
60. Heim, R., D.C. Prasher, and R.Y. Tsien, *Wavelength mutations and posttranslational autoxidation of green fluorescent protein.* Proc Natl Acad Sci U S A, 1994. **91**(26): p. 12501-4.
61. Zolotukhin, S., et al., *A "humanized" green fluorescent protein cDNA adapted for high-level expression in mammalian cells.* J Virol, 1996. **70**(7): p. 4646-54.
62. Ward, W.W. and M.J. Cormier, *An energy transfer protein in coelenterate bioluminescence. Characterization of the Renilla green-fluorescent protein.* J Biol Chem, 1979. **254**(3): p. 781-8.
63. Rizzuto, R., et al., *Chimeric green fluorescent protein as a tool for visualizing subcellular organelles in living cells.* Curr Biol, 1995. **5**(6): p. 635-42.
64. Carrington, W.A., et al., *Superresolution three-dimensional images of fluorescence in cells with minimal light exposure.* Science, 1995. **268**(5216): p. 1483-7.
65. Lynch, R.M., et al., *Metabolic modulation of hexokinase association with mitochondria in living smooth muscle cells.* Am J Physiol, 1996. **270**(2 Pt 1): p. C488-99.
66. Rizzuto, R., W. Carrington, and R.A. Tuft, *Digital imaging microscopy of living cells.* Trends Cell Biol, 1998. **8**(7): p. 288-92.
67. ZhuGe, R., et al., *The influence of sarcoplasmic reticulum Ca2+ concentration on Ca2+ sparks and spontaneous transient outward currents in single smooth muscle cells.* J Gen Physiol, 1999. **113**(2): p. 215-28.
68. de Wet, J.R., et al., *Firefly luciferase gene: structure and expression in mammalian cells.* Mol Cell Biol, 1987. **7**(2): p. 725-37.
69. Kennedy, H.J., et al., *Glucose generates sub-plasma membrane ATP microdomains in single islet beta-cells. Potential role for strategically located mitochondria.* J Biol Chem, 1999. **274**(19): p. 13281-91.
70. Jouaville, L.S., et al., *Regulation of mitochondrial ATP synthesis by calcium: evidence for a long-term metabolic priming.* Proc Natl Acad Sci U S A, 1999. **96**(24): p. 13807-12.
71. Migliaccio, E., et al., *The p66shc adaptor protein controls oxidative stress response and life span in mammals.* Nature, 1999. **402**(6759): p. 309-13.

72. Pelicci, G., et al., *A novel transforming protein (SHC) with an SH2 domain is implicated in mitogenic signal transduction.* Cell, 1992. **70**(1): p. 93-104.
73. Trinei, M., et al., *A p53-p66Shc signalling pathway controls intracellular redox status, levels of oxidation-damaged DNA and oxidative stress-induced apoptosis.* Oncogene, 2002. **21**(24): p. 3872-8.
74. Nemoto, S., et al., *The mammalian longevity-associated gene product p66shc regulates mitochondrial metabolism.* J Biol Chem, 2006. **281**(15): p. 10555-60.
75. Orsini, F., et al., *The life span determinant p66Shc localizes to mitochondria where it associates with mitochondrial heat shock protein 70 and regulates trans-membrane potential.* J Biol Chem, 2004. **279**(24): p. 25689-95.
76. Giorgio, M., et al., *Electron transfer between cytochrome c and p66Shc generates reactive oxygen species that trigger mitochondrial apoptosis.* Cell, 2005. **122**(2): p. 221-33.
77. Bootman, M.D., P. Lipp, and M.J. Berridge, *The organisation and functions of local Ca(2+) signals.* J Cell Sci, 2001. **114**(Pt 12): p. 2213-22.
78. Rizzuto, R., P. Bernardi, and T. Pozzan, *Mitochondria as all-round players of the calcium game.* J Physiol, 2000. **529 Pt 1**: p. 37-47.
79. Duchen, M.R., *Mitochondria and Ca(2+)in cell physiology and pathophysiology.* Cell Calcium, 2000. **28**(5-6): p. 339-48.
80. Pinton, P., et al., *Long-term modulation of mitochondrial Ca2+ signals by protein kinase C isozymes.* J Cell Biol, 2004. **165**(2): p. 223-32.
81. Gopalakrishna, R. and S. Jaken, *Protein kinase C signaling and oxidative stress.* Free Radic Biol Med, 2000. **28**(9): p. 1349-61.
82. Bernardi, P., et al., *A mitochondrial perspective on cell death.* Trends Biochem Sci, 2001. **26**(2): p. 112-7.
83. Gonindard, C., et al., *Synthetic hispidin, a PKC inhibitor, is more cytotoxic toward cancer cells than normal cells in vitro.* Cell Biol Toxicol, 1997. **13**(3): p. 141-53.
84. Lu, K.P., Y.C. Liou, and X.Z. Zhou, *Pinning down proline-directed phosphorylation signaling.* Trends Cell Biol, 2002. **12**(4): p. 164-72.
85. Wulf, G., et al., *Phosphorylation-specific prolyl isomerization: is there an underlying theme?* Nat Cell Biol, 2005. **7**(5): p. 435-41.
86. Zacchi, P., et al., *The prolyl isomerase Pin1 reveals a mechanism to control p53 functions after genotoxic insults.* Nature, 2002. **419**(6909): p. 853-7.

87. Smith, W.W., et al., *Phosphorylation of p66Shc and forkhead proteins mediates Abeta toxicity.* J Cell Biol, 2005. **169**(2): p. 331-9.
88. Schriner, S.E., et al., *Extension of murine life span by overexpression of catalase targeted to mitochondria.* Science, 2005. **308**(5730): p. 1909-11.
89. Pandolfi, S., et al., *p66(shc) is highly expressed in fibroblasts from centenarians.* Mech Ageing Dev, 2005. **126**(8): p. 839-44.
90. Hajnoczky, G. and J.B. Hoek, *Cell signaling. Mitochondrial longevity pathways.* Science, 2007. **315**(5812): p. 607-9.
91. Huebner, K. and C.M. Croce, *FRA3B and other common fragile sites: the weakest links.* Nat Rev Cancer, 2001. **1**(3): p. 214-21.
92. Huebner, K. and C.M. Croce, *Cancer and the FRA3B/FHIT fragile locus: it's a HIT.* Br J Cancer, 2003. **88**(10): p. 1501-6.
93. Ohta, M., et al., *The FHIT gene, spanning the chromosome 3p14.2 fragile site and renal carcinoma-associated t(3;8) breakpoint, is abnormal in digestive tract cancers.* Cell, 1996. **84**(4): p. 587-97.
94. Toledo, G., et al., *Loss of FHIT protein expression is related to high proliferation, low apoptosis and worse prognosis in non-small-cell lung cancer.* Mod Pathol, 2004. **17**(4): p. 440-8.
95. Pekarsky, Y., et al., *FHIT as tumor suppressor: mechanisms and therapeutic opportunities.* Cancer Biol Ther, 2002. **1**(3): p. 232-6.
96. Zanesi, N., et al., *The tumor spectrum in FHIT-deficient mice.* Proc Natl Acad Sci U S A, 2001. **98**(18): p. 10250-5.
97. Dumon, K.R., et al., *FHIT gene therapy prevents tumor development in Fhit-deficient mice.* Proc Natl Acad Sci U S A, 2001. **98**(6): p. 3346-51.
98. Trapasso, F., et al., *Fhit interaction with ferredoxin reductase triggers generation of reactive oxygen species and apoptosis of cancer cells.* J Biol Chem, 2008. **283**(20): p. 13736-44.
99. Bernardi, P., et al., *The mitochondrial permeability transition from in vitro artifact to disease target.* Febs J, 2006. **273**(10): p. 2077-99.
100. Pinton, P., et al., *Calcium and apoptosis: ER-mitochondria Ca2+ transfer in the control of apoptosis.* Oncogene, 2008. **27**(50): p. 6407-18.
101. Rong, Y.P., et al., *Targeting Bcl-2-IP3 receptor interaction to reverse Bcl-2's inhibition of apoptotic calcium signals.* Mol Cell, 2008. **31**(2): p. 255-65.

102. White, C., et al., *The endoplasmic reticulum gateway to apoptosis by Bcl-X(L) modulation of the InsP3R.* Nat Cell Biol, 2005. **7**(10): p. 1021-8.
103. Berridge, M.J., M.D. Bootman, and H.L. Roderick, *Calcium signalling: dynamics, homeostasis and remodelling.* Nat Rev Mol Cell Biol, 2003. **4**(7): p. 517-29.
104. Hajnoczky, G., et al., *Decoding of cytosolic calcium oscillations in the mitochondria.* Cell, 1995. **82**(3): p. 415-24.
105. Gilabert, J.A. and A.B. Parekh, *Respiring mitochondria determine the pattern of activation and inactivation of the store-operated Ca(2+) current I(CRAC).* Embo J, 2000. **19**(23): p. 6401-7.
106. Hajnoczky, G., R. Hager, and A.P. Thomas, *Mitochondria suppress local feedback activation of inositol 1,4, 5-trisphosphate receptors by Ca2+.* J Biol Chem, 1999. **274**(20): p. 14157-62.
107. Giorgi, C., et al., *Structural and functional link between the mitochondrial network and the endoplasmic reticulum.* Int J Biochem Cell Biol, 2009. **41**(10): p. 1817-27.
108. Pinton, P., et al., *Biosensors for the detection of calcium and pH.* Methods Cell Biol, 2007. **80**: p. 297-325.
109. de Brito, O.M. and L. Scorrano, *Mitofusin 2 tethers endoplasmic reticulum to mitochondria.* Nature, 2008. **456**(7222): p. 605-10.
110. Rizzuto, R., et al., *Close contacts with the endoplasmic reticulum as determinants of mitochondrial Ca2+ responses.* Science, 1998. **280**(5370): p. 1763-6.
111. Szabadkai, G., et al., *Drp-1-dependent division of the mitochondrial network blocks intraorganellar Ca2+ waves and protects against Ca2+-mediated apoptosis.* Mol Cell, 2004. **16**(1): p. 59-68.
112. Filippin, L., et al., *Stable interactions between mitochondria and endoplasmic reticulum allow rapid accumulation of calcium in a subpopulation of mitochondria.* J Biol Chem, 2003. **278**(40): p. 39224-34.
113. Pacher, P. and G. Hajnoczky, *Propagation of the apoptotic signal by mitochondrial waves.* Embo J, 2001. **20**(15): p. 4107-21.
114. Scorrano, L., et al., *BAX and BAK regulation of endoplasmic reticulum Ca2+: a control point for apoptosis.* Science, 2003. **300**(5616): p. 135-9.
115. Szado, T., et al., *Phosphorylation of inositol 1,4,5-trisphosphate receptors by protein kinase B/Akt inhibits Ca2+ release and apoptosis.* Proc Natl Acad Sci U S A, 2008. **105**(7): p. 2427-32.

116. Ishii, H., et al., *Components of DNA damage checkpoint pathway regulate UV exposure-dependent alterations of gene expression of FHIT and WWOX at chromosome fragile sites.* Mol Cancer Res, 2005. **3**(3): p. 130-8.
117. Roz, L., et al., *Restoration of fragile histidine triad (FHIT) expression induces apoptosis and suppresses tumorigenicity in lung and cervical cancer cell lines.* Proc Natl Acad Sci U S A, 2002. **99**(6): p. 3615-20.
118. Brenner, C., *Hint, Fhit, and GalT: function, structure, evolution, and mechanism of three branches of the histidine triad superfamily of nucleotide hydrolases and transferases.* Biochemistry, 2002. **41**(29): p. 9003-14.
119. Duchen, M.R., *Mitochondria and calcium: from cell signalling to cell death.* J Physiol, 2000. **529 Pt 1**: p. 57-68.
120. Giorgi, C., et al., *Ca2+ signaling, mitochondria and cell death.* Curr Mol Med, 2008. **8**(2): p. 119-30.
121. Bano, D., et al., *Cleavage of the plasma membrane Na+/Ca2+ exchanger in excitotoxicity.* Cell, 2005. **120**(2): p. 275-85.
122. Song, G., G. Ouyang, and S. Bao, *The activation of Akt/PKB signaling pathway and cell survival.* J Cell Mol Med, 2005. **9**(1): p. 59-71.
123. Manning, B.D. and L.C. Cantley, *AKT/PKB signaling: navigating downstream.* Cell, 2007. **129**(7): p. 1261-74.
124. Whiteman, E.L., H. Cho, and M.J. Birnbaum, *Role of Akt/protein kinase B in metabolism.* Trends Endocrinol Metab, 2002. **13**(10): p. 444-51.
125. Cantley, L.C., *The phosphoinositide 3-kinase pathway.* Science, 2002. **296**(5573): p. 1655-7.
126. Franke, T.F. and L.C. Cantley, *Apoptosis. A Bad kinase makes good.* Nature, 1997. **390**(6656): p. 116-7.
127. Ferguson, K.M., et al., *Structural basis for discrimination of 3-phosphoinositides by pleckstrin homology domains.* Mol Cell, 2000. **6**(2): p. 373-84.
128. Lietzke, S.E., et al., *Structural basis of 3-phosphoinositide recognition by pleckstrin homology domains.* Mol Cell, 2000. **6**(2): p. 385-94.
129. Andjelkovic, M., et al., *Developmental regulation of expression and activity of multiple forms of the Drosophila RAC protein kinase.* J Biol Chem, 1995. **270**(8): p. 4066-75.
130. Jones, P.F., T. Jakubowicz, and B.A. Hemmings, *Molecular cloning of a second form of rac protein kinase.* Cell Regul, 1991. **2**(12): p. 1001-9.

131. Alessi, D.R., et al., *Mechanism of activation of protein kinase B by insulin and IGF-1.* Embo J, 1996. **15**(23): p. 6541-51.
132. Brazil, D.P. and B.A. Hemmings, *Ten years of protein kinase B signalling: a hard Akt to follow.* Trends Biochem Sci, 2001. **26**(11): p. 657-64.
133. Burgering, B.M. and P.J. Coffer, *Protein kinase B (c-Akt) in phosphatidylinositol-3-OH kinase signal transduction.* Nature, 1995. **376**(6541): p. 599-602.
134. Cross, D.A., et al., *Inhibition of glycogen synthase kinase-3 by insulin mediated by protein kinase B.* Nature, 1995. **378**(6559): p. 785-9.
135. Franke, T.F., et al., *The protein kinase encoded by the Akt proto-oncogene is a target of the PDGF-activated phosphatidylinositol 3-kinase.* Cell, 1995. **81**(5): p. 727-36.
136. Alessi, D.R., et al., *Characterization of a 3-phosphoinositide-dependent protein kinase which phosphorylates and activates protein kinase Balpha.* Curr Biol, 1997. **7**(4): p. 261-9.
137. Stephens, L., et al., *Protein kinase B kinases that mediate phosphatidylinositol 3,4,5-trisphosphate-dependent activation of protein kinase B.* Science, 1998. **279**(5351): p. 710-4.
138. Sarbassov, D.D., et al., *Phosphorylation and regulation of Akt/PKB by the rictor-mTOR complex.* Science, 2005. **307**(5712): p. 1098-101.
139. Andjelkovic, M., et al., *Role of translocation in the activation and function of protein kinase B.* J Biol Chem, 1997. **272**(50): p. 31515-24.
140. Carpten, J.D., et al., *A transforming mutation in the pleckstrin homology domain of AKT1 in cancer.* Nature, 2007. **448**(7152): p. 439-44.
141. Kennedy, S.G., et al., *Akt/Protein kinase B inhibits cell death by preventing the release of cytochrome c from mitochondria.* Mol Cell Biol, 1999. **19**(8): p. 5800-10.
142. Zimmermann, S. and K. Moelling, *Phosphorylation and regulation of Raf by Akt (protein kinase B).* Science, 1999. **286**(5445): p. 1741-4.
143. Khan, M.T., et al., *Akt kinase phosphorylation of inositol 1,4,5-trisphosphate receptors.* J Biol Chem, 2006. **281**(6): p. 3731-7.
144. Mikoshiba, K., *The IP3 receptor/Ca2+ channel and its cellular function.* Biochem Soc Symp, 2007(74): p. 9-22.
145. Bare, D.J., et al., *Cardiac type 2 inositol 1,4,5-trisphosphate receptor: interaction and modulation by calcium/calmodulin-dependent protein kinase II.* J Biol Chem, 2005. **280**(16): p. 15912-20.

146. Vermassen, E., et al., *Regulation of the phosphorylation of the inositol 1,4,5-trisphosphate receptor by protein kinase C.* Biochem Biophys Res Commun, 2004. **319**(3): p. 888-93.
147. Clapham, D.E., *Calcium signaling.* Cell, 2007. **131**(6): p. 1047-58.
148. Vanderheyden, V., et al., *Regulation of inositol 1,4,5-trisphosphate-induced Ca2+ release by reversible phosphorylation and dephosphorylation.* Biochim Biophys Acta, 2009. **1793**(6): p. 959-70.
149. Hattori, M., et al., *Distinct roles of inositol 1,4,5-trisphosphate receptor types 1 and 3 in Ca2+ signaling.* J Biol Chem, 2004. **279**(12): p. 11967-75.
150. Tovey, S.C., et al., *Calcium puffs are generic InsP(3)-activated elementary calcium signals and are downregulated by prolonged hormonal stimulation to inhibit cellular calcium responses.* J Cell Sci, 2001. **114**(Pt 22): p. 3979-89.
151. Hajnoczky, G., et al., *Control of apoptosis by IP(3) and ryanodine receptor driven calcium signals.* Cell Calcium, 2000. **28**(5-6): p. 349-63.
152. Fleming, N. and L. Mellow, *Arachidonic acid stimulates intracellular calcium mobilization and regulates protein synthesis, ATP levels, and mucin secretion in submandibular gland cells.* J Dent Res, 1995. **74**(6): p. 1295-302.
153. Zheng, Y. and X. Shen, *H2O2 directly activates inositol 1,4,5-trisphosphate receptors in endothelial cells.* Redox Rep, 2005. **10**(1): p. 29-36.
154. Grynkiewicz, G., M. Poenie, and R.Y. Tsien, *A new generation of Ca2+ indicators with greatly improved fluorescence properties.* J Biol Chem, 1985. **260**(6): p. 3440-50.
155. Johnson, J.D. and J.P. Chang, *Function- and agonist-specific Ca2+ signalling: the requirement for and mechanism of spatial and temporal complexity in Ca2+ signals.* Biochem Cell Biol, 2000. **78**(3): p. 217-40.
156. Roderick, H.L. and M.D. Bootman, *Redoxing calcium from the ER.* Cell, 2005. **120**(1): p. 4-5.
157. Blackshaw, S., et al., *Type 3 inositol 1,4,5-trisphosphate receptor modulates cell death.* Faseb J, 2000. **14**(10): p. 1375-9.
158. Mendes, C.C., et al., *The type III inositol 1,4,5-trisphosphate receptor preferentially transmits apoptotic Ca2+ signals into mitochondria.* J Biol Chem, 2005. **280**(49): p. 40892-900.
159. Jayaraman, T. and A.R. Marks, *T cells deficient in inositol 1,4,5-trisphosphate receptor are resistant to apoptosis.* Mol Cell Biol, 1997. **17**(6): p. 3005-12.

160. Khan, A.A., et al., *Lymphocyte apoptosis: mediation by increased type 3 inositol 1,4,5-trisphosphate receptor.* Science, 1996. **273**(5274): p. 503-7.
161. Calera, M.R. and P.F. Pilch, *Induction of Akt-2 correlates with differentiation in Sol8 muscle cells.* Biochem Biophys Res Commun, 1998. **251**(3): p. 835-41.
162. Ainscow, E.K. and G.A. Rutter, *Mitochondrial priming modifies Ca2+ oscillations and insulin secretion in pancreatic islets.* Biochem J, 2001. **353**(Pt 2): p. 175-80.
163. Rapizzi, E., et al., *Recombinant expression of the voltage-dependent anion channel enhances the transfer of Ca2+ microdomains to mitochondria.* J Cell Biol, 2002. **159**(4): p. 613-24.